ALAMETHICIN: SECONDARY STRUCTURE IN SOLUTION AND INTERACTIONS WITH PHOSPHOLIPID MEMBRANES.

Thesis by

Utpal Banerjee

In Partial Fulfillment of the Requirements

for the Degree of

Doctor of Philosophy

California Institute of Technology

Pasadena, California 91125

1984

(Submitted September 26, 1983)

TO MY PARENTS

Acknowledgements

I thank Professor Sunney Chan for his guidance in this work. His constant encouragement, sound advice and insistence on excellence in research were invaluable. It has been a pleasure to work in his laboratory. I am also grateful to all members of the Chan group for many useful discussions. I wish to thank Craig Martin for his assistance in computer programming and David Blair for introducing me to Raman spectroscopy. Dr. Fai-Po Tsui who moved away from chemistry to broaden his horizons, taught me many tricks of "real chemistry". Thanks are due to dear friends Larry Shapiro and Tim Pearson for many stimulating discussions.I owe my gratitude to Raphael Zidovetzki for sharing the ups and downs of research with me. I cherish my association with him as a friend and colleague. I thank the present and former staff members of the NMR facility, especially Dr. Luciano Mueller for his constant assistance and advice.

Sincere thanks to Professor Israel Pecht whose brief stay at Caltech was a joy for all of us. I am indebted to Dr. J. H. Freed and Leslie Schwartz of Cornell University for providing me with the NMR simulation programs; to Drs. G.B.Whitfield and J.E.Grady of the Upjohn Company for supplying samples of alamethicin used in this project; and to Dr. J.E.Hall for many useful discussions. Dr. Phoebe Dea kindly provided purified chlorophyll A . I thank her for this effort.

The constant encouragement of my teachers and professors in India has made it possible for me to pursue scientific research and the support of my parents has been a source of strength throughout. The "core group" of the Sinhas and Chatterjees, Subirda and Abhijit have added a little touch of sweetness to my stay in Los Angeles. Last but not the least, I thank my friend Arpita for her friendship, patience and understanding and for her help in preparing much of this manuscript.

I acknowledge the use of the Southern California Regional NMR facility funded by grant CHE-7916324 from the National Science Foundation. Financial support during my stay in Caltech was primarily provided by assistantships at the NMR facility funded by the same grant from NSF.

ABSTRACT

The icosapeptide alamethicin (Ac-Aib-Pro-Aib-Ala-Aib-Ala-Gln-Aib-Val-Aib-Gly-Leu-Aib-Pro-Val-Aib-Aib-Glu-Gln-Phol) isolated from the fungus Trichoderma viride induces voltage-gated ionic conductance in black lipid film membranes (Latorre, R. & Alvarez, D. (1981) Physiol. Rev. 61, 77). Single-channel measurements have indicated that passive ion transport across membranes is mediated by alamethicin channels that fluctuate between several conduction states. While these studies provide phenomenological description of the nature of alamethicin-assisted ionic conduction, very few studies probed the molecular structure of this peptide and the nature of its interaction with lipid membranes. These issues are addressed in the present investigation.

An analysis of the proton magnetic resonance spectrum is undertaken. Two-dimensional NMR is employed to achieve a complete assignment of the protons in the molecule to NMR resonances. The spectral assignment is a necessary first step towards molecular interpretations.

Measurement of coupling constants and two-dimensional NOE's suggest a half-helical, half-extended dimeric structure for the molecule in methanol. This proposed model for the secondary structure, consistent with the NMR data as well as a line of other experimental observations erstwhile published, predicts that (a) the amide protons of residues 15 through 20 are intermolecularly hydrogen-bonded with the corresponding residues of the opposing molecule to create a rigid, extended parallel β-pleated structure for the C-terminal end of the molecule; (b) the proline at position 14 breaks the continuity of this structure, and amino acids 10 through 14 are forced into an open, non-hydrogen-bonded

conformation, and (c) amino acids 3 through 9 are folded into an α-helix, with Gln-7 side chains from the two strands in the right juxtaposition to facilitate a hydrogen bond between them. The resultant structure is highly amphipathic: one face is completely hydrophobic with the aliphatic side chains exposed, whereas the other face is primarily hydrophilic with polar side chains and peptide groups lining the extended β-sheet region.

The dimeric structure is further supported by relaxation measurements that indicate that the N-acetyl methyl groups at the N-termini of the two helices in the dimer have distinct proton spin-spin relaxation times. This difference is eliminated once the dimers are dissociated with urea.

Spectral assignments in water are complicated by broadened NMR signals due to aggregation. Standard two-dimensional and decoupling techniques for assignments are inadequate for this case. A successful assignment is achieved by solvent titration from methanol. No changes in coupling constants are noted during the titration, and it is expected that the conformation in water is similar, if not identical, to that in methanol. Relaxation measurements in water are consistent with a tightly bound dimeric unit that micellises to larger aggregates.

The interaction of alamethicin with multilayers is inferred from a spectroscopic investigation of the phospholipid bilayer prepared from dimyristoyl lecithin (DML) in the presence and absence of alamethicin, and, for contrast, in the presence of other membrane active molecules. The dynamics and conformation of phospholipid head group and chains are examined by P31 and H2 NMR. A P31 line shape calculation has helped

identify the dependence of the spectrum on various motional, relaxation and conformational parameters.

As part of the investigation of lipid packing and dynamics in membranes, small bilayer vesicles are also studied. Proton NMR indicates that the outside-facing and inside-facing leaflets of the bilayer in small vesicles have lipids packed in different densities. This is due to the differences in the extent and sign of curvature of the two leaflets. At the high field at which this NMR study is undertaken, the differences in packing show up as distinct proton peaks from the inside and outside chain methylene and methyl groups that differ in width and in chemical shift.

Finally, the interaction of alamethicin with DML multilayers is characterized by P31, H2 and H1 NMR and Raman spectroscopy. The reduction in chemical shift anisotropy ($\Delta\sigma$) of the P31 signal is interpreted in terms of an interaction of the peptide at the water-membrane interface that causes a change in the average head group orientation. Deuterium NMR shows no changes in quadrupolar splittings (and hence C-D order parameters) of the chain deuterons, and Raman spectroscopy shows no change in the gauche-trans ratio of methylene segments in the chain. These results are contrasted with P31 and H2 NMR of the gramicidin S/DML system that shows polymorphism due to partial disruption of the multilayer structure and the chlorophyll A/DML system that exhibits a 7° C change in phase transition temperature as a clear indication of incorporation of the phytol chain into the bilayer.

Taken together, these experiments unequivocally indicate that the peptide interacts with lipid bilayers at the lipid-water interface.

The proposed amphiphilic aggregated solution structure for the peptide is ideally suited for such an interaction. Inasmuch as the conductance characteristics of alamethicin are only explained in terms of transmembrane pore formation, it is proposed that the large dipole moment of this aggregate facilitates the transfer of the peptide into the bilayer once a gradient of field is applied.

Table of Contents

Chapter I.1

Alamethicin: An Icosapeptide Antibiotic from *Trichoderma viride*

Alamethicin was discovered in the culture broth of the fungus *Trichoderma viride* by Meyer and Reusser in 1966. They established the antibiotic properties of this peptide and demonstrated that it exclusively inhibits the growth of gram-positive bacteria. The peptide is cataloged as Antibiotic U22324. Interest in the peptide surged with the discovery by Mueller and Rudin (1968) that alamethicin induces voltage-dependent conductance in bilayer membranes. This was a remarkable finding since electrical conductivity properties such as negative resistance, delayed rectification, bistable charges of electromotive force as well as single or rhythmic action potentials, which were erstwhile thought of as characteristic of nerve membrane proteins (Hodgkin and Huxley, 1952) and excitability-inducing material (Bean et al., 1969), were shown to be exhibited by this small peptide.

The primary structure of alamethicin was thought to be cyclic (Payne, 1970), and it was not until 1975 that NMR investigations confirmed it to be linear (Martin and Williams, 1975). Both termini of the peptide are modified--the N-terminus by acetylation and the C-terminus by reduction to an alcohol. Martin and Williams' proposed structure is branched at the C-terminus; it has been shown later that this structure belongs only to a minor component in native alamethicin. The isolated mixture has been separated by high-pressure liquid chromatography into twelve components by Balasubramanian and co-workers (1981). Solid and liquid phase methods have now been developed by several groups to synthesize the major fraction (Gisin, 1977; Marshall et al., 1979; Nagaraj & Balaram, 1981). These investigators have now

reached a consensus on the primary structure of the major component. It is a linear sequence of twenty amino acids given below:

```
    1               5                  10                  15
Ac-Aib-Pro-Aib-Ala-Aib-Ala-Gln-Aib-Val-Aib-Gly-Leu-Aib-Pro-Val-Aib-
                20
Aib-Glu-Gln-Phol
```

The unusual features of this primary structure are the amino acid Aib (α-aminoisobutyric acid) and the reduced C-terminus amino acid phenylalaninol (Phol). The combination of Aib and Phol has now been found in several peptides leading to the interesting nomenclature for this class of compounds as "peptaibphol" antibiotics (Pandey et al., 1977). The presence of Aib units necessitates that the peptide be biosynthesized by a nongenetic pathway. It has been demonstrated (Mohr & Kleinkauf, 1978) that the biosynthesis is initiated on a multienzyme complex. The N-terminal Aib remains bound on the surface of the synthetase until synthesis of the chain is completed; cleavage is followed by acetylation of the N-terminus by acetyl Co-A.

The mechanism of the bactericidal action of alamethicin is not clear; however, a number of investigators have looked at the effect of alamethicin on more advanced biological systems. These studies, while not of much importance to the native action of the peptide itself, shed light on its mode of action across the cell membranes. It was shown, for example, that the peptide can be incorporated into the node of Ranvier of frog (Calahan & Hall, 1982). Multiple pore state and the "inactivation phenomenon" (Donovan & Latorre, 1979) can be observed in this system when Ca^{+2} ions, quaternary ammonium ions or local anesthetics are present. It has also been shown that alamethicin causes hemolysis in red blood cells

Figure I.1 Amino acid sequence of alamethicin (Gisin et al.1977; Pandey et al. 1977).

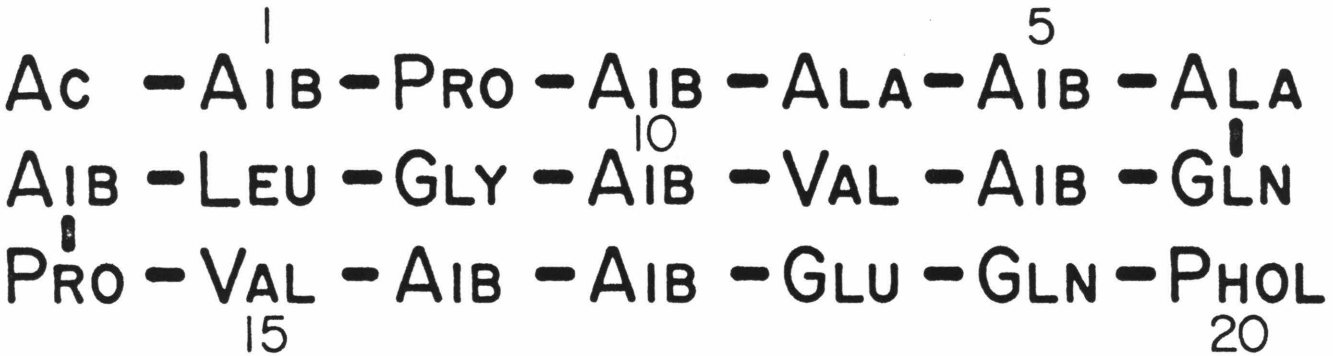

Aib: α Amino Iso-Butyric Acid

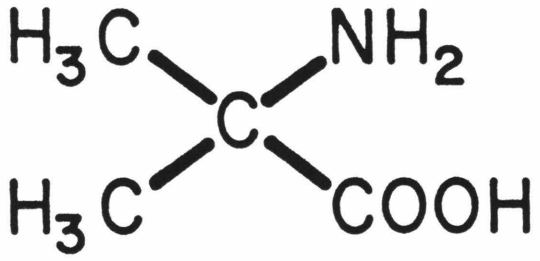

Phol: Phenylalaninol

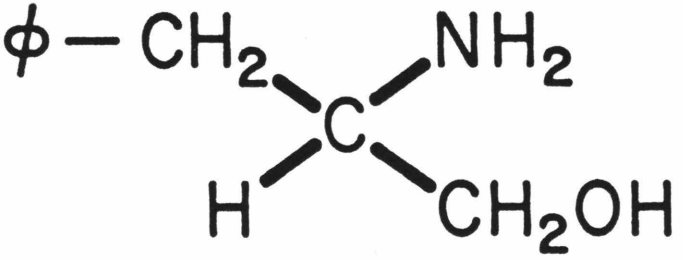

(Irmscher & Jung, 1977), acts as an uncoupler of mitochondrial oxidative phosphorylation in rat liver mitochondria (Mathew et al., 1981), and has an unmasking effect on Na^+-K^+ ATPase, β-adrenergic receptor coupled adenylate cyclase and c-AMP dependent protein kinase activity of cardiac sarcolemmal vesicles (Jones et al., 1980).

The aforementioned experiments nonwithstanding, the focus of the alamethicin literature has been centered on the peptide's curious conductance behavior in black lipid films. Gordon and Haydon (1972) published the first evidence that alamethicin exhibits discreet steps in conductance; the most comprehensive study on alamethicin conductance patterns followed by Eisenberg and co-workers (1973). The results from these experiments indicated that alamethicin shows at least five conductance states that are not simple multiples of one another (Fig. I.2). While each pore state shows ohmic conductance in single channel measurements, the overall macroscopic current-voltage curve is nonlinear and even shows a region of negative resistance. This is shown in Fig. I.3.

The conductance has a high-order dependence on salt and alamethicin concentration; the number of pores n created at voltage V is given by (Eigenberg et al., 1973)

$$n = n_c(C_{salt})^4 \, (C_a)^9 \exp\left(\frac{V - k}{3.94}\right) \qquad (I.1)$$

where C_{salt} and C_a are the salt and alamethicin concentrations, respectively, n_c is the number of pores at the "characteristic voltage" as defined by Eisenberg et al. (1973) and K is a constant that depends on the type of salt and membrane area. Further characterization of

Figure I.2 Single channel measurements on alamethicin doped black PE-decane film membrane. Current vs time trace shows up to 6 levels of conductance (from Eisenberg et al. 1973).

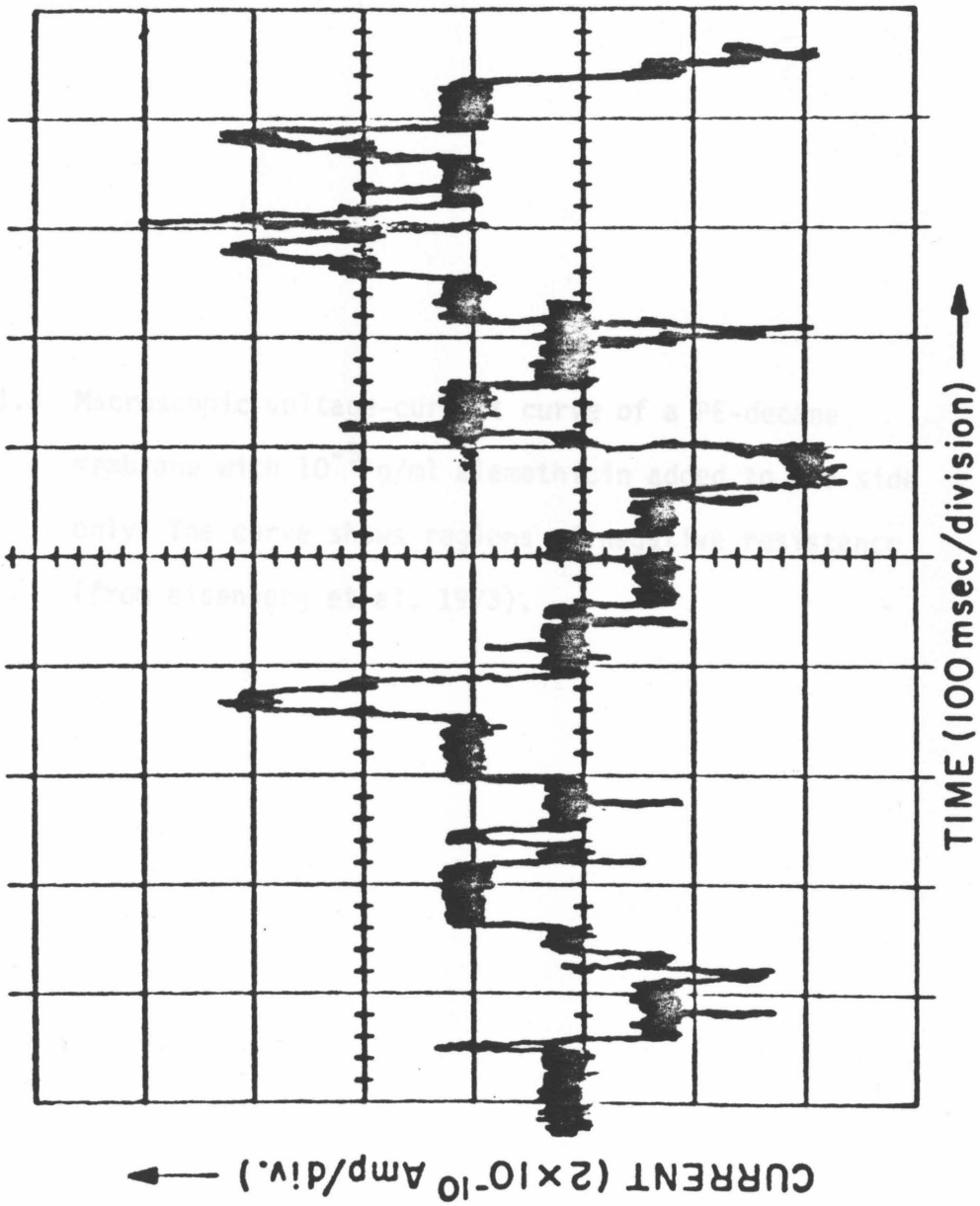
CURRENT (2×10⁻¹⁰ Amp/div.)
TIME (100 msec/division)

Figure I.3 Macroscopic voltage-current curve of a PE-decane membrane with 10^{-5} g/ml alamethicin added to one side only. The curve shows regions of negative resistance (from eisenberg et al. 1973).

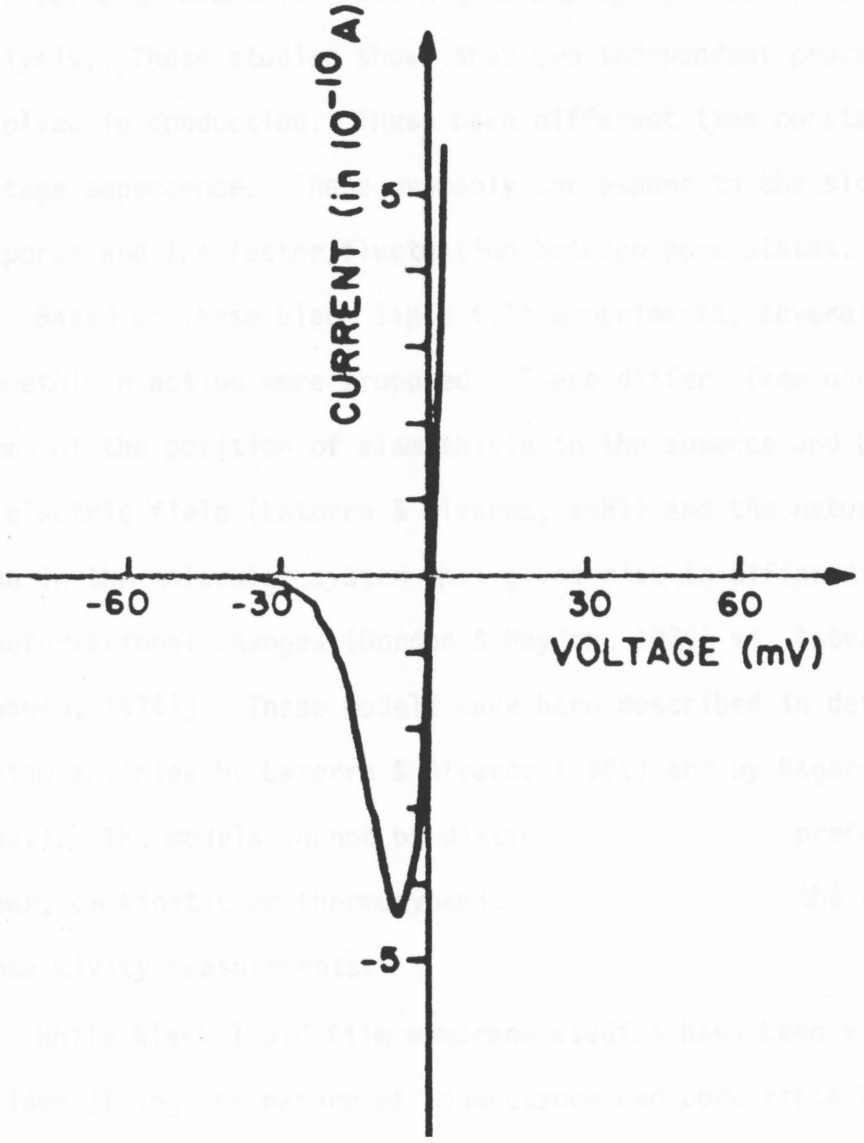
CURRENT (in 10^{-10} A)
5
-5
-60
-30
30
60
VOLTAGE (mV)

the multipore conduction of alamethicin was accomplished by Boheim and co-workers (Kolb & Boheim, 1978); Boheim & Kolb, 1978) by voltage-jump current-relaxation techniques and by auto-correlation and spectral analysis. These studies show that two independent processes are involved in conduction. These have different time constants and voltage dependence. These probably correspond to the slow formation of pores and the faster fluctuation between pore states.

Based on these black lipid film experiments, several models for alamethicin action were proposed. These differ from one another in terms of the position of alamethicin in the absence and presence of electric field (Latorre & Alvarez, 1981) and the nature of fluctuation in the molecular system that gives rise to different pore states [conformational changes (Gordon & Haydon, 1976) vs. lateral diffusion (Boheim, 1974)]. These models have been described in detail in review articles by Latorre & Alvarez (1981) and by Nagaraj & Balaram (1981). The models cannot be distinguished, one in preference to the other, on kinetic or thermodynamic grounds based on the electrical conductivity measurements.

While black lipid film membrane studies have been very successful in identifying the nature of conductance and pore state of alamethicin, these methods are inadequate for predicting the molecular events underlying the conductance phenomenon. To achieve this, it is necessary to employ methods for direct observation of the peptide molecule. Recently a number of biophysical studies have addressed the question of alamethicin secondary structure, aggregation and interaction with lipid membranes. Ultracentrifugation and interfacial tension

measurements by McMullen and Stirrup (1971) showed that the molecule is highly aggregated in water (~ 17 monomers/micelle). The micelles are only partially disrupted in 6M urea solution. Dipole moment measurements are also indicative of aggregation; the investigation by Yantorno, et al. (1977) shows that the molecule exists mostly as a monomer, but to a small degree as a dimer in octanol with a dipole moment of ~75D; larger aggregates are formed when dioxane is added to the system. The secondary structure of the peptide has been discussed in detail later in this report. Earlier, a circular dichroism study indicated that 40% of the structure is α helical. More recently, partial α helical character has been indicated by C13 NMR by Jung and co-workers (1982) while the crystal structure has indicated α helix along the entire length of the molecule with the inevitable break at Pro-14 (Fox & Richards, 1982). Davis and Gisin (1981) have published a proton NMR assignment for alamethicin at 600 MHz without any reference to the secondary structure. The assignments at 600 MHz are in agreement with the results presented in this thesis. NMR, IR and crystallographic investigations of N-terminus fragments of alamethicin have shown β turns and 2_{10} helical structures for these subunits (Nagaraj & Balaram, 1981a, 1981b; Balasubramanian et al., 1981).

Spectroscopic investigations of lipid-alamethicin mixed systems have been scarce. Hauser et al. (1970) studied the interaction of alamethicin with lipid vesicles and reported perturbation of lipid head groups and chains (Hauser et al., 1970). It was shown later, however, that the observed changes are explained by alamethicin-induced vesicle fusion. Lau and Chan suggested that alamethicin interacts with membranes at

the water-lipid interface. These investigators also demonstrated channel-forming capability of alamethicin in artificial lipid vesicles (Lau & Chan, 1975, 1976). The proposed surface interaction has been contradicted in the recent literature by two reports that emphasize that the peptide is incorporated into the bilayer in the absence of a field. The first of these studies is on lipid multilayers using infrared-attenuated total reflection spectroscopy by Fringeli and Fringeli (1979). The second report is on vesicles by Latorre et al. (1981) which is based on photolabeling of alamethicin by activated lipids.

The present investigation addresses the question of secondary structure and aggregation state of alamethicin and, in the next part, the interaction of alamethicin with phospholipid membranes in the absence of a transmembrane potential.

Chapter I.2
High-Field Two-Dimensional Fourier-Transform NMR

The first NMR experiments were reported in 1946 by Purcell et al. (1946), and a general formalism for the NMR phenomenon was developed by Bloch et al. (1946) the same year. Since then, this branch of spectroscopy has flourished and improved to attain its current status as a leading technique for structural analysis in solution as well as for studies in motional dynamics (Seiter & Chan, 1973), kinetics (den-Hollander et al., 1979), imaging (Hoult & Lauterbur, 1979) and conformational analysis (Bystrov, 1976). Until recently, however, NMR methods in solution were only applicable to small molecules. The extension of the method to accommodate studies of biological macromolecules has been made possible by later developments in instrumentation as well as with the newer applications of the theory of NMR. The two most important technical developments that aided the rapid growth of this technique have been the manufacture of large homogenous magnets and dedicated computer systems with fast Fourier-transform and multiple pulse generation capabilities. For most of the work described in this thesis a 11.7 Tesla superconducting magnet was employed that can provide the necessary resolution and sensitivity for spectral assignments in large peptides. The advancement in technology has been complemented by several theoretical developments in NMR in the last decade that have resulted in newer techniques. An important milestone in these developments has been the creation of two-dimensional NMR. The unambiguous assignment of about two hundred protons in alamethicin to resonance patterns was made possible mainly due to the use of this technique. In light of the relevance to the current work and its rather recent use as a general technique, the basic methodology

of two-dimensional NMR is discussed in this chapter.

Two-dimensional NMR was first proposed by Jeener (1971, unpublished; Jeener et al, 1979); the theoretical foundations were subsequently laid and chemical applications cited by Aue et al. (1976), Ernst (1975) and Freeman et al. (1977). Applications to macromolecules were pioneered by Wüthrich and co-workers (Nagayama & Wüthrich, 1981 and references therein). In one-dimensional Fourier-transfer NMR a radiofrequency pulse excites all spins in the system. The amplitude of magnetization is then monitored as a function of time. The signal $S(t_2)$ thus acquired is then Fourier transformed to obtain the frequency domain spectrum $S(f_2)$. The logical extension to two dimensions would require another parameter in the acquired spectrum. This is usually another time, but may be rf field strength, frequency or magnetic gradients. Most commonly the acquired signal is of the form $S(t_1,t_2)$ which is related by double Fourier transform to $F(\omega_1,\omega_2)$. A two-dimensional representation of the data is termed a "two-dimensional spectrum." In spite of its appearance, a two-dimensional spectrum is not a stacked plot of many one-dimensional spectra. The complete correlated representation is a single spectrum obtained from one composite pulse sequence. All 2D Fourier-transform experiments are characterized by three temporal phases. These are shown in Fig. I.4 and have been named by Aue et al. (1976) in accordance with their functional significance:

1. Preparation period ($t < 0$)

The spin system is allowed to relax to a state of Boltzman energy distribution. An initial state described by the density

Figure I.4 General scheme for two dimensional NMR spectroscopy defining time periods and pulses. In the final Fourier transformed representations, coupled NMR resonances, A and B, give rise to cross peaks AB and AB'.

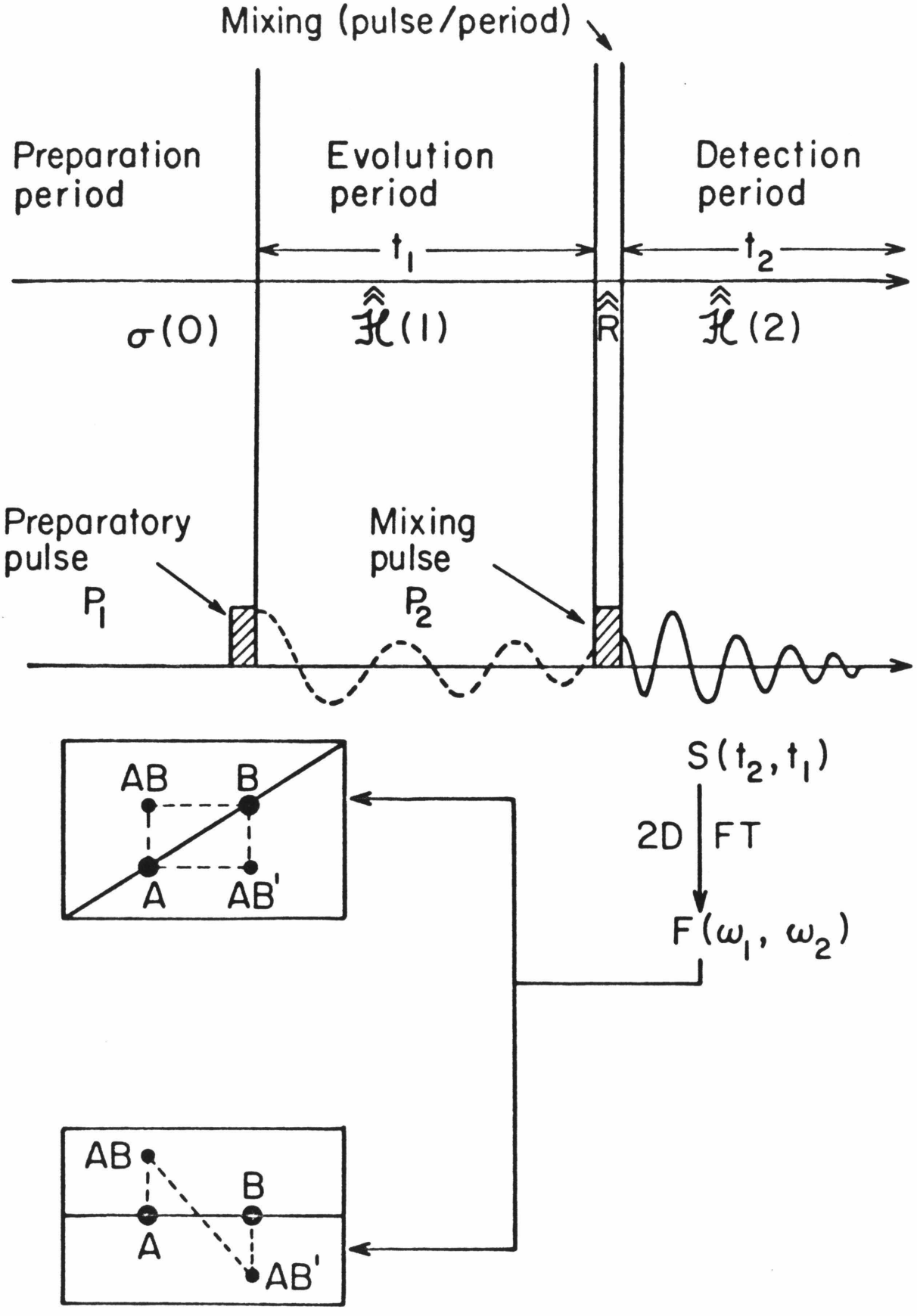
Mixing (pulse/period)
Preparation period
Evolution period
Detection period
t_1
t_2
$\sigma(0)$
$\hat{\hat{\mathcal{H}}}(1)$
$\hat{\hat{R}}$
$\hat{\hat{\mathcal{H}}}(2)$
Preparatory pulse
P_1
Mixing pulse
P_2
AB
B
A
AB'
$S(t_2, t_1)$
2D FT
$F(\omega_1, \omega_2)$
AB
B
A
AB'

operator $\sigma(0)$ and suitable for the particular 2D experiment is then created in the preparatory pulse P_1.

2. Evolution period ($0 < t < t_1$)

The system evolves under the influence of a Hamiltonian $\hat{\hat{H}}^{(1)}$. The transverse magnetization during this period depends upon $\hat{\hat{H}}^{(1)}$ and t_1. In all 2D experiments FID's are collected as a function of t_1. At the end of this period, a short and strong perturbation (usually a 90° rf pulse) is employed to rotate the generated spin states.

3. Detection period ($t_1 < t$)

The system evolves under the influence of another Hamiltonian $\hat{\hat{H}}^{(2)}$. The signal is detected as a function of t_2. The final spin state for the system is described by the density operator $\sigma(t_1,t_2)$ given by

$$\sigma(t_1,t_2) = \exp(-i\,\hat{\hat{H}}^{(2)}t_2)\,\hat{\hat{R}}\,\exp(-i\,\hat{\hat{H}}^{(1)}t_1)\,\sigma(0) \qquad \text{I.2}$$

Here $\hat{\hat{R}}$ represents a mixing operator whose components connect the two sets of transitions during the time periods t_1 and t_2. The transverse magnetization is given by

$$M_y(t_1,t_2) = \mathrm{Tr}\,[F_y\,\sigma(t_1,t_2)] \qquad \text{I.3}$$

where F_y is the total spin for the system along the observation axis. The NMR signal $S(t_1,t_2) \propto M_y(t_1,t_2)$ is double Fourier transformed to given the frequency-dependent spectrum $F(\omega_1,\omega_2)$. The order of Fourier transformation is not important, although it is usually most convenient to first transform the free induction decays along t_2; "interferograms" are then constructed using corresponding points from

different spectra along t_1. These are transformed to obtain the 2D spectrum.

A variety of two-dimensional experiments may be created that differ from one another in a) the components of the density matrix in the initial state ($\sigma_{lm}(0)$), b) the Hamiltonians $\hat{\hat{H}}^{(1)}$ and $\hat{\hat{H}}^{(2)}$ that determine the resonance frequencies along the two dimensions, or c) the components of the rotational operator $R_{ij,lm}$ that determine how the transition frequencies are connected during the mixing period by the mixing pulse(s). There are, however, two major classes of single quantum two-dimensional methods. Most experiments can be classied into one of these classes or a combination of the two:

1. Resolved NMR

Here $\sigma_{lm} \neq 0$, $R_{ij,lm} = \delta_{(ij)(lm)}$ and $\hat{\hat{H}}^{(1)} \neq \hat{\hat{H}}^{(2)}$. Common examples are homonuclear J resolved NMR and dipolar NMR.

2. Correlated NMR

$\sigma_{lm} \neq 0$; $R_{ij,lm} \neq \delta_{(ij)(lm)}$ $\hat{\hat{H}}^{(1)} = \hat{\hat{H}}^{(2)}$. Examples are chemical shift correlated NMR and spin echo correlated spectroscopy.

Four kinds of 2D spectroscopies have been most popular in the current literature. These are: 2D-J resolved spectroscopy, correlated spectroscopy (COSY), spin echo correlated spectroscopy (SECSY) and nuclear Overhauser enhancement spectroscopy (NOESY). SECSY and COSY are related by conformal mapping and have the same information content. SECSY involves a smaller data matrix requiring lesser memory space and is therefore more useful in studies of macromolecules. In what follows, a short description of each of these methods is presented. SECSY and NOESY have been used later for

assignments and structural analysis. 2D-J resolved spectroscopy has not been used here, but is included in this chapter because of its importance as an NMR technique.

2D-J Resolved Spectroscopy

2D-J resolved spectroscopy is useful for identification of multiplet structure in a crowded region of spectrum and for the measurement of coupling constants. The apparently higher resolution afforded by this technique as compared to a regular one-dimensional experiment is because each multiplet in the spectrum is rotated about its center by an angle (usually 90°). The spin coupling (J) and the chemical shift (δ) are displayed along separate axes, thus enhancing the digital accuracy in the measurement of J.

The pulse sequence for the experiment (Nagayama et al., 1977, 1979) (Fig. I.5) is

$$[90° - t_1/2 - 180° - t_1/2 - t_2]_n$$

The nonselective 90° preparatory pulse frequency labels the spins. In the middle of the evolution period a 180° pulse is applied. The spin echo generated at the end of t_1 is then acquired as a FID over the time period t_2. To construct the interferograms in the second dimension, the experiment is repeated with increasing t_1 values. The data matrix $S(t_1,t_2)$ generated is Fourier transformed to produce the desired spectrum $S(\omega_1,\omega_2)$.

Homonuclear Correlated Spectroscopy (COSY and SECSY)

COSY and SECSY manifest connectivities between NMR peaks of spins that are J coupled. These two methods circumvent the

Figure I.5 Pulse sequences for the common homonuclear two-dimensional NMR methods.

A. 2D-J Resolved Spectroscopy

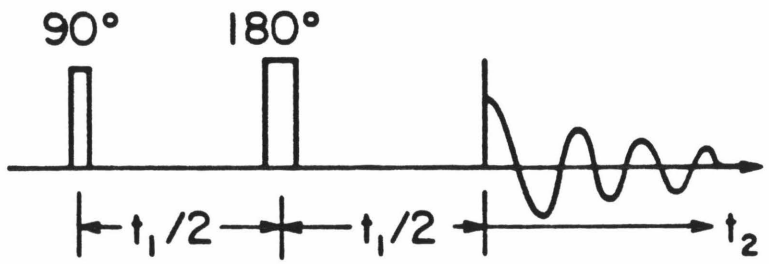

B. 2D-Correlated Spectroscopy (COSY)

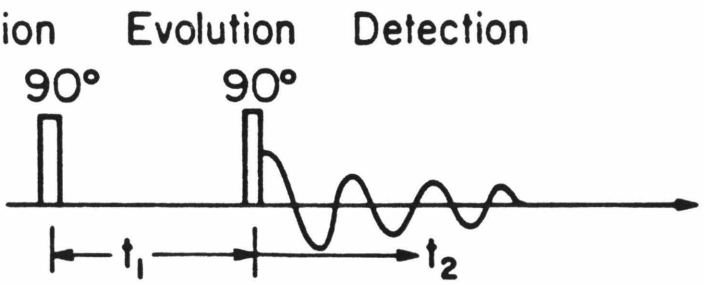

C. 2D-Spin Echo Correlated Spectroscopy (SECSY)

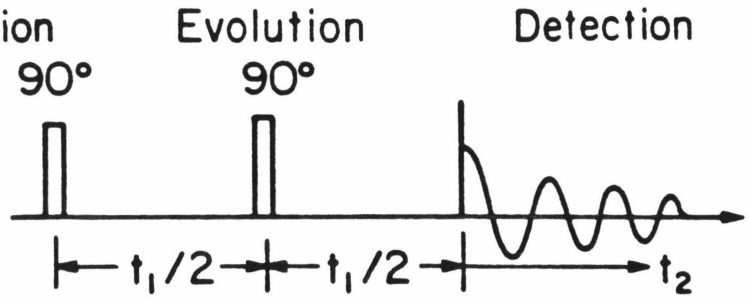

D. 2D-Nuclear Overhauser Enhancement Spectroscopy (NOESY)

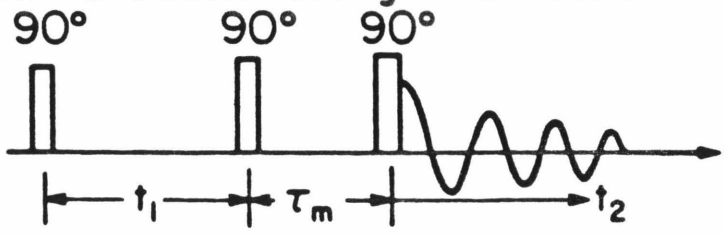

conventional decoupling technique with the advantage that the complete information about all connectivities in the spectrum is obtained from one instrumental setting and the absence of decoupler frequency helps gain arbitrarily high selectivity. COSY and SECSY are identical in their information content, and either one of them is of great importance in assignment of peaks in complicated NMR spectra, especially from large molecules.

The pulse sequences for these experiments are the following (Kumar et al.,1980a ; Nagayama et al., 1979), (Fig. I.5):

COSY: $[90° - t_1 - 90° - t_2]_n$

SECSY: $[90° - t_1/2 - 90° - t_1/2 - t_2]_n$

The pulse following or during the evolution period is 90° as compared to 180° for J resolved. In SECSY, an echo is generated at the end of the evolution period. In COSY, however, no echo is generated since the observation period directly follows the mixing pulse. As a result the final data representation is different in the two cases (Fig. I.4). These two representations are related by conformal mapping.

Nuclear Overhauser Enhancement Spectroscopy (NOESY)

Nuclear Overhauser enhancement is defined as the functional change in the intensity of one NMR peak when another is saturated. Such an exchange of magnetization is observed only for spins that are close together in space and are coupled by dipolar interactions. NOESY manifests NOE connectivities as cross peaks between resonances that correspond to nuclei close together in space. Unlike the one-

dimensional experiment, no irradiation frequency for saturation is used, thus avoiding all spill-over problems. In addition, all NOE's in the molecule may be obtained from a single experiment.

The pulse sequence for the NOESY experiment is (Kumar et al., 1980a, 1980b) (Fig. I.5):

$$[90° - t_1 - 90° - \tau_m - 90° - t_2]_n$$

All spins are frequency labeled during t_1. During the mixing delay τ_m, cross relaxation leads to incoherent magnetization exchange. The spectrum is acquired following the third 90° pulse as a function of t_2. The data representation is similar to that in COSY except the cross peaks now correspond to NOE-coupled spins. The delay τ_m determines the extent of truncation in the transfer of magnetization. NOE's over only small distances are picked up for short τ_m. In principle τ_m could be varied to generate a 3D experiment with challenging display possibilities.

In the current investigation, 2D NMR has assumed an important role in determination of structure of the icosapeptide alamethicin. As described in the next chapter SECSY was used for a complete assignment of all peaks in this molecule and NOESY provided important structural predictions that are consistent with our proposed model for alamethicin.

Chapter I.3

NMR Study of Alamethicin in Solution: Assignment of Proton Resonances

A. INTRODUCTION

The pore forming characteristics of alamethicin in lipid membranes is expected to be closely linked to its structure in solution. Modern developments in high field NMR have afforded access to structural investigations on proteins and polypeptides. This chapter describes structural studies on alamethicin by ^{1}H NMR spectroscopy at 500 MHz. Two-dimensional spin echo correlated spectroscopy is combined with double resonance experiments to afford a complete assignment of NMR resonances to protons in the molecule. Coupling constants and two-dimensional nuclear Overhauser enhancements are also reported. In the following chapter, these results have been combined to deduce the conformation of alamethicin in a methanolic solution. The effect of water on the solution conformation was followed by solvent titration experiments. No pronounced conformational difference was noted between the two solvent systems despite a significant increase in the aggregation of the molecule in water.

B. MATERIALS AND METHODS

Alamethicin from three different sources was used in this study. The first sample is a generous gift from Dr. G. B. Whitfield, Jr., of the Upjohn Company and was used without further purification. The second one is a highly purified sample ('fraction 4' by HPLC) that was prepared in the laboratory of Professor G. R. Marshall (Balasubramanian et al., 1981).

The third sample was purchased from PHLS, Wiltshire, England. This latter sample was found to be impure and give 8 bands on TLC. The mixture was therefore purified on a 2 mm silica gel 60 F_{254} precoated preparative TLC plate. Each band was then recovered and run on 0.5 mm preparative TLC plates. The fraction that showed spectroscopic resemblance to 'fraction 4' of Marshall's purified alamethicin was collected at Rf 0.47 using the solvent system: $CHCl_3$:CH_3OH:H_2O v/v/v 65:24:4.

All solutions of alamethicin were made in NMR tubes to prevent loss in handling. Typically, the concentration of the peptide was in the millimolar range. The amide protons exchange with different rates in deuterated methanol and are all replaced by deuterons in about a day's time. Before such a deuterated peptide is reused for further experiments to investigate the amides, it was back-exchanged in a CH_3OH-H_2O mixture for several days. The protonated solvent was then blown off with dry nitrogen. The tube was kept under vacuum overnight and then fresh solutions were made in deuterated solvents immediately before the experiment. The measured pD value of an alamethicin solution was typically 6.84 in CD_3OD and 6.52 in D_2O. In view of the closeness of these values to neutrality, no PD adjustments were made.

All NMR spectra were recorded on a Bruker WM500 spectrometer operating at a field strength of 11.74 Tesla (500.13 MHz proton frequency). Spectra were recorded at 298 K. Conventional NMR spectra were acquired in the Fourier transfer (FT) mode with either 16K or 32K data points using quadrature-phase detection, a 60^{o} pulse width, a cycling time between scans of 1.7 seconds, and a spectral width of 6000 Hz. The spectra were resolution-enhanced to facilitate spectral assignments and coupling constant measurements. This was achieved with a Gaussian multiplication routine that involved multiplying the free induction decay (FID) with a Gaussian centered

at 15% of the total decay time and a negative line broadening of -7 Hz.

The complete assignment of the proton NMR spectrum of alamethicin in methanol was achieved with the aid of spin echo correlated spectroscopy (SECSY) and double resonance experiments. Conformation of the molecule was established by coupling constant measurements. Predictions about the conformation of the C terminal end based on these measurements were confirmed by two-dimensional nuclear Overhauser spectroscopy (NOESY).

The SECSY spectrum was obtained using the two-pulse sequence $(90^{o}\text{-}t_1\text{-}90^{o}\text{-}t_2)_n$ (Aue et al., 1976). With this sequence all the spins are frequency labeled during time t_1, and exchange of magnetization between J-coupled spins takes place during the application of the second pulse. The free induction decay is acquired as a function of t_2. Collection of several such FID's for different t_1 values yields a data matrix $f(t_1,t_2)$ that is Fourier transformed in two dimensions to obtain the 2D spectrum $s(\omega_1,\omega_2)$, where ω_2 is the regular chemical shift axis and ω_1 is the frequency of J coupling. In our experiments, after zero filling, the number of data points used in the ω_1 and ω_2 dimensions was 1K and 4K, respectively. A sixteen-phase cycling was used for each t_1 to prevent distortions and axial peaks. The phases used for the SECSY experiment were the ones suggested by Bruker for use with their FTNMR and FTNMR2D software packages. To obtain the best presentation of data, multiple level contour plots were used to join local regions of equal intensity. Cross peaks that indicate J connectivity show up symmetrically about a centrally placed one-dimensional spectrum. For a 'square plot', coupled cross peaks fall on a segment that makes an angle of 135^{o} to the central axis.

Homonuclear decoupling was performed with the gated low power decoupler on the WM500 spectrometer. The power levels used were high enough to decouple the peaks but without significant spilling over to nearby resonances.

The 2D-NOE spectrum was obtained using three 90^{o} pulses with a mixing time τ_m between the last two (Anil Kumar et al., 1980)

$$(90^{o}\text{-}t_1\text{-}90^{o}\text{-}\tau_m\text{-}90^{o}\text{-}t_2)_n$$

The mixing time used was 350 msec. The data used after Fourier transformation was 1K and 4K along the ω_1 and ω_2 axes, respectively. A line broadening of 1 Hz along the t_1 axis and a cosine squared bell along the t_2 axis were applied to enhance the signal-to-noise ratio. Very few clear cross peaks showed up in the 2D NOE spectrum for reasons elaborated upon later in the chapter. The phase sequence used to obtain a diagonally projected spectrum was kindly provided by Dr. J. Wright of the University of California, San Diego, and consisted of 16 phase cyclings to reduce axial peaks.

C. RESULTS

(a) Spectrum in Methanol

A list of chemical shifts of all protons in the alamethicin molecule in CD_3OD is presented in Table I.1. Different regions of the proton magentic resonance spectrum of alamethicin in this solvent system are shown in Figure I.6. All spectra reported here correspond to those of the sample of alamethicin received from the Upjohn Company. All measured coupling constants in the molecule are also summarized in Table I.1.

Table I.1 Proton NMR Chemical Shifts and ^{1}H-^{1}H Coupling Constants of Alamethicin in Methanol-d_4. Chemical Shifts Are in ppm from TMS.

Amino Acid; Proton Group	Chemical Shift (δ), ppm (± 0.01)	Coupling Constants, Hz (± 0.2)
Proline-2		
αCH	4.24	$J_{\alpha\beta_1}$ = 8.1
βCH(1)	1.78	$J_{\alpha\beta_2}$ = 8.1
βCH(2)	2.30	
γCH_2	2.06	
γCH(1)	3.49	
δCH(2)	4.00	
Alanine-4		
NH	7.55	$J_{\alpha\text{-NH}}$ = 5.7
αCH	4.11	$J_{\alpha\text{-}CH_3}$ = 7.0
βCH_3	1.52	
Alanine-6		
NH	7.92	$J_{\alpha\text{-NH}}$ = 5.5
αCH	4.02	$J_{\alpha\text{-}CH_3}$ = 7.0
βCH_3	1.53	
Glutamine-7		
NH	8.00	$J_{\alpha\text{-NH}}$ = 5.2
αCH	3.90	
βCH_2	2.27	

Table I.1 Continued

Amino Acid; Proton Group	Chemical Shift (δ), ppm (± 0.01)	Coupling Constants, Hz (± 0.2)
Valine-9		
NH	7.48	$J_{\alpha\text{-NH}} = 5.5$
αCH	3.58	$J_{\alpha\text{-}\beta} = 9.5$
βCH	2.23	
$\gamma CH_3(1)$	1.06	$J_{\beta\text{-}\gamma_1} = 6.6$
$\gamma CH_3(2)$	0.98	$J_{\beta\text{-}\gamma_2} = 7.4$
Glycine-11		
NH	8.33	$J_{\alpha\text{-NH}} = 6.1$
αCH(1)	3.93	$J_{\alpha_1\text{-}\alpha_2} = 16.4$
αCH(2)	3.66	
Leucine-12		
NH	8.09	$J_{\text{NH-}\alpha} = 8.0$
αCH	4.45	$J_{\alpha\text{-}\beta_1} = 3.7$
$\beta;\gamma\text{-}CH_2$	1.94	$J_{\alpha\text{-}\beta_2} = 11.0$
$\delta CH_3(1)$	0.91	$J_{\gamma\text{-}CH_3^1} = 6.3$
$\delta CH_3(2)$	0.93	$J_{\gamma\text{-}CH_3^2} = 6.0$
Proline-14		
αCH	4.37	$J_{\alpha\text{-}\beta_1} = 7.3$
βCH(1)	1.78	$J_{\alpha\text{-}\beta_2} = 7.3$
βCH(2)	2.30	
γCH_2	2.06	
δCH(1)	3.71	
δCH(2)	3.88	

Table I.1 Continued

Amino Acid; Proton Group	Chemical Shift (δ), ppm (± 0.01)	Coupling Constants, Hz (± 0.2)
Valine-15		
NH	7.58	$J_{NH-\alpha} = 7.7$
αCH	3.72	$J_{\alpha-\beta} = 9.6$
βCH	2.25	$J_{\beta-\gamma_1} = 6.6$
$\gamma CH_3(1)$	1.13	$J_{\beta-\gamma_2} = 6.2$
$\gamma CH_3(2)$	1.00	
Glutamic acid-18		
NH	7.90	$J_{NH-\alpha} = 7.7$
αCH	4.15	
βCH_2	2.02	
γCH	2.39	
Glutamine-19		
NH	7.78	$J_{\alpha-NH} = 7.6$
αCH	4.05	
βCH_2	2.10	
Phenylalaninol-20		
NH	7.36	$J_{\alpha-NH} = 9.1$
ring-ortho	7.29	$J_{O-m} = 7.7$
-meta	7.22	$J_{m-p} = 7.3$
-para	7.13	$J_{\alpha-\beta_1} = 9.0$
αCH	4.15	$J_{\beta_1-\beta_2} = 14.0$
βCH(1)	2.74	$J_{\alpha-\beta_2} = 5.9$
βCH(2)	2.93	$J_{\alpha-\beta(OH)} = 5.5$
$\beta CH_2(OH)$	3.61	

Table I.1 Continued

Amino Acid; Proton Group	Chemical Shift (δ); ppm (± 0.01)	Coupling Constants, Hz (± 0.2)
α-Aminoisobutyric acid-1,3,5,8,10,13, 16 and 17		
α-CH_3	1.2-1.7	
N-acetyl	2.05	

Amide Protons. The amide protons appear between 8.4 and 7.3 ppm downfield of TMS. These protons typically exchange out in this deuterated solvent in a few hours. The glycine amide peak can be readily identified from its coupling pattern since it is the only amide signal that shows up as a triplet. As expected, all the α-aminoiosbutyric acid amide protons appear as singlets from lack of an α proton. The remaining amide protons show up as doublets. A weak resonance (labeled Val x in Figure I.6A) is seen at 7.47 ppm. By tracing its connectivity to α, β and γ protons, this peak has been identified as belonging to a valine. This signal is absent in the purified 'fraction 4' and is therefore assigned to one of the minor components of alamethicin in the Upjohn sample.

αCH Protons. The αCH protons are quite well resolved at 500 MHz and the various multiplets can be easily examined and analyzed. These protons occur between 4.5 and 3.4 ppm along with the δ protons of the prolines. The αCH protons of the glycine are chemical-shift nonequivalent and are separated by 135 Hz. The αCH proton multiplets simplify as the amide protons exchange out (cf. Figures I.6B and I.6C). This exchange has been taken advantage of in the assignment of the spectrum and in the determination of coupling constants ($J_{NH-\alpha CH}$ and $J_{\alpha CH-\beta CH}$).

Side Chain Protons. The β and γ CH_2 resonances are seen between 1.7 and 3 ppm downfield from TMS. All the β and δ protons can be quite easily identified although overlapping resonances do obscure the structural details of some of the multiplets and make it impossible to determine coupling constants in these cases. The γ and δ methyls of the two valines and the single leucine are very well resolved. The two methyls attached to a given valine are nonequivalent. They are chemically shifted by 40 Hz

Figure I.6 H1 NMR spectrum of alamethicin in methanol-d_4 at 500 MHz.

a. Amide and aromatic protons.

b. αCH protons prior to exchange of amide protons in the deuterated solvent.

c. αCH protons after amide exchange.

d. β and γ CH_2 protons.

e. Methyl protons.

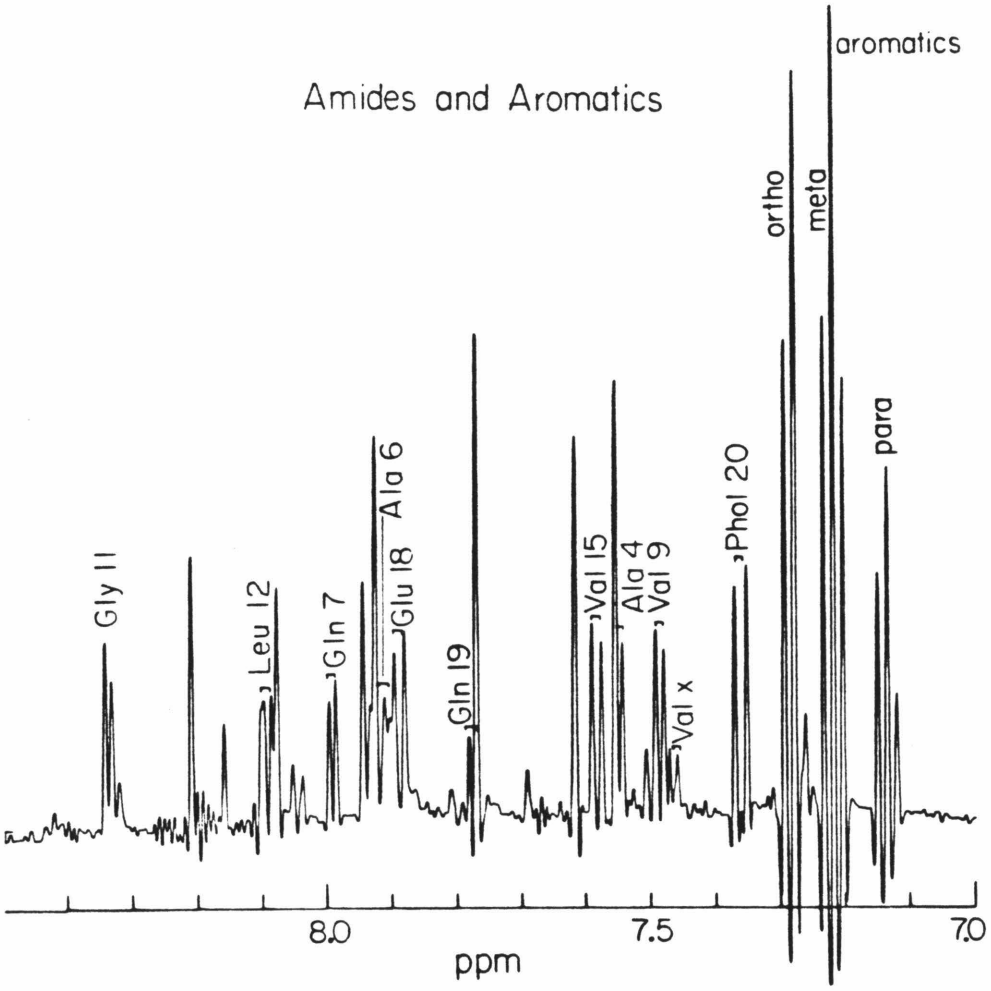
Amides and Aromatics
aromatics
ortho
meta
para
Gly 11
Leu 12
Gln 7
Ala 6
Glu 18
Gln 19
Val 15
Ala 4
Val 9
Val x
Phol 20
8.0
7.5
7.0
ppm

Figure I.6a.

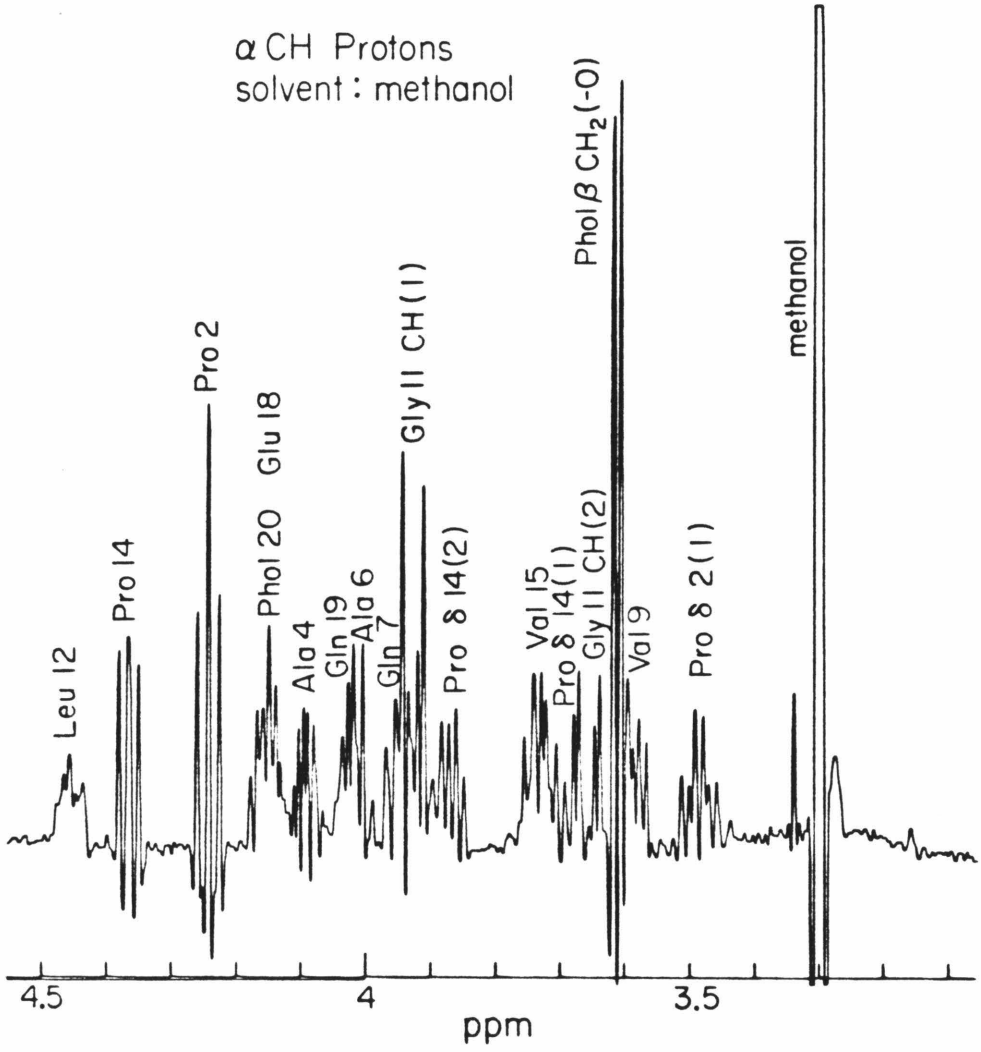
α CH Protons
solvent : methanol
Leu 12
Pro 14
Pro 2
Glu 18
Phol 20
Ala 4
Gln 19
Ala 6
Gln 7
Gly 11 CH(1)
Pro δ 14(2)
Val 15
Pro δ 14(1)
Gly 11 CH(2)
Phol β CH2(-O)
Val 9
Pro δ 2(1)
methanol
4.5
4
3.5
ppm

Figure I.6b.

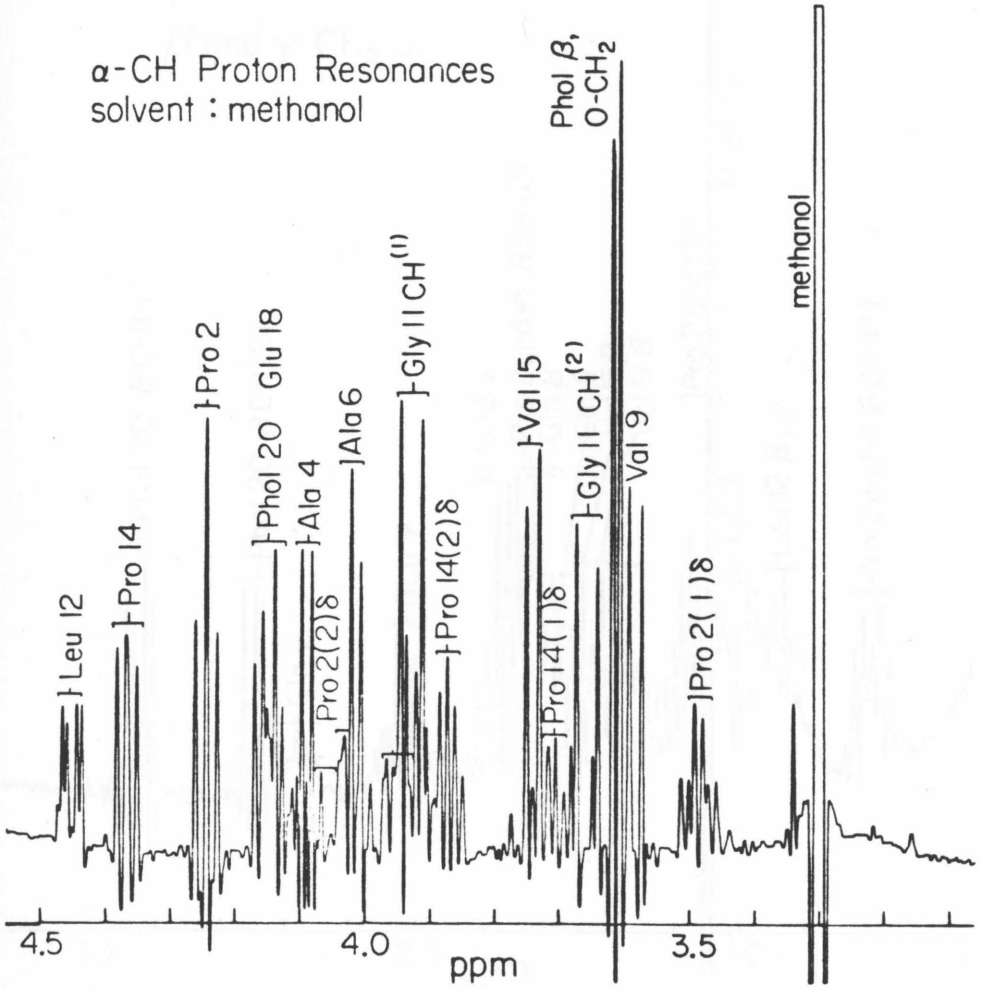
α-CH Proton Resonances
solvent : methanol
Leu 12
Pro 14
Pro 2
Phol 20
Glu 18
Ala 4
Pro 2(2)δ
Ala 6
Gly 11 CH(1)
Pro 14(2)δ
Val 15
Pro 14(1)δ
Gly 11 CH(2)
Phol β, O-CH2
Val 9
Pro 2(1)δ
methanol
4.5
4.0
3.5
ppm

Figure I.6c.

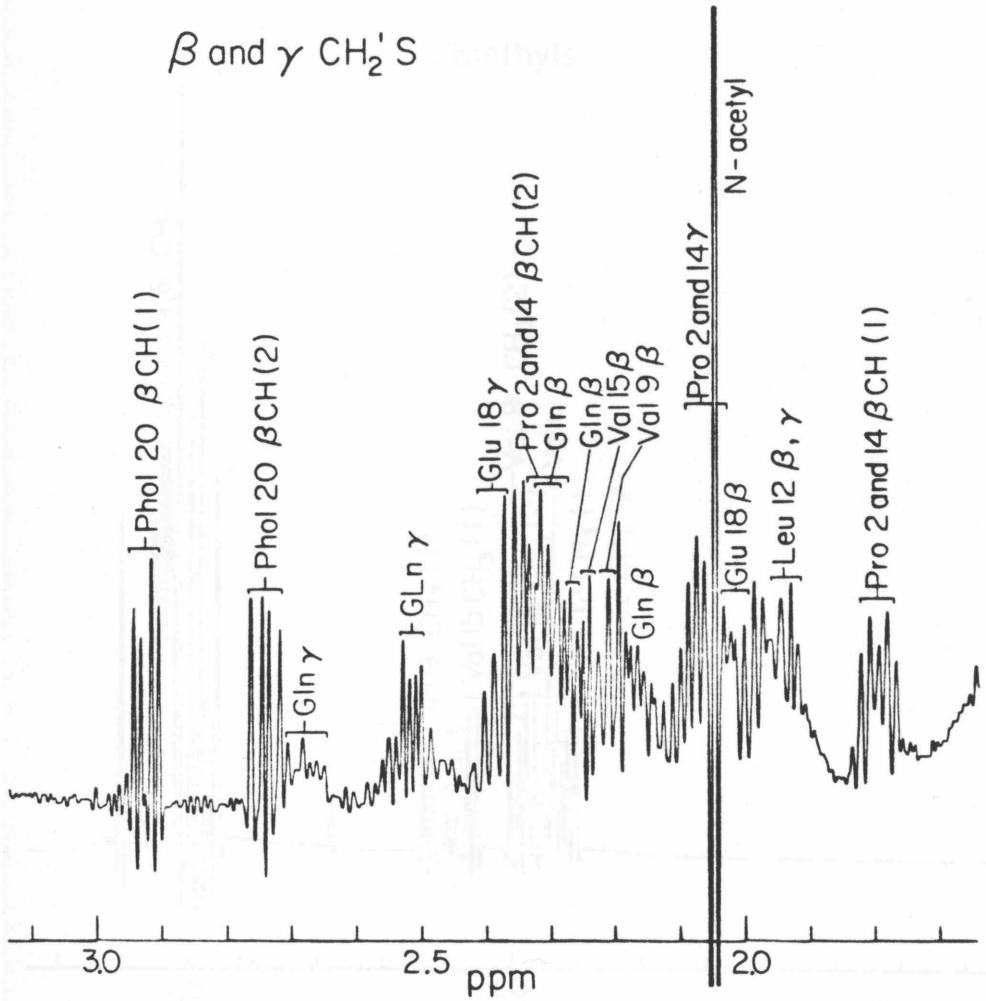
β and γ CH2's
Phol 20 βCH(1)
Phol 20 βCH(2)
Gln γ
GLn γ
Glu 18 γ
Pro 2and14 βCH(2)
Gln β
Gln β
Val 15β
Val 9 β
Gln β
Pro 2and14γ
N-acetyl
Glu 18β
Leu 12 β, γ
Pro 2 and 14 βCH (1)
3.0
2.5
ppm
2.0

Figure I.6d.

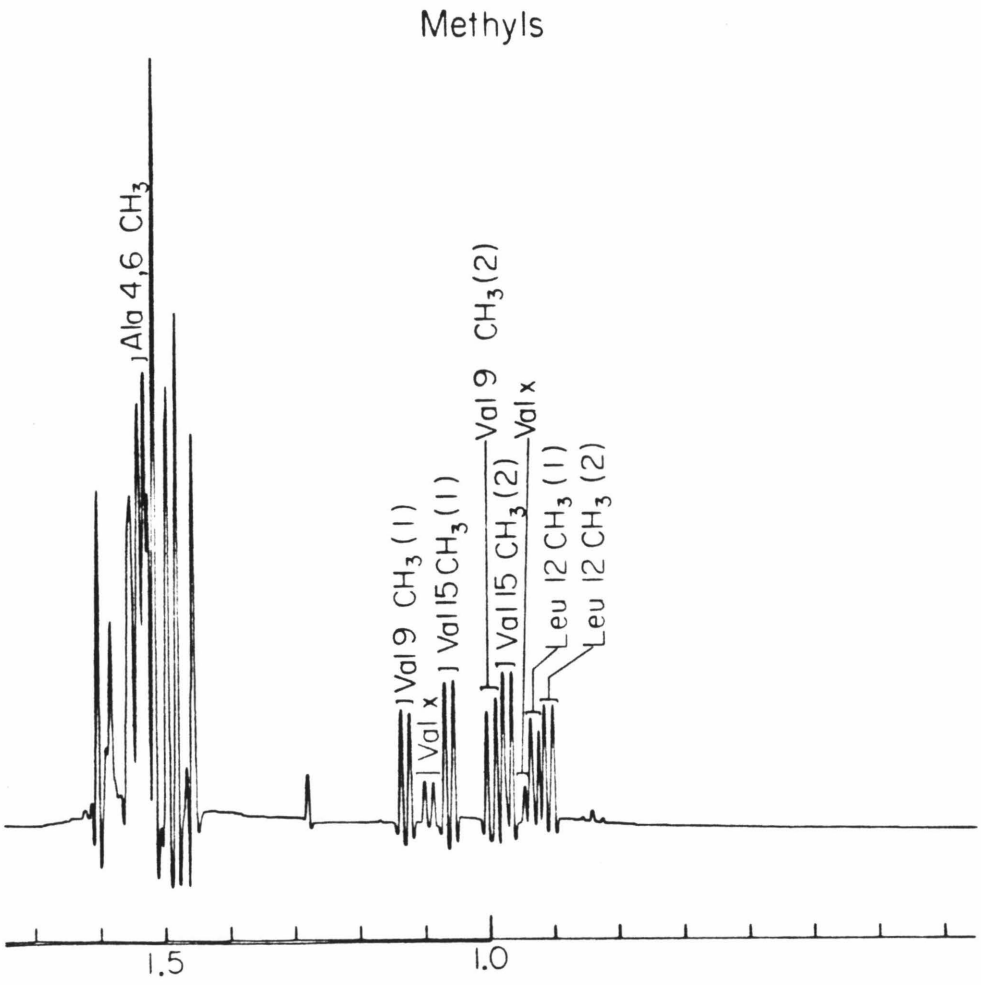
Methyls
Ala 4,6 CH3
Val 9 CH3 (1)
Val x
Val 15 CH3 (1)
Val 9 CH3 (2)
Val 15 CH3 (2)
Val x
Leu 12 CH3 (1)
Leu 12 CH3 (2)
1.5
1.0

Figure I.6e.

for Val-15 and by 65 Hz for Val-9. The methyls of the alanine and the α-aminoisobutyric acid residues are seen between 1.4 and 1.7 ppm. The two alanine methyls can be distinguished from the eight α-aminoisobutyric acid methyls by tracing their scalar connectivity to the CH protons by spin decoupling. The aromatic protons belonging to the phenylalaninol ring resonate between 7.1 and 7.3 ppm and are easily identified. The assignment of ortho, meta and para protons can be made from their intensities and the multiplet structure. The N acetyl peak occurs at 2.05 ppm.

The assignment of resonances in methanol was primarily accomplished by 2D spin echo correlated spectroscopy. Figure I.7 shows a contour plot that exhibits all the connectivities. The plot shown here is 'square', i.e. the number of Hertz per centimeter along the two axes is identical. In this plot the central axis represents a contour of the one-dimensional spectrum, and two cross peaks corresponding to J-coupled resonances fall on a line that makes an angle of 135^{o} with the central axis, as shown in Figure I.7. Independent confirmations of all 2D assignments have been made by spin decoupling. Decoupled and undecoupled spectra were recorded separately and were compared visually. Difference spectra were not used since Bloch-Siegert shifts on nearby resonances could give inaccurate assignments and shifts. The 2D method has distinct advantages over decoupling in that all the information about coupling can be obtained from a single spectrum, and problems regarding spillover of decoupler power are avoided. In some cases 2D offers specific advantages over decoupling in spectral assignments, as in the case of the glycine amide proton. Here, the amide proton is easily exchanged and appears as a broad triplet. These characteristics render decoupling assignments difficult, but the 2D spectrum shows the connectivity quite clearly.

Figure I.7 Contour plot of two-dimensional spin echo spectrum of alamethicin in methanol-d_4. Connectivities due to J coupling between protons are indicated.

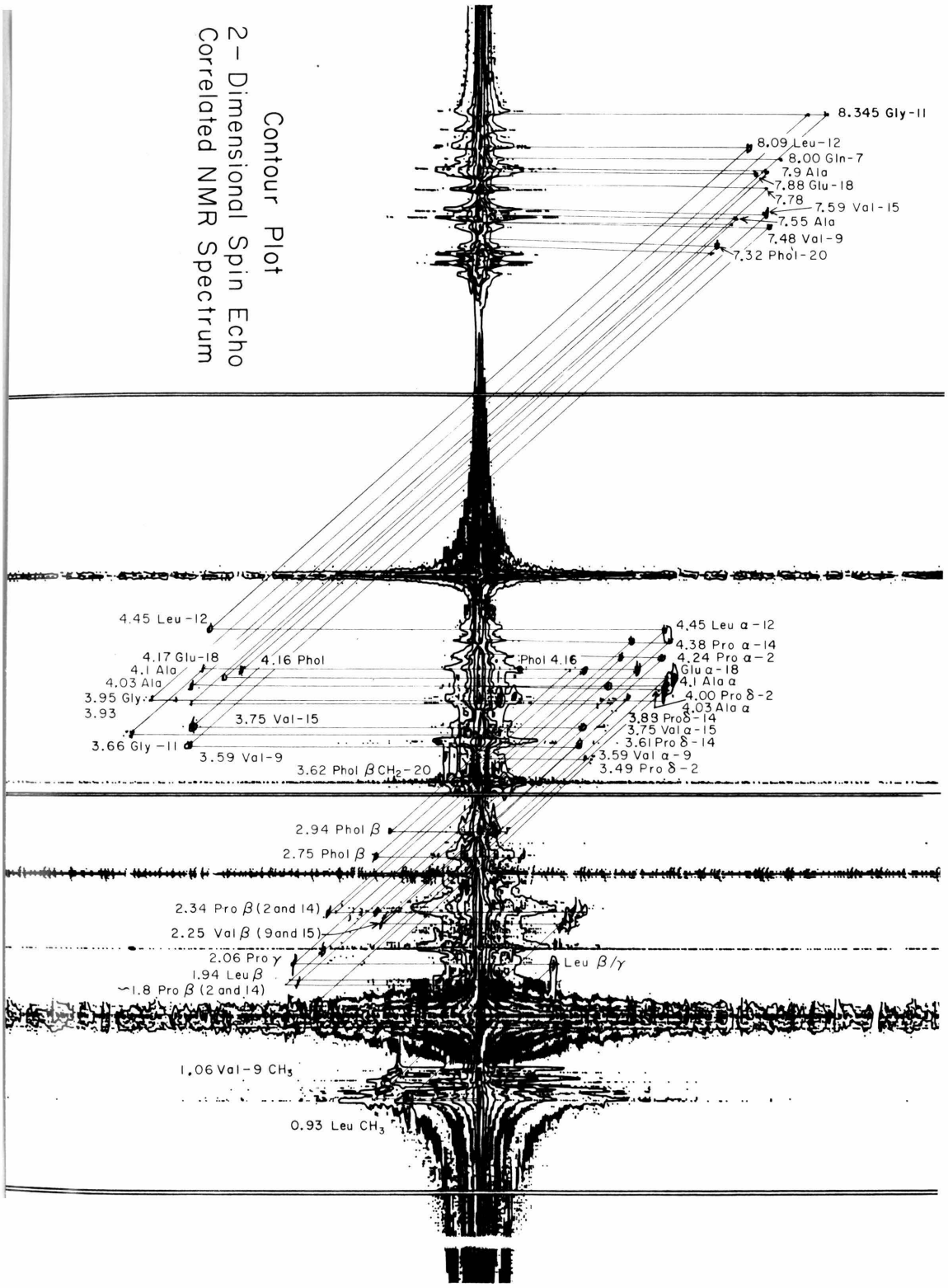
Contour Plot
2 - Dimensional Spin Echo
Correlated NMR Spectrum
8.345 Gly-11
8.09 Leu-12
8.00 Gln-7
7.9 Ala
7.88 Glu-18
7.78
7.59 Val-15
7.55 Ala
7.48 Val-9
7.32 Phol-20
4.45 Leu-12
4.17 Glu-18
4.1 Ala
4.03 Ala
3.95 Gly
3.93
3.66 Gly-11
4.16 Phol
3.75 Val-15
3.59 Val-9
3.62 Phol βCH2-20
Phol 4.16
4.45 Leu α-12
4.38 Pro α-14
4.24 Pro α-2
Glu α-18
4.1 Ala α
4.00 Pro δ-2
4.03 Ala α
3.83 Pro δ-14
3.75 Val α-15
3.61 Pro δ-14
3.59 Val α-9
3.49 Pro δ-2
2.94 Phol β
2.75 Phol β
2.34 Pro β (2 and 14)
2.25 Val β (9 and 15)
2.06 Pro γ
1.94 Leu β
~1.8 Pro β (2 and 14)
Leu β/γ
1.06 Val-9 CH3
0.93 Leu CH3

Several amino acids are repeated in the primary sequence of alamethicin. Most of the repeating residues are Aib units that are conformationally uninformative. No attempt has therefore been made to assign individually the amide and methyl protons of this amino acid. The remaining degeneracies in amino acid assignments have been solved using a variety of experimental evidence. The observed NOE between the ortho proton of Phol-20 and a valine α-CH identifies the latter proton as belonging to Val-15. Val-9 is spatially distant from Phol-20, and a proximity between the two would necessitate a pseudocyclic conformation with increased steric hinderances. The proximity of Val-15 and Phol-20 is, in fact, a natural consequence of the conformation of alamethicin suggested in Chapter I.7. Pro-2 has been distinguished from Pro-14 by the earlier N-terminal cleavage and shift reagent experiments of Martin and Williams (1976). Gln-19 can be identified from Gln-7 based on the trends in the coupling constants. The glutamine amide peak with $J_{NH\text{-}\alpha CH}$ coupling constant of 5.2 Hz is assigned to Gln-7 since the amino acids flanking this residue have a similar coupling constant and form part of an α helix. The distinction between Ala-4 and Ala-6 is largely tentative.

Amide Coupling Constants. Table I.2 shows the amide coupling constants ($J_{NH\text{-}\alpha CH}$) for the various amide protons along the polypeptide chain. There exists a pattern for the magnitude of these coupling constants along the chain. The values are typically 5.0-5.5 Hz for the N-terminal half of the molecule and 7-9 Hz for the C-terminal end. This is an important observation and suggests that the molecule may be apportioned into two regions, each with a different secondary structure. These two regions appear to be separated from one another by the bend introduced by Pro-14.

Table I-2. Amide-αCH Proton Coupling Constants ($J_{NH-\alpha}$) of Alamethicin in Methanol-d_4.

Amino Acid	$J_{\alpha-NH}$ (Hz)	Conformation
Aib-1	-	
Pro-2	-	
Aib-3	-	
Ala-4	5.7	
Aib-5	-	
Ala-6	5.5	α helix
Gln-7	5.2	
Aib-8	-	
Val-9	5.5	
Aib-10	-	
Gly-11	6.1	
Leu-12	8.0	extended open
Aib-13	-	
Pro-14	-	
Val-15	7.7	
Aib-16	-	
Aib-17	-	
Glu-18	7.7	extended β sheet
Gln-19	7.6	
Phol-20	9.1	

The amide coupling constants measured for the alamethicin protons in methanol-d_4 are quite different from those measured for the corresponding amino acids in N-terminal fragments in DMSO-d and chloroform-d (Nagaraj and Balaram, 1981). The values of the coupling constants for the whole molecule are consistently lower.

Low temperature measurements showed that the values of amide coupling constants are thermally invariant within errors of measurement. Thus, $J_{NH-\alpha CH}$ for Gln-7, Val-9, Val-15, and Phol-20 are 5.18, 5.69, 7.56, and 9.32 Hz, respectively, at 298 K, and 5.05, 5.89, 7.35, 9.37 Hz, respectively, at 278 K.

2D-NOE Studies. The nuclear Overhauser effect has often been used to infer proximity relationships for nuclear spins in a molecule. This information is often helpful in conformational analysis (Wagner et al., 1981). The two-dimensional NOE spectrum of alamethicin in methanol-d_4 is shown in Figure I.8. A stacked plot in the diagonal representation is shown. In this representation, lines drawn parallel to the two frequency axes through a cross peak intersect the diagonal at positions corresponding to peaks that show the cross relaxation.

As is true for all 2D studies, the information content of a 2D-NOE spectrum depends upon the number of cross peaks. Unfortunately, the 2D-NOE spectrum of alamethicin in methanol shows only a few cross peaks. This is a result of the rotational time scale of the peptide being comparable to the reciprocal of the NMR frequency ($\omega\tau_c \sim 1$). This conclusion was supported by the fact that one-dimensional NOE difference spectra for this system did not yield significant enhancements either. The correlation time of tumbling for the peptide is estimated to be 4-6 x 10^{-10} sec in

Figure I.8 Stacked plot of two-dimensional nuclear Overhauser spectrum of alamethicin in methanol-d_4. There were only a few cross peaks (see text); prominent ones are labeled A,B and C.

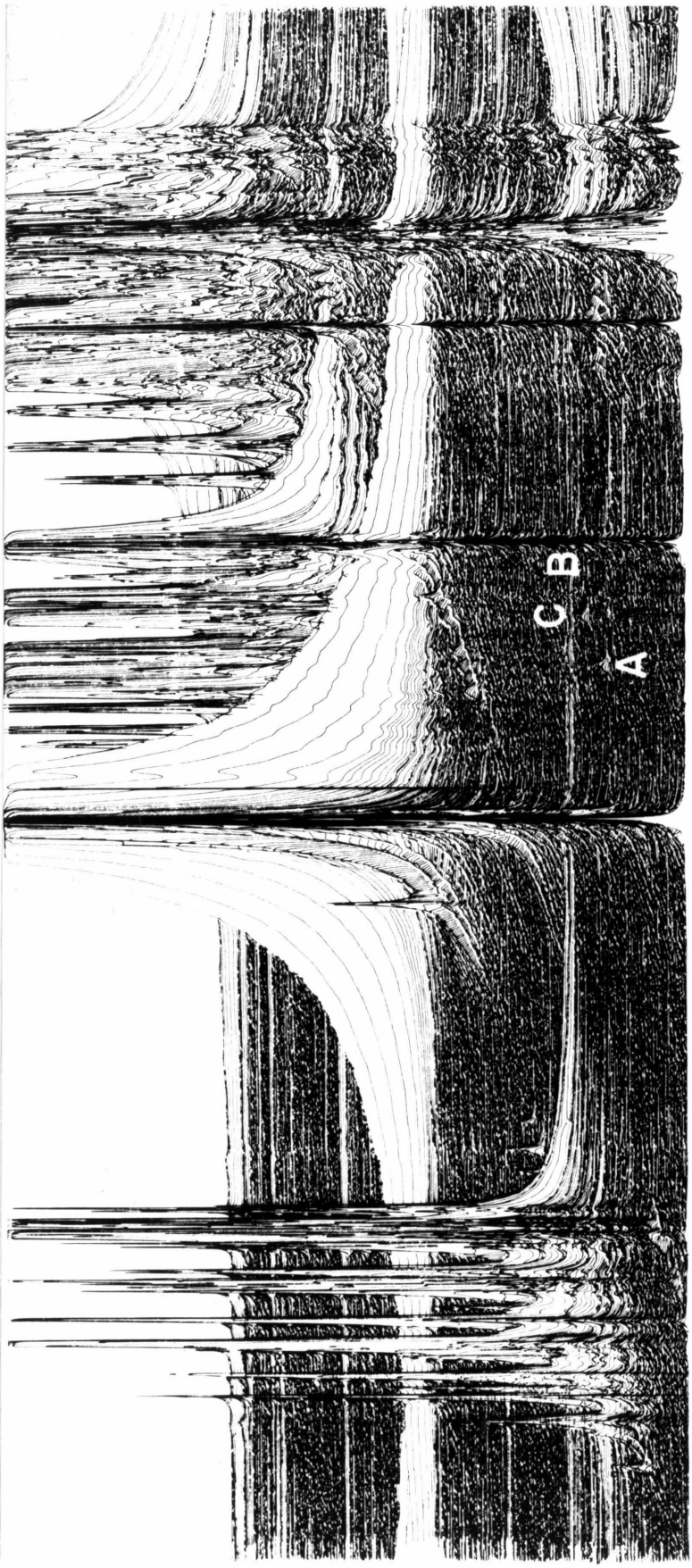
C
B
A


C
B
A

methanol. At 500 MHz, this gives $\omega\tau_c$ = 1.2-1.8. The fractional enhancement in the intensity of one spin I when a different spin S is irradiated depends upon the correlation time τ_c and the NMR frequency ω according to (Balaram et al., 1973):

$$f_I(S) = \frac{5 + \omega^2\tau_c^2 - 4\omega^4\tau_c^4}{10 + 23\omega^2\tau_c^2 + 4\omega^4\tau_c^4} \qquad \text{I.4}$$

For these conditions, we predict, $f_I(S)$ = -0.036. This small value for the enhancement factor would explain the lack of many cross peaks.

In the 2-D NOE stacked plot, three weak cross peaks are clearly discerned. These are labeled A, B and C in Figure I.8. A is a cross peak between Gln-19 αCH and Gln-19 NH, B is a very weak cross peak between the Phol-20 βCH_2 and the ortho ring proton of Phol-20 and C between Val-15 αCH and the ortho proton of Phol-20. Note that the protons responsible for the cross peak C are on amino acids that are five residues apart. Inasmuch as magnetization transfer is seen only for spins in very close spatial proximity, this result imposes restrictions on the conformation of the near the C-terminal end.

(b) Spectrum in Water

The biological activity of alamethicin is manifested in aqueous solutions, at the membrane interface and inside the membrane itself. Accordingly, it is important to study the conformation and properties of this peptide in an aqueous medium. Alamethicin is expected to be aggregated at the concentrations chosen for our experiments (McMullen and Stirrup, 1971). This is reflected in the NMR spectrum as broad lines.

Usual methods of assignments are not applicable for such broad resonances. To alleviate this problem, the proton NMR spectrum was followed carefully by solvent titration. A methanolic solution of alamethicin was titrated with water, and the positions of the peaks were traced through the titration.

All the resonances become broader with increasing amounts of water added to the methanolic solution. Part of this broadening is heterogeneous, resulting from overlapping resonance, but the bulk of the broadening arises from short T_2's. Figure I.9 shows the αCH, aromatics, β and γ methylenes and methyl regions of the alamethicin spectrum in D_2O. Following the above methid, it was possible to assign most of the peaks. However, there is too much overlap of the resonances in the region of β and γ methylene protons to allow meaningful individual assignments.

Figure I.10 shows the variation in the chemical shifts with the addition of water for αCH and methyl protons. The proton resonances are shifted in both directions upon the addition of water. For example, while the α-CH proton of Pro-2 is shifted upfield, the corresponding proton in Pro-14 moves downfield. In a number of cases, the peaks 'cross over', as in the case of the αCH protons of Leu-12 and Pro-14. On the other hand, a few protons like the αCH protons of the alanines seem to be solvent inert, presumably reflecting their lesser exposure to solvent molecules.

The coupling constants of various residues can be determined from the spectrum through part of the titration. No change is observed in the J values, suggesting a similar conformation of the molecule in methanol and in methanol-water mixtures.

Figure I.9 H1 NMR spectrum of alamethicin in D_2O at 500 MHz.

a. Aromatic protons from Phol-20.

b. αCH protons.

c. β,γCH_2 and methyl protons

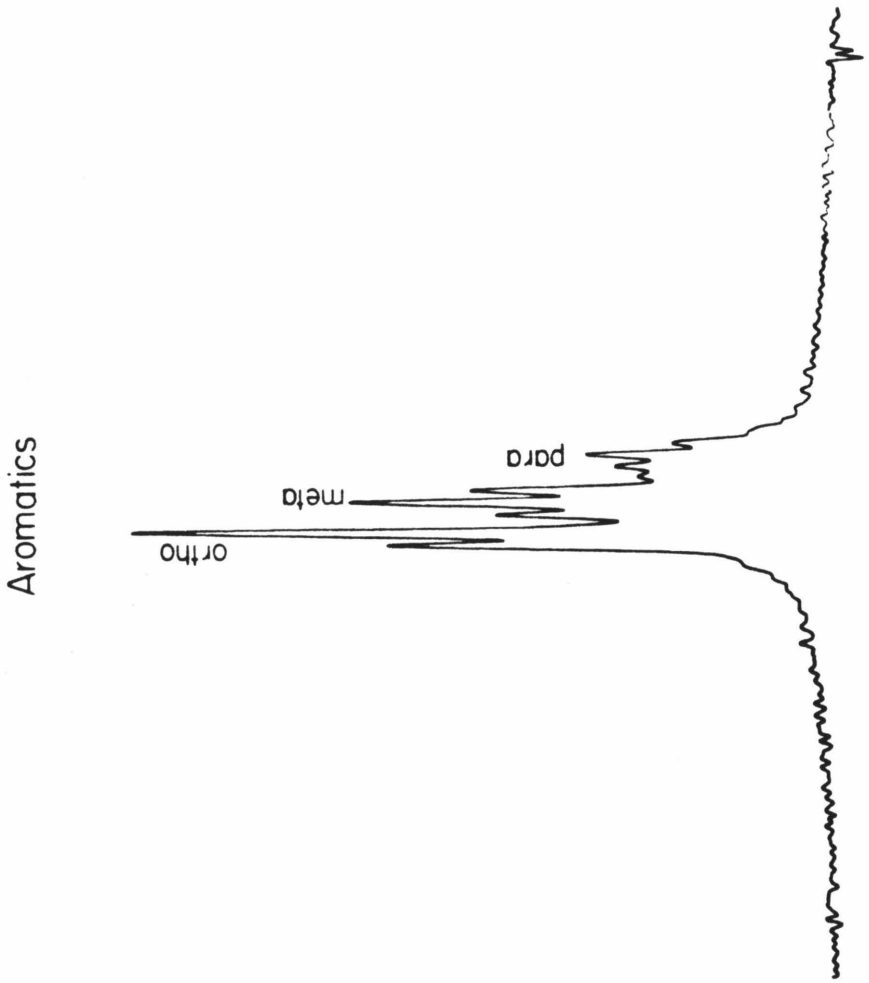

Figure I.9a.

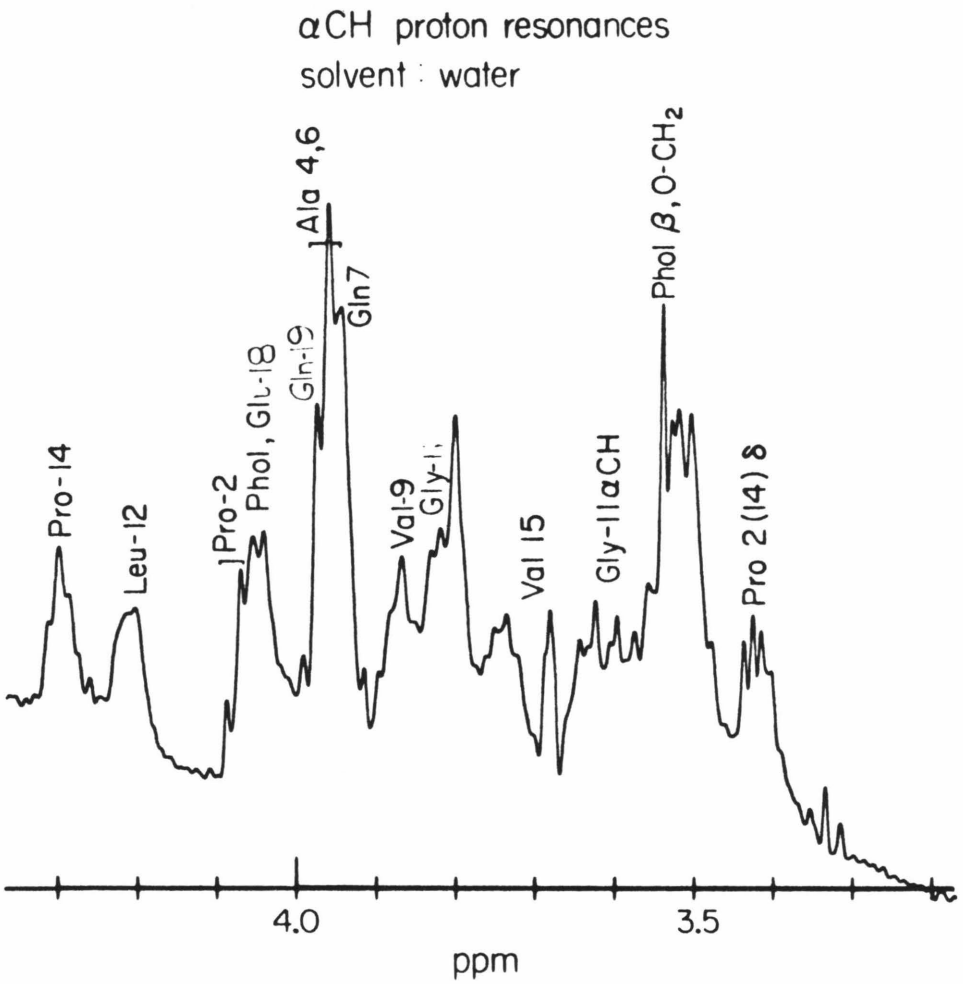
αCH proton resonances
solvent : water
Pro-14
Leu-12
Pro-2
Phol, Glu-18
Gln-19
Ala 4,6
Gln7
Val-9
Gly-1
Val 15
Gly-11αCH
Phol β, O-CH2
Pro 2(14) δ
4.0
3.5
ppm

Figure I.9b.

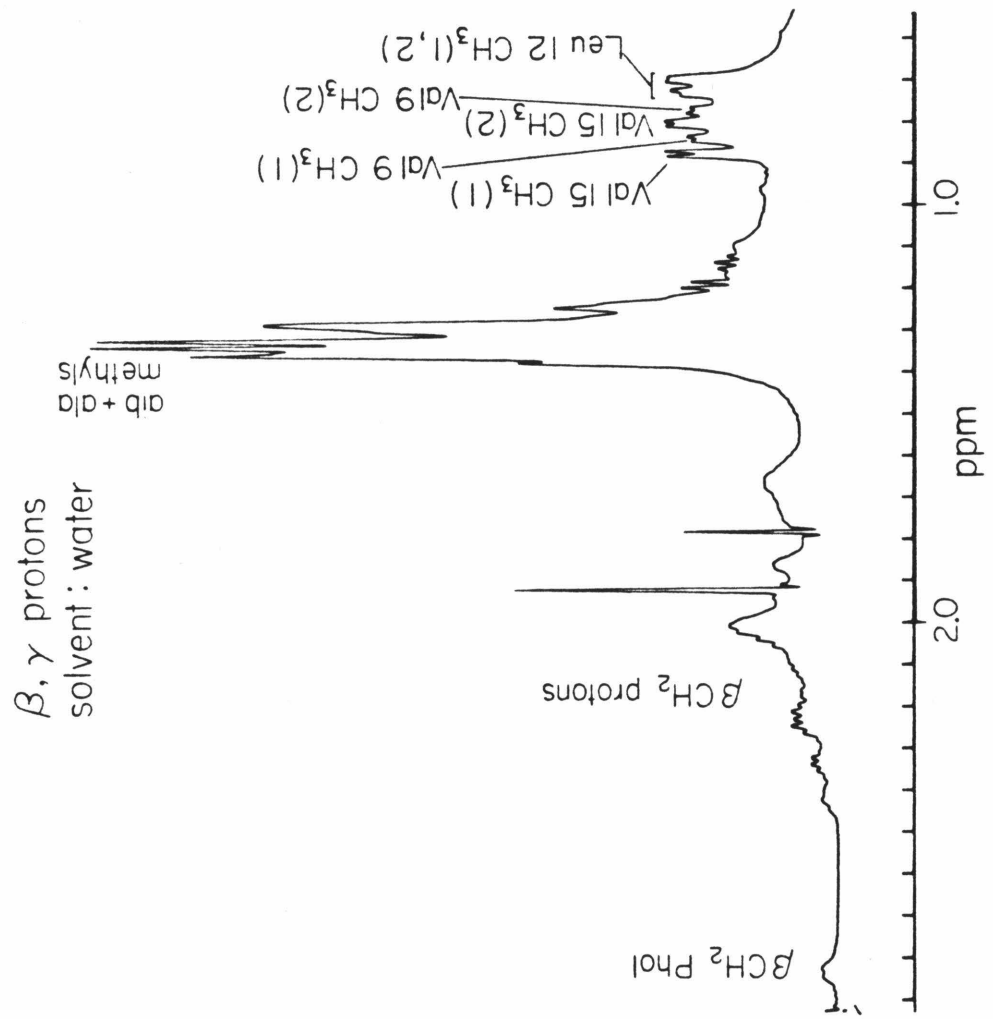
β, γ protons
solvent : water
ala + ala methyls
Val 15 CH3 (1)
Val 9 CH3 (1)
Val 15 CH3 (2)
Val 9 CH3 (2)
Leu 12 CH3 (1,2)
β CH2 protons
β CH2 Phol
2.0
1.0
ppm

Figure I.9c.

Figure I.10 Solvent titration curves for selected protons of alamethicin in methanol-water mixtures.

a. Chemical shifts of αCH protons.

b. Chemical shifts of methyl protons.

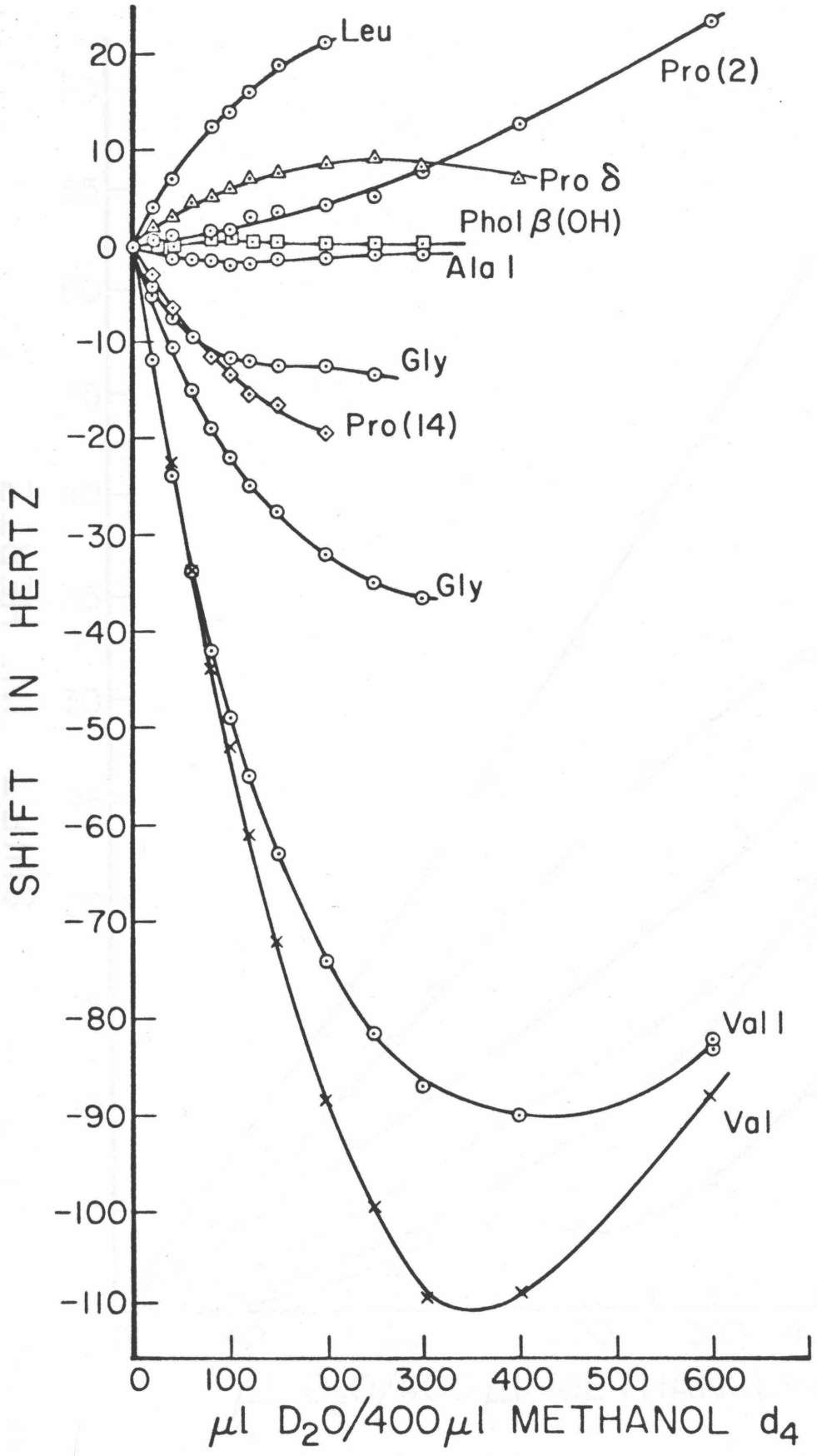
Leu
Pro(2)
Pro δ
Phol β(OH)
Ala I
Gly
Pro(14)
Gly
Val I
Val
SHIFT IN HERTZ
20
10
0
-10
-20
-30
-40
-50
-60
-70
-80
-90
-100
-110
0
100
00
300
400
500
600
μl D2O/400μl METHANOL d4

Figure I.10a.

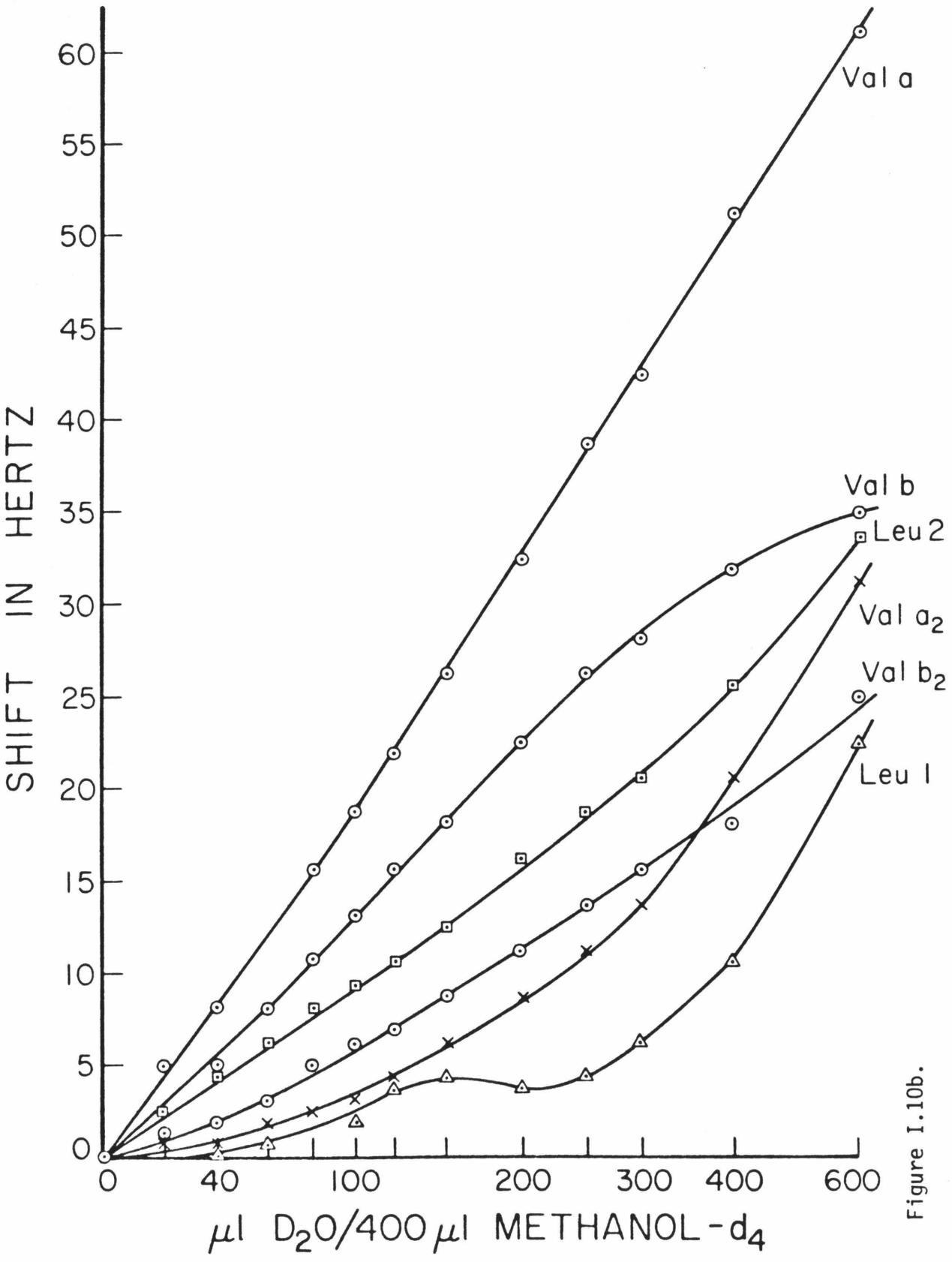
SHIFT IN HERTZ
0
5
10
15
20
25
30
35
40
45
50
55
60
0
40
100
200
300
400
600
μl D2O/400 μl METHANOL-d4
Val a
Val b
Leu 2
Val a2
Val b2
Leu 1

Figure I.10b.

Chapter I.4

Proposed Structure of Alamethicin in Solution

A. INTRODUCTION

Ever since the pioneering work on alamethicin by several investigators (Mueller and Rudin, 1968; Gordon and Haydon, 1976; Eisenberg et al., 1973; Boheim, 1974) the structure of alamethicin and the nature of the alamethicin ionic channel have received considerable attention. Initial efforts to deduce the molecular basis for the gated ionic conductance of alamethicin in black lipid film membranes were impeded by a lack of understanding of the structure of the icosapeptide. In fact, early attempts at structural studies were led astray by an incorrect primary structure of the molecule. The situation has been rectified by the subsequent NMR work (Martin and Williams, 1976) as well as synthetic efforts (Marshall et al., 1979; Gísin et al., 1981). Despite these efforts as well as those of others (Nagaraj and Balaram, 1981; Fringeli and Fringeli, 1979) the secondary structure of alamethicin in solution, not to mention in lipid bilayers, has remained elusive. With the advent of high field NMR spectroscopy and with the aid of the modern techniques of two-dimensional NMR (Nagayama, 1981; Aue et al., 1976), the determination of the solution structure of peptides and proteins has become more of a tractable problem (Wagner and Wüthrich, 1982; Wüthrich et al., 1982).

In the previous chapter the complete assignment of the alamethicin spectrum was presented. Spin-spin coupling constants measured therefrom is combined with two-dimensional NMR results to propose here a model for alamethicin structure in solution.

B. CONFORMATION IN METHANOL

Probably the most important results emerging from the NMR work described in Chapter I.3 are the amide coupling constants ($J_{NH-\alpha CH}$) since they provide a diagnostic for the secondary structure of the peptide. There exists a remarkable pattern to these coupling constants along the chain of the peptide. The N-terminal end of the molecule beginning with Ala-4 through Val-9 gives $J_{NH-\alpha CH}$'s around 5.3 Hz. This value suggests an alpha helix towards this end of the molecule. The C-terminal end, on the other hand, shows coupling constants ranging from 7.2 up to 8.2 Hz. These higher values are more consistent with a β-pleated sheet structure (Bystrov, 1976; Dickerson and Geis, 1969). Since no discernable temperature dependence is observed for these coupling constants, it is surmised that the secondary structure of alamethicin is quite rigid under the conditions of the present experiments, and the larger coupling constants observed for the C-terminal do not correspond to an average rotomer population, but rather reflect a rigid, extended structure for this region of the peptide.

It is now well established that alamethicin is a linear peptide (Martin and Williams, 1976). Accordingly, an extended β-sheet structure in a part of the molecule could only be stabilized by intermolecular hydrogen bonds. A dimer of alamethicin which is consistent with these NMR observations is shown in Figure I.9. Here, the amide protons of residues 15 through 20 are intermolecularly hydrogen bonded to residues on the opposing molecule to create a rigid, extended, β-pleated type structure for the C-terminal end of the molecule. The proline at position 14, of course, breaks the continuity of this structure and forces amino acids 10

through 14 into an open structure. In accordance with the coupling constant data, amino acids 3 through 9 are folded into an α helix. Interestingly, this structure brings the Gln-7 side chains from the two strands in the right juxtaposition to facilitate a hydrogen bond between them.

Photographs of a CPK model illustrating the proposed structure are shown in Figure I.11. Different views are depicted to illustrate different features of the structure. Examination of the structure reveals that it is highly amphiphilic, with one face (Figure I.11A) completely hydrophobic and the other face (Figure I.11B) lined with polar groups towards the C-terminal half of the molecule. The polar groups arise from two sources: (i) the polar side chains of amino acids 18 through 22 and (ii) the exposed backbone amide groups of residues 10 through 14. It is possible that this amphiphilic nature of the dimer structure plays a role in the formation of the alamethicin channel.

Two important structural features are apparent from the model. First, the α-CH proton of Val-15 and the ortho proton of the phenyl ring of Phol-20 are in very close proximity (Figure I.11C). This is in accordance with the appearance of a cross peak between Val-15 αCH and Phol-20 ortho proton in the 2D-NOE spectrum. Second, it is an asymmetric structure, the two halves of the dimer being partly inequivalent. This feature has been explored in detail in Chapter I.5 and a relaxation technique has been devised to confirm the aggregation state in methanol and in water.

In the proposed structure, seven out of the twenty amino acids are arranged into an α helix. Earlier CD data (McMullen et al., 1971) had indicated that 40% of the molecule is α helical. The model is also consistent with infrared attenuated total reflection spectroscopic investigations

Figure I.11 Photographs of CPK models depicting the proposed structure of alamethicin in methanol.

a. The hydrophobic face

b. The hydrophilic face showing the polar originating from the polar side chains and amide residues.

c. Side view of the dimer, showing the close proximity of ring ortho proton of Phol 20 and the αCH proton of Val 15.

d. The N-terminus of the molecule showing the intermolecularly hydrogen bonded Gln 7's and the two αhelices.

Figure. I.11a

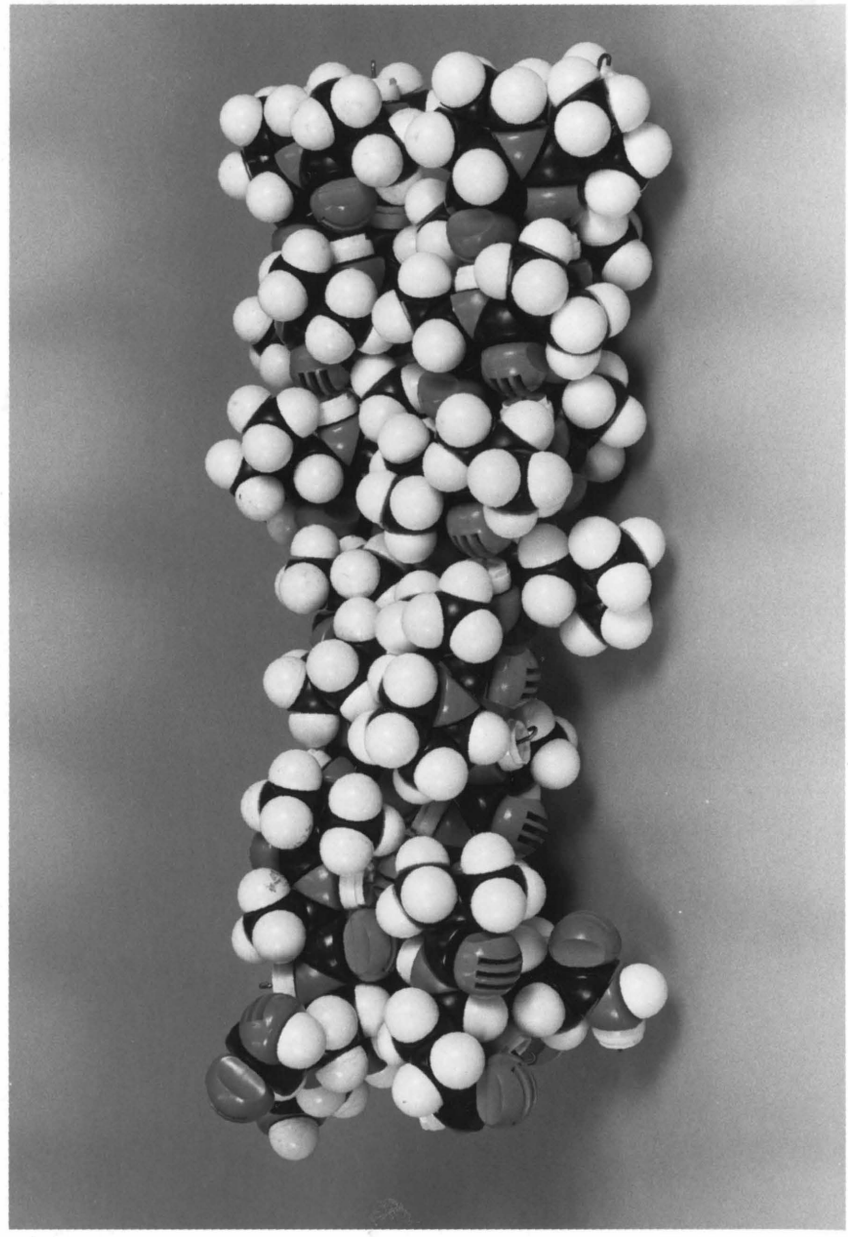

Figure I.11b

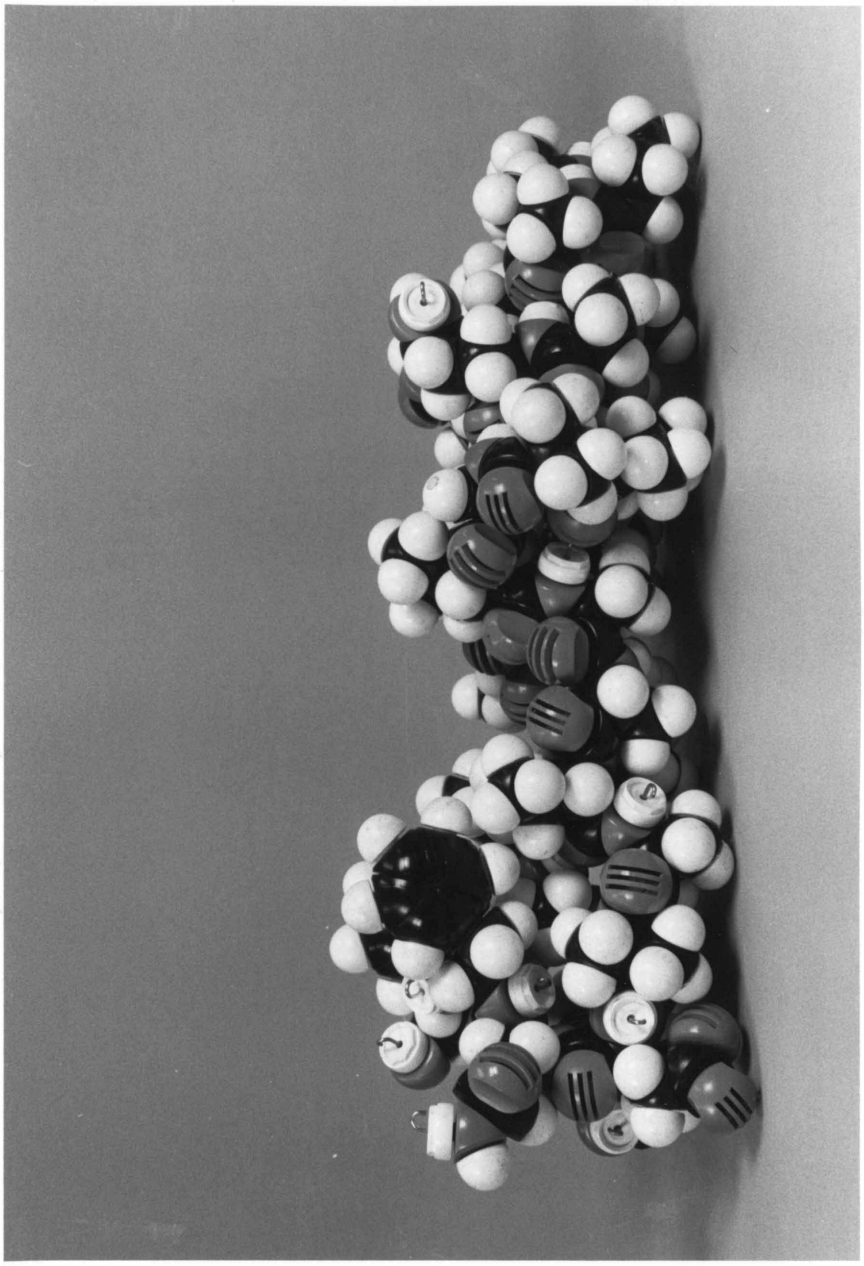

Figure I.11c

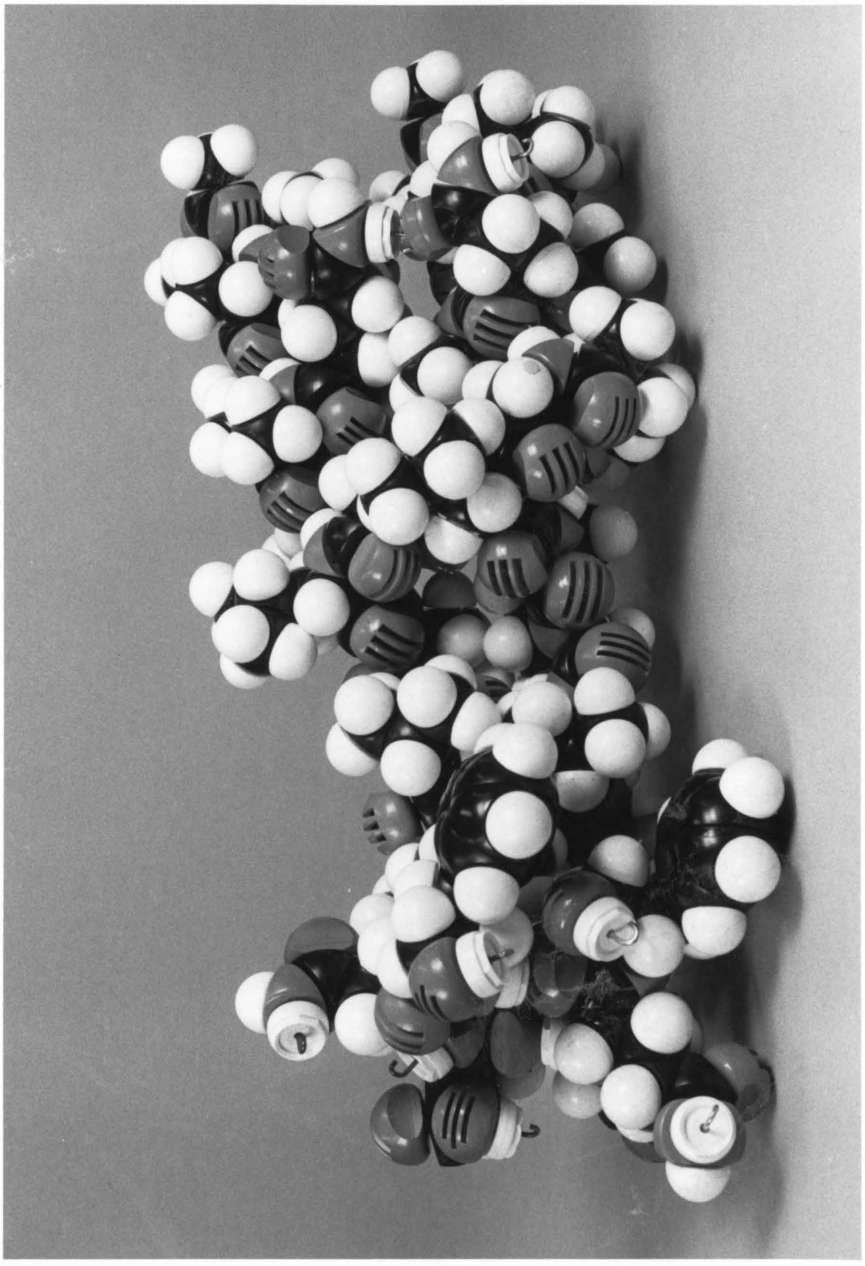

Figure I.11d

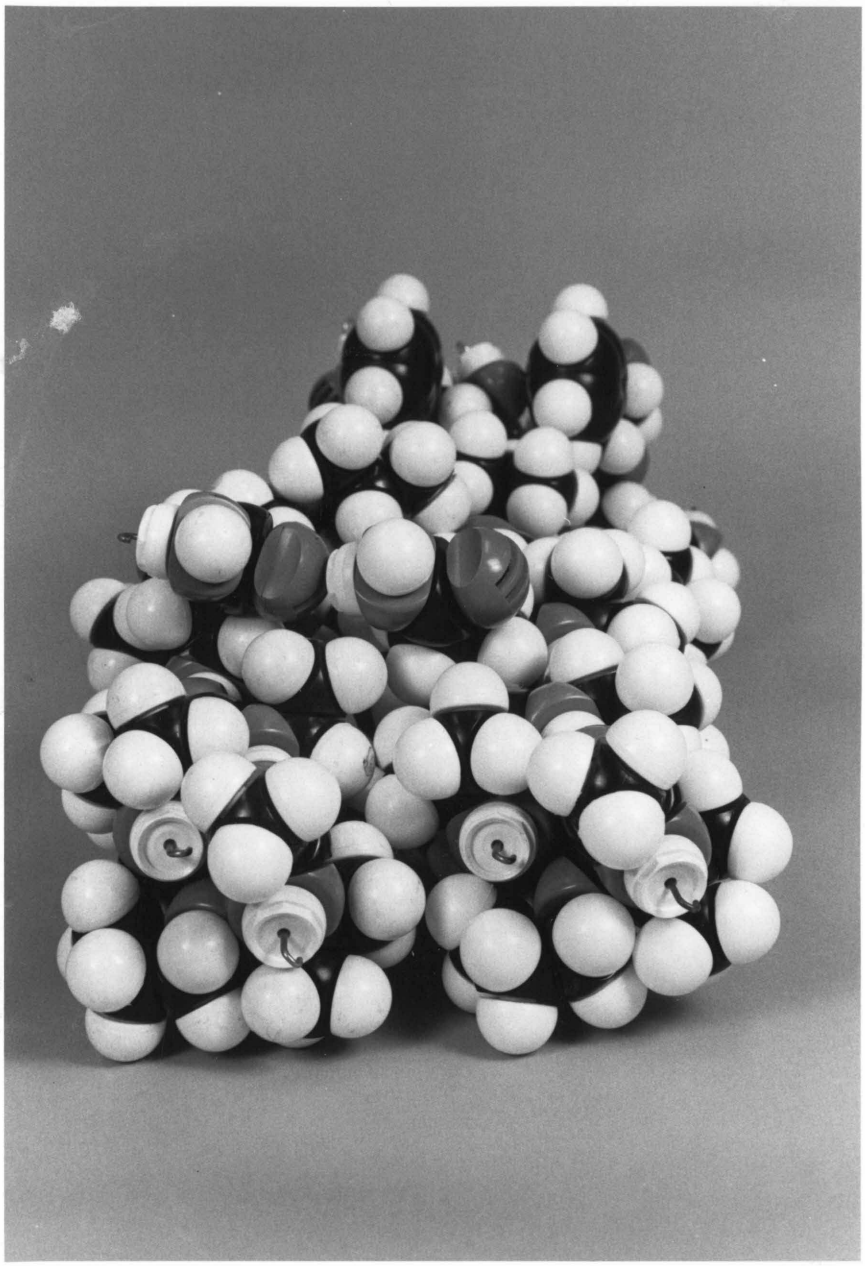

(Fringeli and Fringeli, 1979). These workers presented evidence that the molecule is entirely α helical in the dry state, but that upon addition of water, the molecule rearranges to form a β-pleated sheet structure. Although these results were obtained in the presence of lipids, we attribute them primarily to a solvent effect with the lipids providing a hydrophobic surface for the adsorption and further stabilization of the structure. The amide proton exchange rates recently reported by Davis and Gisin (1981) are also in accord with our proposed structure. These investigators reported that the proton exchange rates for Ala-4, Ala-6, Gln-7, and Val-9 are very slow, while those for Gly-11, Leu-12, and Val-15 are much faster. Since the amide protons are tied up in intramolecular hydrogen bonding in the α-helical N-terminus of the molecule, they are expected to exchange very slowly, while the amide protons in the exposed region between the two more structured ends should undergo exchange more rapidly.

C. CONFORMATION IN AQUEOUS SOLUTION

The dimeric structure proposed above is highly amphiphilic and one expects further aggregation of the peptide when alamethicin is transferred from methanol to an aqueous environment. This expectation is confirmed by the NMR spectrum of alamethicin in water. The spectrum is broad and ill-defined, and the homogeneous broadening of resonances seen in this solvent system clearly indicates a longer correlation time for tumbling of the molecular units, indicative of extensive aggregation even in the millimolar concentration range. This observation is in agreement with earlier sedimentation studies (McMullen and Stirrup, 1971).

Spectral assignments in water were made by solvent titration. Large chemical shifts were observed in going from methanol to water, particularly for the hydrophobic residues. These solvent shifts may well reflect the greater exposure of the hydrophobic groups in methanol compared to water as these groups are expected to be sequestered away from water through hydrophobic association to form larger aggregates. A detailed quantitative analysis of the shift data, however, is beyond the scope of this work and is not attempted here.

While the state of aggregation of alamethicin is significantly more extensive in water than in methanol, there is no evidence for a change in the secondary structure of the molecule in going from one solvent system to the other. All the coupling constants that were possible to be measured remain unchanged throughout the solvent titration. This result is not inconsistent with the mode of aggregation depicted above; namely, that the aggregates in water are formed by the hydrophobic association of the dimeric units observed in methanol.

Chapter I.5

Solution Structure of Alamethicin: Confirmation by NMR Relaxation Studies

A. INTRODUCTION

In Chapter I.4 a secondary structure for alamethicin in solution has been described based on NMR coupling constant measurements and 2-D NOE results. In this chapter relaxation results are discussed which contribute further evidence in favor of the proposed dimeric model. The experiments undertaken to achieve this derive from the motional dependences of the two NMR relaxation times (spin-lattice relaxation time T_1 and spin-spin relaxation time T_2). T_1 is the time constant for non-radiative exchange of energy with the lattice that restores Boltzman equilibrium in the spin system once the exciting rf pulse is turned off. The spin-spin relaxation time, T_2, on the other hand, results from an interaction between spins. This process governs the line width of NMR peaks. The width at half height $\nu_{\frac{1}{2}}$ for a Lorentzian line shape is given by

$$\nu_{\frac{1}{2}} = \frac{1}{\pi T_2} + \frac{\Delta H_o \gamma}{2\pi} \qquad (I.5)$$

where ΔH_o is the inhomogeneity in the magnetic field.

The T_1 and T_2 relaxation processes arise from fluctuations in locally generated magnetic fields due to the motions in molecules. T_1 processes are affected by fluctuations perpendicular to the direction of the field, while T_2 arises from fluctuations along any of the three directions. The range of motional fluctuation in a molecule is

contained in the spectral density functions $J(n\omega_o)$; n = 0,1,2 (Abragam, 1961). The relaxation times are related to these functions in a straightforward way. For dipolar interaction mediated relaxation in a many-spin system, for example,

$$\frac{1}{T_1} = \frac{3}{2}\gamma^4\hbar^2 I(I+1) \sum_{i,k}' \{(J_1)_{ik}(\omega_I) + (J_2)_{ik}(2\omega_I)\} \qquad (I.6)$$

$$\frac{1}{T_2} = \gamma^4\hbar^2 I(I+1) \sum_{i,k}' \{\frac{3}{8}(J_o)_{ik}(0) + \frac{15}{4}(J_1)_{ik}(\omega_I) + \frac{3}{8}(J_2)_{ik}(2\omega_I)\} \qquad (I.7)$$

Here the summation is over all pairs of spin. These expressions are of particular significance in macromolecular systems where a large range of motions is allowed. Since the expression for T_2 contains a spectral density at zero frequency while T_1 has spectral densities only at around Larmor frequency, we expect that slow motions would only affect T_2 and not T_1, while high-frequency processes would affect both T_1 and T_2.

In the proposed solution structure for alamethicin, the two helices at the N-terminal end of the proposed dimer are held rigidly together and are energetically stabilized by a side chain amide hydrogen bond between the two Gln-7's. Extensive hydrophobic interaction between the side groups in the helical region no doubt contributes to the stability of the structure as well. Since one helical strand must be necessarily twisted slightly with respect to the other in this structure, an interesting consequence is that the two acetyl methyl groups at the

N-termini of the dimer are inequivalent in terms of the angle subtended by them with respect to the long axis of the dimer. Since this is the principal rotor axis, it follows on the basis of the Woessner et al. (1969) treatment of the relaxation of symmetric top methyl groups attached to the side chain of an anisotropically tumbling ellipsoid, that the two sets of N-acetyl methyl protons should exhibit different spin-spin relaxation times (T_2's). The T_1's for the two sets of N-acetyl methyl protons, on the other hand, are expected to be identical. This contrast in the angular dependence of the two relaxation times originates from the slow motion dependence of T_2 but not of T_1 and has been discussed in detail later in the chapter. The C-termini of the dimer are also inequivalent, but since the individual units are related to one another by a two-fold screw axis, the side groups in this part of the molecule are symmetrically displaced with respect to the principal rotor axis of the aggregate. Protons from the two aromatic rings on the individual strands, for example, subtend the same angle to the rotor axis and should therefore exhibit equal spin-spin relaxation times.

The relaxation time measurements discussed in this chapter are consistent with the above expectations. T_1 and T_2 measurements for selected protons in alamethicin have been undertaken in methanol, in water, and in the presence of urea under conditions that would break up intermolecularly hydrogen-bonded oligomers. On the basis of these relaxation measurements, estimates of the correlation times and orientations of the acetyl groups in the molecule have been obtained.

B. MATERIALS AND METHODS

Alamethicin used in this study is a generous gift of Dr. G. B. Whitfield, Jr., of the Upjohn Company. The experiments were repeated and confirmed with the highly purified "fraction 4" kindly supplied by Professors G. R. Marshall and T. M. Balasubramanian, and with alamethicin purchased from PHLS England. D_2O was purchased from Aldrich Chemical Company, Inc. and CD_3OD from Merck, Inc. Perdeuterated urea was prepared by repeated evaporation of a solution in D_2O.

All solutions of alamethicin were made in NMR tubes to prevent loss in handling. Typically, the concentration of the peptide used was in the millimolar range. The measured pD value of an alamethicin solution was typically 6.84 in CD_3OD and 6.52 in D_2O. In view of the closeness of these values to neutrality, no pD adjustments were made. Prior to T_2 measurements, oxygen was eliminated from the solution by bubbling dry gaseous nitrogen into the sample. Samples for T_2 measurements in the presence of urea were made by dissolving alamethicin in saturated solutions of perdeuterated urea in CD_3OD or D_2O.

500 MHz NMR spectra were recorded on a Bruker WM 500 spectrometer operating at a field strength of 11.74 Tesla, and 200 MHz NMR spectra were acquired on a Varian XL-200 spectrometer operating at a field strength of 4.69 Tesla. All spectra were recorded at 298 K. NMR spectra were acquired in the Fourier transform (FT) mode using quadrature-phase detection and a cycling time between pulses of 5 seconds. 32 K and 8 K data points and spectral widths of 6000 Hz

and 2500 Hz were used to acquire the 500 MHz and 200 MHz spectra, respectively.

The Carr-Purcell-Meiboom-Gill repetitive two-pulse sequence (Farrar & Becker, 1971) $90_x,[-\tau-180_y,-\tau]_n$ was used for the measurement of spin-spin relaxation time (T_2). The value of τ used was 0.5 msec and 2 msec for the experiments at 500 MHz and 200 MHz, respectively. The advantages of the CPMG method over the simple Hahn echo technique are: (a) the short value of τ minimizes the effects of molecular diffusion on the measurement of T_2; and (b) the phase shift in the 180^o pulse with respect to the 90^o pulse eliminates errors introduced by inaccuracies in the measurement of length of the 180^o pulse. Using this technique, echo signals were generated at increasing time intervals. When a NMR peak is describable by a single spin-spin relaxation time (T_2), the intensity derived from Fourier-transformation of the echo signal is expected to decay exponentially with a time constant T_2 (Farrar & Becker, 1971), i.e.,

$$I(t) = A \exp(-t/T_2) \qquad (I.8)$$

where $I(t)$ is the intensity of the resonance derived from Fourier-transformation of the n^{th} echo signal and $t = 2n\tau$ for the n^{th} echo. For a composite peak described by two component T_2's, the time decay of total intensity is nonexponential and may be described by

$$I(t) = C_A \exp(-t/T_{2A}) + C_B \exp(-t/T_{2B}) \qquad (I.9)$$

The Fourier-transformed spectra were scaled in the "absolute intensity mode." No spectral resolution enhancements or line broadenings were used. Sample tubes were not spun during spectral

acquisition to prevent artifactual modulation of T_2's introduced by sample spinning. Accurate measurement of intensity was accomplished by cutting out peaks and weighing them on a Mettler balance.

Spin lattice relaxation times (T_1) were determined by the inversion recovery method using the standard 180-τ-90 pulse sequence. Data manipulation was accomplished by the automatic T_1 determination routine available in the Bruker software.

C. RESULTS

The proton NMR spectra of alamethicin in methanol and in water have been assigned (Banerjee et al., 1983). This chapter emphasizes the N-acetyl methyl protons at 2.05 ppm and the aromatic ring protons of phenylalaninol centered around 7.2 ppm. As expected, the measured ratio of the intensity of these two peaks is 5/3.

Since the N-acetyl methyl protons on the two strands of the proposed dimer are not symmetrically positioned with respect to the principal tumbling axis, they were expected to show differences in spin-spin relaxation times. On the other hand, the more symmetrically disposed aromatic groups at the extended C-terminal end of the molecules should relax with essentially the same time constant. Figure I.12 shows a plot of the time dependence of the logarithm of the intensity

of the acetyl and aromatic protons of alamethicin in methanol as derived from the Fourier transforms of the various echo signals in the CPMG experiment. These measurements were made at 500 MHz. It is clear from the plot that while the contribution to the echo signal from the aromatic protons followed an exponential time course, that from the acetyl resonance was nonexponential, describable only by a minimum of two component T_2's. The number of protons contributing to the slower decay may be ascertained by linear extrapolation of this component to zero time. If the intensity of the signal from the aromatic residues is normalized to five protons, one finds that the long time constant component of the acetyl group resonance corresponds to 1.5 protons only. Thus, it seems that half of the N-acetyl protons have a significantly longer spin-spin relaxation time than the other half. The acetyl resonance relaxation data were readily fitted to a sum of the two exponentials. A three-parameter constrained fit and a four-parameter unconstrained fit yielded similar results. The relative weights of the two exponentials needed to fit the N-acetyl relaxation data are equal, and the average values (from several measurements) of the time constants are 457 and 168 msec. In contrast, the aromatic proton relaxation data were readily fitted to a single exponential with a time constant of 570 msec.

Figure I.12a Semilog plots of the intensity of the N-acetyl methyl protons (●) and the phenylalaninol aromatic protons (▲) of alamethicin as measured from Fourier transformed spectra of echo signals obtained for various total time intervals between pulses in a Carr-Purcell-Meiboom- Gill T_2 experiment. Solvent, methanol. Temperature, 298K. The broken curve for the N-acetyl methyl protons is calculated using the best fit parameters obtained from Figure I.12c.

Figure I.12b The effect of a saturated solution of urea in methanol on the decay of transverse magnetization of the N-acetyl methyl protons in a Carr-purcell-Meiboom-Gill (CPMG) experiment. The decay of transverse magnetization was determined by measuring the intensity of the N-acetyl resonance in Fourier transformed spectra of the echo signal at various total time intervals between the excitation pulses.

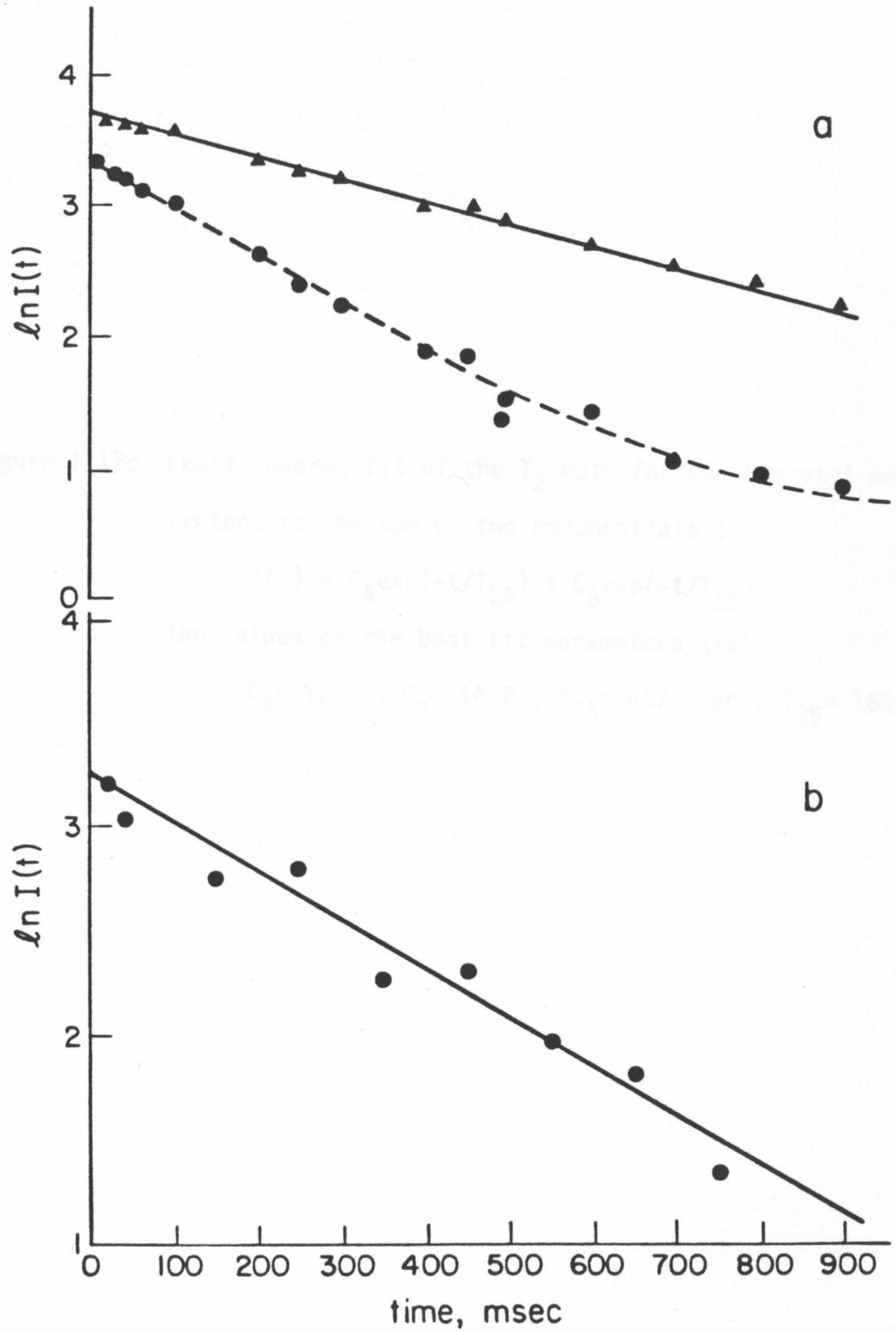
a
b
ℓn I(t)
ℓn I(t)
4
3
2
1
0
4
3
2
1
0
100
200
300
400
500
600
700
800
900
time, msec

Figure I.12c Least squares fit of the T_2 data for the N-acetyl methyl protons to the sum of two exponentials :

$$I(t) = C_A \exp(-t/T_{2A}) + C_B \exp(-t/T_{2B})$$

The values of the best fit parameters are :

$C_A = 12.9$, $C_B = 14.2$; $T_{2A} = 457$ msec , $T_{2B} = 168$ msec.

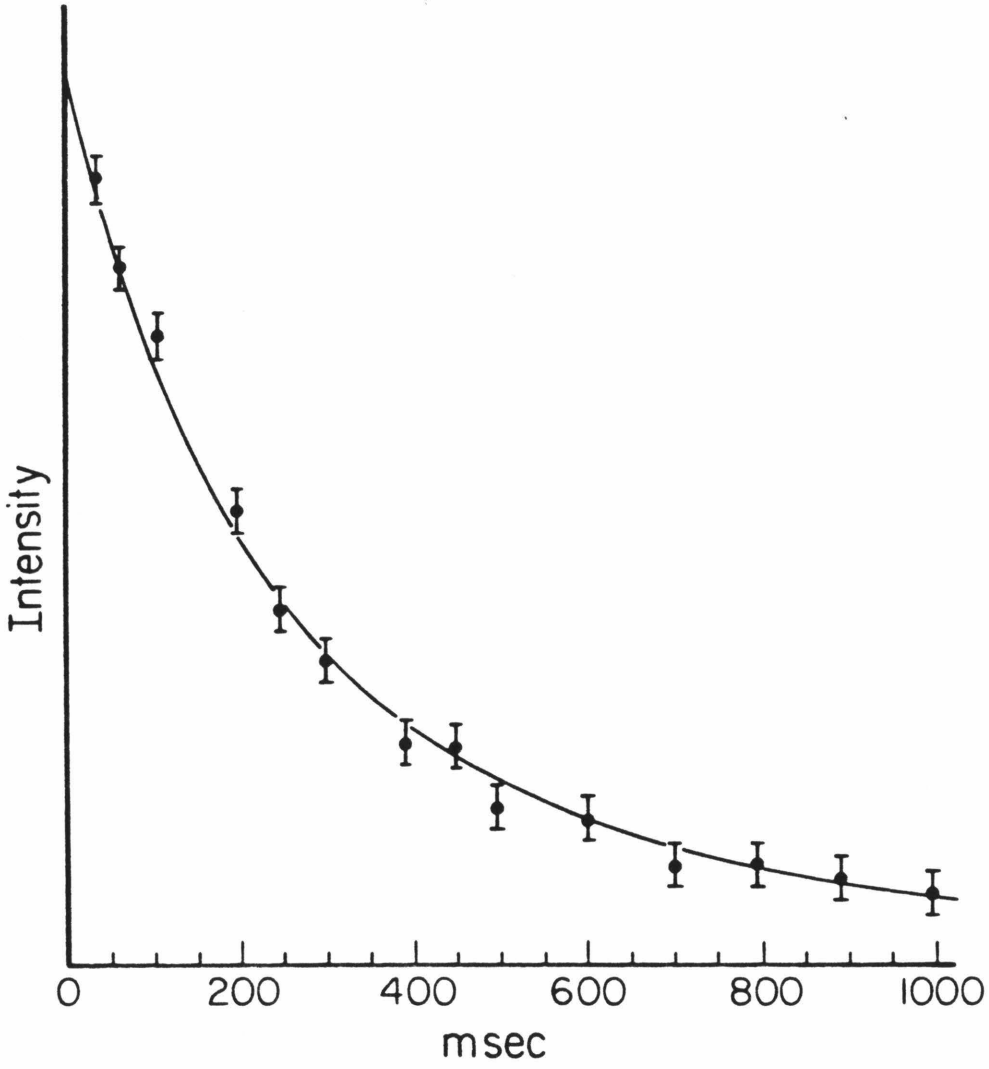
Intensity
0
200
400
600
800
1000
msec

Similar measurements of the spin-spin relaxation times were also made at 200 MHz with methanol as a solvent and at 500 and 200 MHz in water. The aromatic protons showed a normal single exponential relaxation behavior in all cases while the acetyl resonance showed two-component T_2's in both solvents and at both fields. The two T_2's in methanol at 200 MHz are 465 msec and 153 msec. In water, however, additional aggregation reduces the T_2's further, and the corresponding values at 500 MHz are 213 msec and 96 msec. Whereas in methanol the two-relaxation components contributed equally to the intensity of the echo signal, in water the situation was more complicated. Within the error limits in the measurement of intensity of broad and overlapping lines, the best least-squares fit to the relaxation data was obtained when the relative contribution of the slower relaxation component (longer T_2) is 1.56 times that of the faster one.

The above results may be taken as direct evidence in support of the dimer model for alamethicin in methanolic solutions proposed in Chapter I.3. It was verified that the component T_2's arise from the acetyl residues on the two strands of a tightly bound asymmetric dimer by undertaking similar spin-spin relaxation measurements in a saturated solution of urea at 308 K. The results of this experiment are plotted in Figure I.12b. In the saturated urea solution, it was found that the contribution to echo signal from the N-acetyl methyl resonance followed a simple single

exponential time course. The slope of this plot indicated a T_2 of 295 msec. A similar experiment in water gave identical results although the fit to the data are not as good, probably on account of incomplete disruption of the secondary structure in this solvent system.

In contrast to the T_2's, the spin lattice relaxation behavior for the N-acetyl methyl group followed a single exponential time course. At 500 MHz, the T_1 for the N-acetyl methyl group in methanol was determined to be 1.42 ± .1 sec.

D. DISCUSSION

A relaxation study of the methyl protons of the N-terminal acetyl group of alamethicin is described in this chapter. NMR data revealed nonexponential decay for the transverse magnetization due to these protons. In methanol, the decay can be decomposed into two exponential components of equal weight, and from the amplitude of these components relative to that of the phenyl ring protons, it is surmised that the smallest aggregate unit of the molecule that is consistent with these observations is the dimer in this solvent system. This result reinforces the structural conclusions derived from analysis of the amide coupling constants and the 2D NOE data,

including the invariance of the amide coupling constants with the enhanced aggregation noted in water. Another important corollary of the nonexponential T_2 decay observed for the N-acetyl methyls, for this picture to be totally self-consistent, is that the dimer must dissociate only slowly on the timescale of these experiments. This slow dissociation is expected for a structure like the one proposed here since there are seven hydrogen bonds, in addition to hydrophobic interactions, holding the two subunits together.

As it was clear from the inspection of a CPK model of the dimer structure proposed, the methyl groups that are attached to the side chains on the N-termini of the two molecules are distinct from one another in terms of the angle subtended with respect to the long axis of the aggregate. The two N-acetyl groups may be visualized as a pair of rapidly rotating symmetric tops attached by short and rigid stems to a bulky and slowly tumbling prolate ellipsoid. The relaxation behavior of such symmetric top methyl groups attached to an asymmetrically tumbling ellipsoid has been well studied (Woessner, 1969). Here the primary mechanism for relaxation is the magnetic dipole-dipole interaction among the proton spins of the rotor, and the spin lattice and spin-spin relaxation times are given by (Woessner, 1962)

$$\frac{1}{T_1} = \frac{9}{8}\gamma^4\hbar^2 R_0^{-6}\{J_1(\omega_0) + J_2(2\omega_0)\} \tag{I.10}$$

$$\frac{1}{T_2} = \frac{9}{32}\gamma^4\hbar^2 R_0^{-6}\{J_0(0) + 10J_1(\omega_0) + J_2(2\omega_0)\} \tag{I.11}$$

where γ is the gyromagnetic ratio of the proton spins; R_0, the inter-proton distance; and $J_n(n\omega_0)$ denote the spectral densities at frequencies $n\omega_0$ $(n = 0,1,2)$.

Figure I.13 represents the alamethicin molecule as a prolate ellipsoid and indicate the principal motions that may contribute to the relaxation of the methyl protons. r_i denotes the rates of reorientations about the specified axes. α is the angle subtended by the axis of a methyl rotor relative to the long axis of the molecule. Following Woessner et al. (1969), the relevant correlation times are

$$\begin{aligned}
\frac{1}{\tau_A} &= 6r_2 \\
\frac{1}{\tau_B} &= r_1 + 5r_2 \\
\frac{1}{\tau_C} &= 4r_1 + 2r_2 \\
\frac{1}{\tau_{i2}} &= \frac{1}{\tau_i} + r_{rot}
\end{aligned} \tag{I.12}$$

where i = A, B, C.

Figure I.13 The principal axes of rotation of a methyl group rigidly attached to an ellipsoid. r_1, r_2, r_{rot} represent the rates of rotation about the axes indicated.

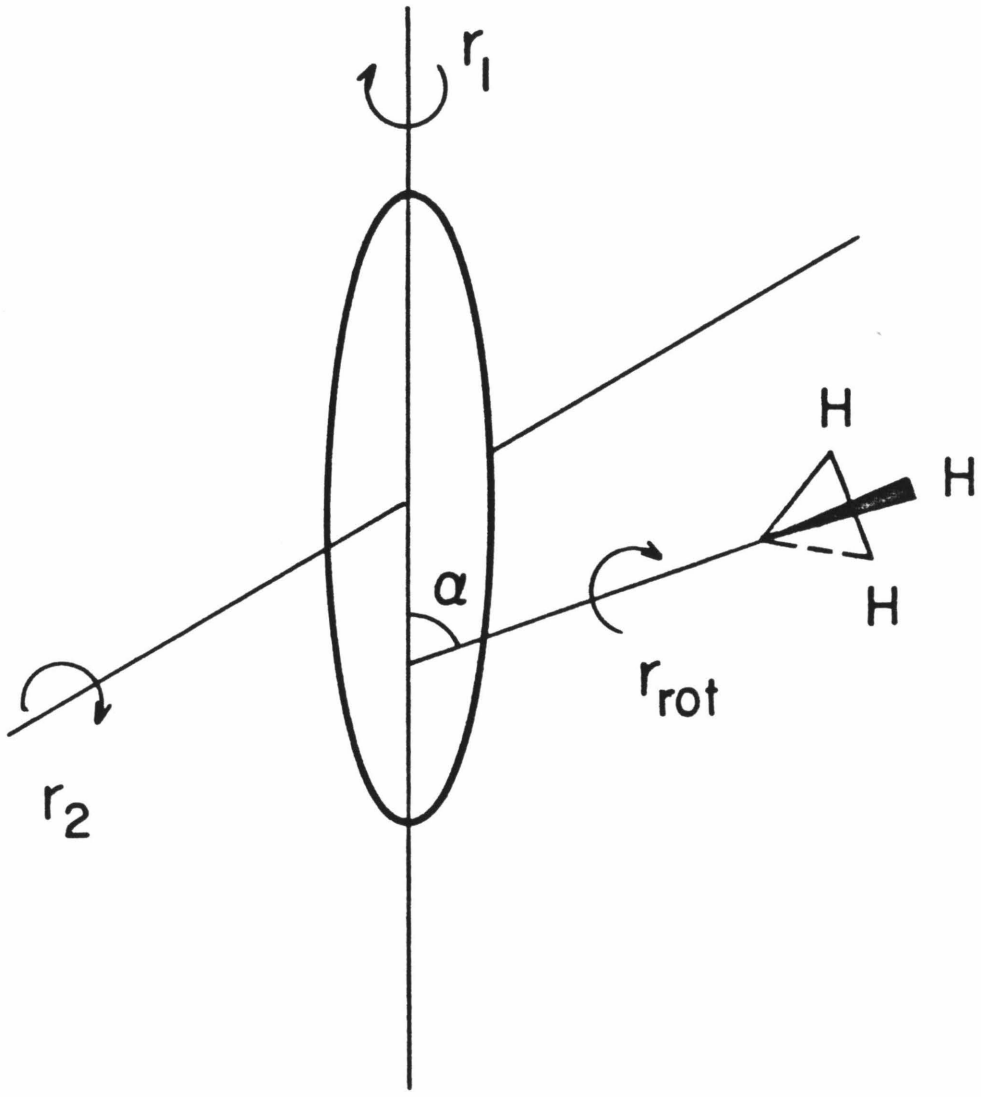
r_1
H
H
H
α
r_{rot}
r_2

A considerable simplification of the Woessner results obtains for the present problem since (i) the relaxation vectors connecting the protons of the methyl group are perpendicular to the rotor axis; and (ii) for a macromolecule of the size of alamethicin, the reorientation rates r_1 and r_2 for the whole molecule are much slower than the rate of fast reorientation of the methyl group, r_{rot}. Under these conditions, the spectral densities are given by

$$J_0(0) = \frac{1}{10}\left[\frac{(3\cos^2\alpha - 1)^2}{6r_2} + \frac{3\sin^2 2\alpha}{r_1 + 5r_2} + \frac{3\sin^4\alpha}{2(2r_1 + r_2)}\right] \qquad (I.13)$$

$$J_n(n\omega_o) = \frac{1}{60}\left[\frac{(3\cos^2\alpha - 1)^2}{6}\frac{(1/r_2)}{1 + (n\omega_0/6r_2)^2} + 3\sin^2 2\alpha\,\frac{1/(r_1 + 5r_2)}{1 + n^2\omega_0^2/(r_1 + 5r_2)^2}\right.$$

$$\left. + 3\sin^4\alpha\,\frac{1/(4r_1 + 2r_2)}{1 + n^2\omega_0^2/(4r_1 + 2r_2)^2} + 12\,\frac{1/r_{rot}}{1 + (n\omega_0/r_{rot})^2}\right]; \; n = 1,2. \qquad (I.14)$$

Given the rotational diffusion times anticipated for the macromolecule, i.e., $r_{rot} >> r_1, r_2$, one expects $J_0(0) >> J_1(\omega_0)$ and $J_2(2\omega_0)$. This is verified experimentally by the observations that (i) $T_1 >> T_2$ and (ii) T_2's at 200 MHz and 500 MHz for the acetyl resonance are identical within errors of measurement. Also for a long prolate ellipsoid, r_2 is much slower than r_1. Making this assumption and

substituting values for the internuclear distance between protons and the gyromagnetic ratio, one obtains the following expressions for T_1 and T_2:

$$\frac{1}{T_1} = \frac{1.5 \times 10^{10}}{r_{rot}} \left[\frac{1}{1 + (\omega_0/r_{rot})^2} + \frac{1}{1 + (2\omega_0/r_{rot})^2} \right] \qquad (I.15)$$

$$\frac{1}{T_2} = 7.9 \times 10^7 \frac{(3\cos^2\alpha - 1)^2}{r_2} \qquad (I.16)$$

Let us now consider T_1 and T_2 in turn.

T_1: The above T_1 expression in conjunction with the T_1 data for the N-acetyls yield a reorientation rate r_{rot} of 2.0×10^{10} sec^{-1}. This reorientation rate places the motion in the extreme narrowing limit, and a frequency dependence of T_1 is not expected as long as $(\omega_0/r_1)^2$, $(\omega_0/r_2)^2 >> 1$. This is in accordance with the experimental observations. Finally, since the spin lattice relaxation rates are dominated by the rapid rotation of the methyl groups, the spectral densities $J_1(\omega_0)$ and $J_2(2\omega_0)$ are independent of α. We have observed rather similar T_1's for all the N-acetyl groups.

T_2: The above expression for $1/T_2$ predicts that T_2 would depend on α, the angle subtended by the rotor axis of the N-acetyl group vis a vis the long axis of the prolate ellipsoid. This angle

is not known a priori for either N-acetyl group of the alamethicin dimer. However, a relation between them may be deduced from the T_2 data since

$$\frac{T_{2A}}{T_{2B}} = \frac{(3\cos^2\alpha_A - 1)^2}{(3\cos^2\alpha_B - 1)^2} = \frac{457}{168} = 2.7$$

The angles α_A and α_B can be estimated from a CPK model of alamethicin; they are approximately 70^o and 80^o. This would predict a T_2 ratio of ~ 2, in reasonable correspondence with the measured value of 2.7. Substitution of these angles in the T_2 expression gives $r_2 \sim 1.3 \times 10^7$ sec^{-1} and $\tau_A = 1/6r_2 \sim 1.2 \times 10^{-8}$ sec. This correlation time for the reorientation of the molecule about the short axis is in excellent agreement with the value of 1×10^{-8} sec predicted for a 45 Å long ellipsoid in methanol from hydrodynamic theory using Perrin's equation for long ellipsoids to calculate the frictional coefficients (Perrin, 1934).

Independent confirmation of the above interpretation of the NMR relaxation results has come from the urea experiments. In the presence of urea, the decay of the x-y plane magnetization becomes exponential, indicating that the nonexponential decay in methanol is a consequence of the secondary structure of the molecule in this solvent system. In contrast to the urea results, the relaxation data in water indicates greater complexity. This is not surprising since a further aggregation of the dimer units is expected by the sequestering of the hydrophobic

units away from water. A detailed analysis of the T_2 in water in terms of motional parameters would involve more correlation times than have been considered for the case of methanol and would not be warranted by the limited data.

Finally, it should be emphasized that the conclusions on relaxation measurements have been based on samples from three different sources including the highly purified "fraction 4" obtained from Marshall and Balasubramanian (Marshall & Balasubramanian, 1979; Vodyanoy et al., 1982). All of these alamethicin samples showed nonexponential T_2's in methanol for the terminal acetyl methyl group, thus excluding the possibility of contribution from an impurity.

E. CONCLUSION

The NMR relaxation measurements reported in the present study lend further support to the dimeric structure of alamethicin proposed in the previous chapter. In the latter work coupling constant measurements indicated that the N-terminus of the molecule (amino acids 1 through 9) is α helical and that the C-terminus (amino acids 15 through 20) is in an extended β-pleated sheet conformation. The "bend region" (amino acids 10 through 14) has peptide groups forced into a nonhydrogen bonded extended structure. The conclusions regarding the N-terminus are consistent with the crystal structure of

alamethicin recently reported (Fox & Richards, 1982) as well as recent C13 NMR studies by Jung and coworkers (Oekonomopulos et al., 1982) on analogs of alamethicin. However, there seems to be some ambiguity about the secondary structure of the C-terminus. The x-ray crystal structure indicated α-helix for the C-terminus as well, with the expected break of continuity at Pro-14. The NMR coupling constants measured by us for this end of the molecule (J_{NH-CH} = 7.6-9.1 Hz) are not consistent with an α-helix. These data suggest instead that the C-terminus exists in a more extended structure. Jung and coworkers (Oekonomopulos et al., 1982) have proposed that the C-terminus in alamethicin analogs might be in a more disordered secondary structure, and the present results are largely in agreement with this suggestion. However, evidence presented here confirms that alamethicin exists as a dimer in methanolic solution and that the β-pleated sheet toward the C-terminus is most probably stabilized by intermolecular hydrogen bonding between the two opposing molecules.

The disparity between the solution results and the crystal structure may not be so surprising and emphasizes the importance of solvent in determining the secondary structure of peptides. Earlier reflection spectroscopy studies (Fringeli & Fringeli, 1979) have indicated that alamethicin is all helical in the dry state, but the molecule undergoes a helix to β-sheet transition in the presence of hydrated

lipids, an observation which can be accounted for simply by the solvation of the peptide. This structure is consistent with CD measurements in ethanol, which indicated that only 40% of the molecule is α-helical (McMullen et al., 1971).

The structure proposed by the NMR studies is highly amphiphilic; it has one face that is completely hydrophobic, while the other is partly lined with polar groups. The additional aggregation observed in water is consistent with these features of the structure. Such an amphiphilic unit may play an important role in the pore formation and antibiotic characteristics of alamethicin.

Chapter II.1
NMR of Biological Membranes

A. INTRODUCTION

The solution structure of alamethicin as discussed in Part I is an amphiphilic aggregate suitable for pore formation in membranes. In order to investigate the nature of interaction of alamethicin with membranes, it was considered necessary first to choose a suitable method for characterizing lipid bilayers. The first half of this part therefore discusses lipid organizations in planar lipid multilayers and NMR methods that can be used to describe motional order and configuration of the head group and chains. The experimental results described in Chapter II.2 are supplemented by a density matrix calculation of the P31 NMR spectrum of phosphate head group in DML to achieve a clearer understanding of the parameters that lead to changes in its line shape. The characterization of the bilayers is followed in Chapter II.3 by a study of the interaction of alamethicin with multilayers. A comprehensive study with granucidin S and chlorophyll a is utilized to confirm the position of alamestricin relative to the bilayer and its nature of interaction with membranes in the absence of an applied potential.

B. NMR AS A PROBE FOR DYNAMICS OF LIPIDS IN MULTILAYERS

Phospholipid multilayers are large membrane units; the dimensions are on the order of microns and overall tumbling motions are slow enough to be considered static at least on the NMR time scale. The local motions of the lipids are anisotropic and usually axial. The unoriented multilayer has lipid molecules arranged in all possible directions (Israelachvili et al.,

1980). In the solid state, these differently oriented lipids could give rise to individual NMR peaks that superimpose to result in a "powder pattern" (Bocian and Chan, 1978). In a bilayer membrane, the rapid internal motion and rotational diffusion of lipids cause a partial averaging of this "powder pattern", but the residual spectrum is still quite broad. The broadening is caused by quadrupolar coupling for the case of deuterium NMR spectra and by chemical shift anisotropy for proton decoupled phosphorus spectra.

P31 NMR

The P31 NMR spectrum at 11.7 tesla (202.49 MHz for phosphorus resonance) from the lipid head group of DML multilayers is a broad line covering from about 10 KHz (50 ppm) to about 18 KHz (90 ppm), depending upon the temperature. The primary contributions to the width of the spectrum are from chemical shift anisotropy of phosphorus and dipolar interaction between protons and phosphorus. The latter can be reduced by proton decoupling. This, however, requires high power ($\sim$100W) proton irradiation not achievable on regular spectrometers. The use of solid state spectrometer to improve line shapes is described in this work. The static chemical shift tensor for P31 is nonaxial, the values of the principal components have been measured in the solid state (Kohler and Klein, 1976;1977). Many reports interpreting P31 data from bilayers, in particular, simulations that assume an axially symmetric tensor (McLaughlin et al., 1975; de Knight et al., 1976) are therefore wrong. Due to the nonaxiality of the tensor, at least two order parameters are needed to describe the P31 spectrum. These have been denoted by S_{11} and S_{33} (Seelig, 1978) and are the order parameters of

the principal axis connecting the two esterified and two nonesterified oxygens, respectively. The residual chemical shift anisotropy $\Delta\sigma$ after complete axial motional averaging determines the overall width of the spectrum and is given by (Seelig, 1978)

$$\Delta\sigma = S_{11}(\sigma_{11} - \sigma_{22}) + S_{33}(\sigma_{33} - \sigma_{22}) \qquad \text{II.1}$$

Here, σ_{11}, σ_{22} and σ_{33} are the components of the static chemical shift tensor. Using values for these tensor elements measured by Kohler and Klein (1977),

$$\Delta\sigma(\text{ppm}) = -56S_{11} + 133S_{33} \qquad \text{II.2}$$

The motional dependence of $\Delta\sigma$ has been taken advantage of in this work in predicting the nature of DML-alamethicin interaction.

H2 NMR

Studies on chain deuterated lipids have been useful in investigating lipid chain dynamics (Mantsch et al., 1977). As is the case with P31 NMR, the deuterium pattern in membranes is axially averaged, but unlike the case for P31, the quadrupolar splitting for H2 is determined by a single order parameter $S_{C\text{-}D}$. Each individual C-D bond order parameter has been measured by H2 NMR of specifically deuterated lipids (Seelig and Seelig, 1976). The order parameter rises rapidly up the bottom half of the chain and plateaus off near the backbone region (Seelig, 1977). This is in agreement with theoretical predictions (Petersen and Chan, 1977). A non-oriented sample of deuterated lipids used in the current study gives rise to a superposition of quadrupolar patterns from each C-D moeity. The

maximum splitting for the ith C-D group (ν_D^i) is given by

$$\nu_D^i = \frac{3}{2}\left(\frac{e^2qQ}{h}\right) S_{C-D}^i \qquad \text{II.3}$$

This expression assumes axial motional averaging (asymmetry parameter $\eta = 0$). (e^2qQ/h) is the static quadrupolar splitting constant. The dependence of the splitting ν_D^i on the order parameter of the chain deuterons S_{C-D}^i makes this technique attractive for study of chain motions and perturbations. The method has been used in this work for looking at DML-alamethicin interaction.

Chapter II.2

P31 and H2 NMR Study of Phospholipid Multilayers

A. MATERIALS AND METHODS

Dimyristoyl Phosphatidyl Choline (DML) was purchased from Sigma chemicals and was checked on TLC for purity. Chain perdeuterated Dimyristoyl Phosphatidyl Choline (d-54 DML) was purchased from Serdary Chemicals, Canada. D_2O used was from Aldrich chemicals.

Multilayers were made by dissolving lipid or a mixture of lipid and alamethicin in methanol in an NMR tube; the solvent was then evaporated off by dry nitrogen and the tube was kept under vacuum for at least eight hours. The thin film formed was hydrated with a 25mM Tris buffer solution (pD: 7.4) in D_2O by alternately vortexing on a mixer and gentle warming with a heat gun. The vortexing was done for about five minutes till a uniform white suspension was formed. The samples all had a 1:10 w/v ratio of lipid to water. Proper hydration and prolonged vortexing wereimportant in obtaining a uniform lipid mixture. Incomplete hydration shows up prominently in the P31 spectra as nonaxial or isotropic spectra. For measurements at higher ionic strengths the buffer solution was made in 0.5M NaCl. Samples for H2 NMR were prepared with a 2:1 mixture of normal DML with d-54 DML. All samples for H2 NMR were checked by P31 spectra for the integrity and nature of the multilayer. Before beginning the NMR experiments, all samples were maintained at $30^{o}C$.

NMR spectra were acquired at 11.7 tesla (500.13 MHz H1, 202.49 MHz P31 and 76.78 MHz H2 frequency) on a Bruker WM500 spectrometer equipped with an aspect 2000 computing system; and a variable temperature unit that

maintains the temperature of the sample constant within +/- 0.5°C. P31 spectra were acquired using a spectral width of 50 KHz, a 75° pulse and a relaxation delay of 1.5 seconds. Gated broad band decoupling at 10W was employed while acquiring most spectra. Deuterium NMR spectra were acquired with a quad echo sequence. A 166 KHz spectral width and a refocusing time of 50 usec were used. H1 spectra were obtained with usual parameters.

B. P31 NMR OF PHOSPHOLIPID HEAD GROUPS

The P31 NMR spectrum of the head group phosphorus in phospholipid multilayers has an axially averaged powder pattern (Seelig, 1978). Figure II.1 shows a typical spectrum of fully hydrated DML multilayers above the gel-liquid crystalline phase transition temperature. The static chemical shift tensor for the head group phosphorus is nonaxial and in the principal coordinate system it is described by three components: σ_{xx}, σ_{yy} and σ_{zz}. These have been measured for phospholipids in the solid state by Kohler and Klein (1977). Hydration of the lipid molecules results in rapid intramolecular rotation of the phosphate group and allows rotational diffusion about the long molecular axis. These motions cause axial time averaging of the tensor components giving rise to the shift tensors $\sigma_{\perp}$ and $\sigma_{\parallel}$ where

$$\sigma_{\parallel} + 2\sigma_{\perp} = \sigma_{xx} + \sigma_{yy} + \sigma_{zz} \qquad \text{II.4}$$

The anisotropic part of the time averaged tensor is defined as

$$\Delta\sigma = \sigma_{\parallel} - \sigma_{\perp} \qquad \text{II.5}$$

This chemical shift anisotropy ($\Delta\sigma$) is measured as the splitting between

Figure II.1 Proton decoupled (10 Watts) P31 NMR spectra at 202.49 MHz of DML multilayers. Temperatures are:

a. 26°C (above T_c).

b. 16°C (below T_c).

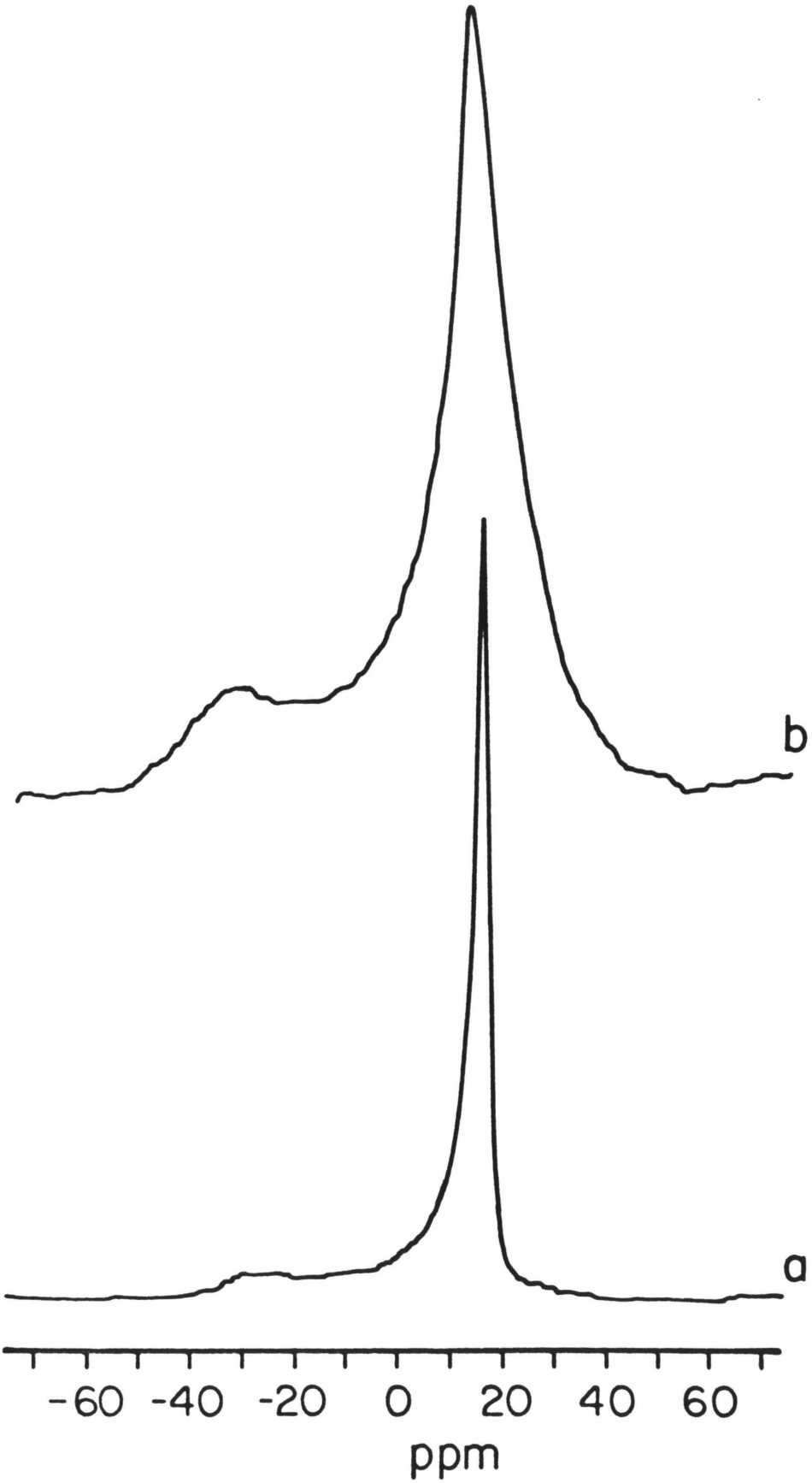
b
a
-60
-40
-20
0
20
40
60
ppm

the edges of the spectrum at the half height of the low frequency "foot" (Fig. II.1) can also be expressed in terms of the order parameters for the system (Seelig, 1978):

$$\Delta\sigma = S_{11}(\sigma_{xx} - \sigma_{yy}) + S_{33}(\sigma_{zz} - \sigma_{yy}) \qquad \text{II.6}$$

Due to the nonaxiality of the static chemical shift tensor, two order parameters S_{11} and S_{33} are necessary to describe a spectrum. The dependence of the experimentally measured $\Delta\sigma$ on the order parameters makes it a useful parameter to evaluate the mobility and order of the phospholipid head group. It is possible, for example, to follow the changes in order parameter and mobility of the head group with temperature by monitoring the corresponding values of $\Delta\sigma$. Figure II.2A shows $\Delta\sigma$ of DML multilayers plotted as a function of temperature. The sharp increase in $\Delta\sigma$ at $24^{o}C$ corresponds to the gel-liquid crystalline phase transition of the phospholipids (Cullis, 1976). Another parameter that is useful in describing the P31 spectra of multilayers is the width at half height — $\Delta\nu_{1/2}$ (Seelig and Gally, 1976). While this is an empirical parameter and is not a measure of the true linewidths of the superposed spectra, it is, however, dependent on the H1-P31 coupling and hence on the motional behavior of the system. Figure II.2B shows the dependence of $\Delta\nu_{1/2}$ of DML multilayers on temperature in the presence and absence of 10W broad band proton decoupling. Above phase transition temperature and decoupling of P31 from protons results in lowering of $\Delta\nu_{1/2}$. Below the phase transition temperature, our maximum decoupler power setting of 10W is unable to eliminate the strong dipolar P31-H1 couplings. $\Delta\nu_{1/2}$ loses its significance as an empirical parameter describing the system at low temperatures where

Figure II.2A Variation of the P31 chemical shielding anisotropy (in parts per million) with temperature. Data for DML multilayers (10% lipid 90% tris buffer, 25 mM)

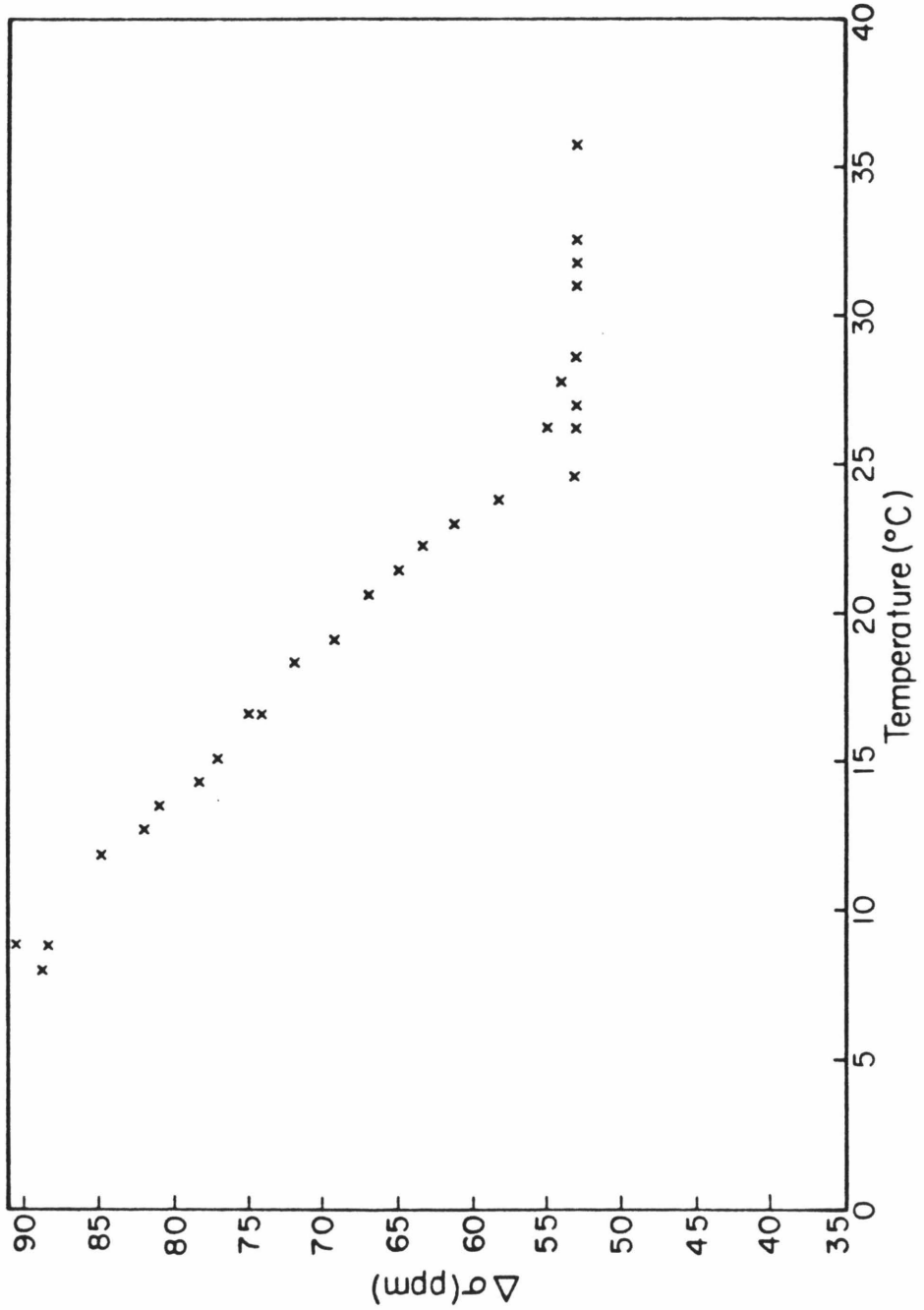
Δ q(ppm)
Temperature (°C)
90
85
80
75
70
65
60
55
50
45
40
35
0
5
10
15
20
25
30
35
40

Figure II.2B Temperature dependence of the width at half-height parameter $\Delta\nu_{\frac{1}{2}}$ for powder type P31 NMR spectrum of DML multilayers.

(*--*) no proton decoupling applied.

(+--+) 10W proton decoupling applied.

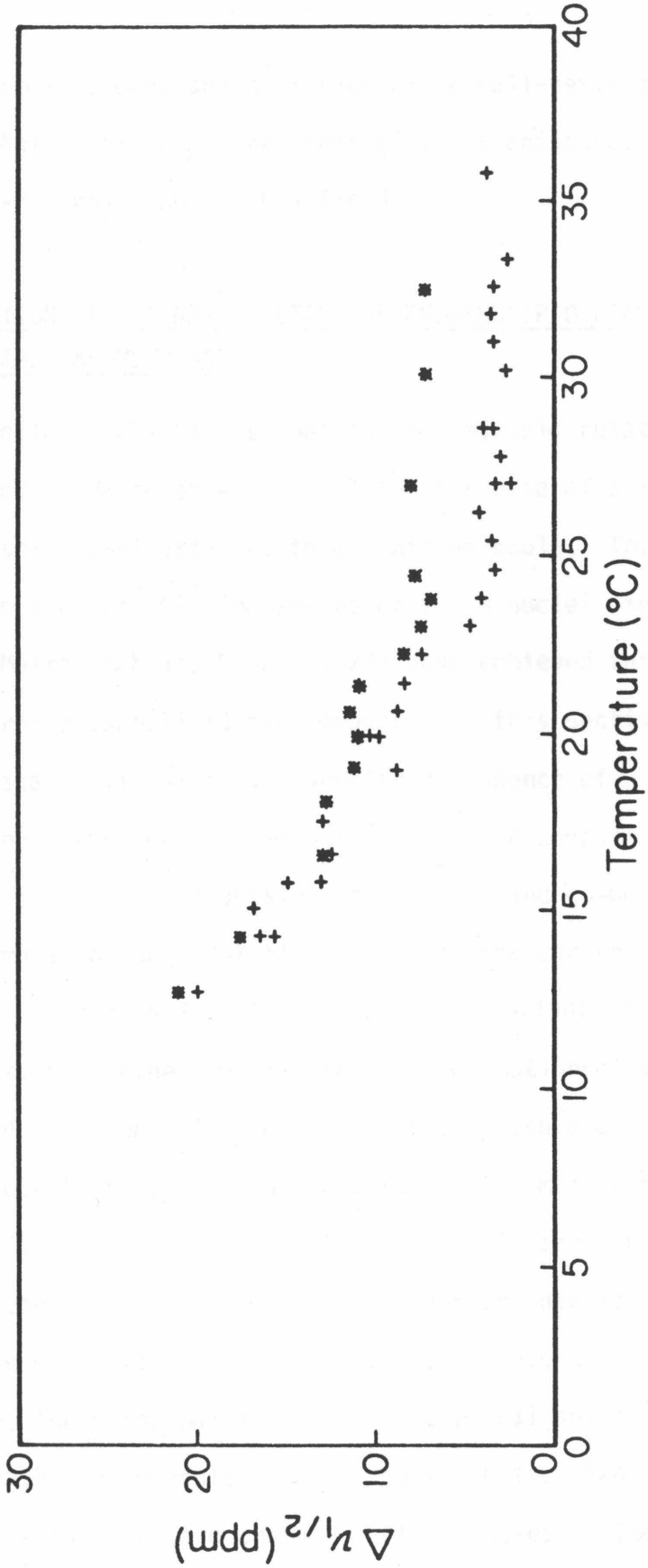
Δ ν1/2 (ppm)
0
10
20
30
0
5
10
15
20
25
30
35
40
Temperature (°C)

the spectrum is broad, and no longer has a well-defined low field edge. We found that unlike $\Delta\nu_{\frac{1}{2}}$, the chemical shift anisotropy ($\Delta\sigma$) is not sensitive to H1-P31 coupling at this field.

C. SIMULATION OF P31 NMR SPECTRUM OF PHOSPHOLIPID HEAD GROUPS IN MULTILAMELLAR MEMBRANES

Slow motional ESR line shapes for anisotropic rotational diffusion have been modeled by Mason et al. (1974) for the case of a rapidly rotating nitroxide spin label attached to a lipid molecule. This method can be extended to predict NMR line shapes of $I = \frac{1}{2}$ nuclei in the lipid molecules. Campbell, Meirovitch and Freed (1979) have achieved this to simulate the P31 spectrum from phospholipid head groups. In this section a study of the diffusion constant, linewidth and angular dependence of $\Delta\sigma$ is described based on the Campbell-Meirovitch-Freed treatment. A computer program for ESR simulation on a PDP 1134 obtained from Freed and co-workers was adapted for P31 NMR simulation on a VAX 11/780 to suit the current needs.

In the Freed formalism for anisotropic reorientation of lipid molecules in bilayers, the rather complicated set of motions of the head group is represented by three diffusion constants. These are, (a) a rotational diffusion constant $D_{||}$ for the fast rotational motion of the lipid molecules, (b) a very slow tumbling diffusion constant $D_{\perp}$ and (c) a rapid internal diffusion constant corresponding to bond reorientations D_I. The principal axis of the magnetic interaction for the P31 nucleus in the lipid multilayer (i.e. the principal axis for the chemical shift tensor) is not coincident with the molecule fixed diffusion axis. Two angles θ and ϕ that relate these two axes are termed "tilt angles". These angles are

defined in Figure II.3. The anisotropic P31 spectrum is simulated with $D_\perp$, $D_{||}$, D_I, θ, ϕ and T_2^{-1} as input parameters where T_2^{-1} is related to the line width of the constituent lorentzian envelopes that make up the powder pattern.

The theoretical formalism of an ab initio simulation of slow motional spectra has been described in detail by Freed and co-workers (1979). The spin Hamiltonian for the problem is set up in a proper coordinate system to account for the tilted diffusion frame of the molecule. Local motions are incorporated by solving a stochastic Liouville's equation to obtain coefficients of the eigenfunction expansion of the density matrix. The absorption spectrum is then calculated from these coefficients (Freed et al., 1971). This simulation technique is superior to that used by others (Seelig and Gally, 1976; Kohler and Klein, 1977) that only fit the value of $\Delta\sigma$ to two order parameters S_{11} and S_{33} (equation II.6) to simulate the line shape to fit overlapping Lorentzians without any explicit involvement of motional parameters. This simplified approach requires that the rotation about the director be so fast that residual time dependent effects of any process that lead to line broadening etc. are negligible while motion perpendicular to the director is so slow that its effects on the spectrum are negligible. According to Freed and co-workers, these assumptions are valid only for $D_{||} \geq 2 \times 10^7\ s^{-1}$ and $D_\perp \leq 5\ s^{-1}$. While those conditions are met for lipid membranes above the phase transition temperature, they may not be rigorously valid at low temperatures or in the presence of proteins or other perturbations.

Figure II.3 Schematic representation of the PO_4 group in the DML molecule. X,Y and Z denote the principal axes of the chemical shift tensor of the P31 nucleus and θ and ϕ define the orientation of the diffusion axis v. Axis Y lies within the O-P-O plane and approximately bisects the O-P-O angle, where the O's are the nonesterified oxygens.
(Reproduced from Campbell et al. 1979).

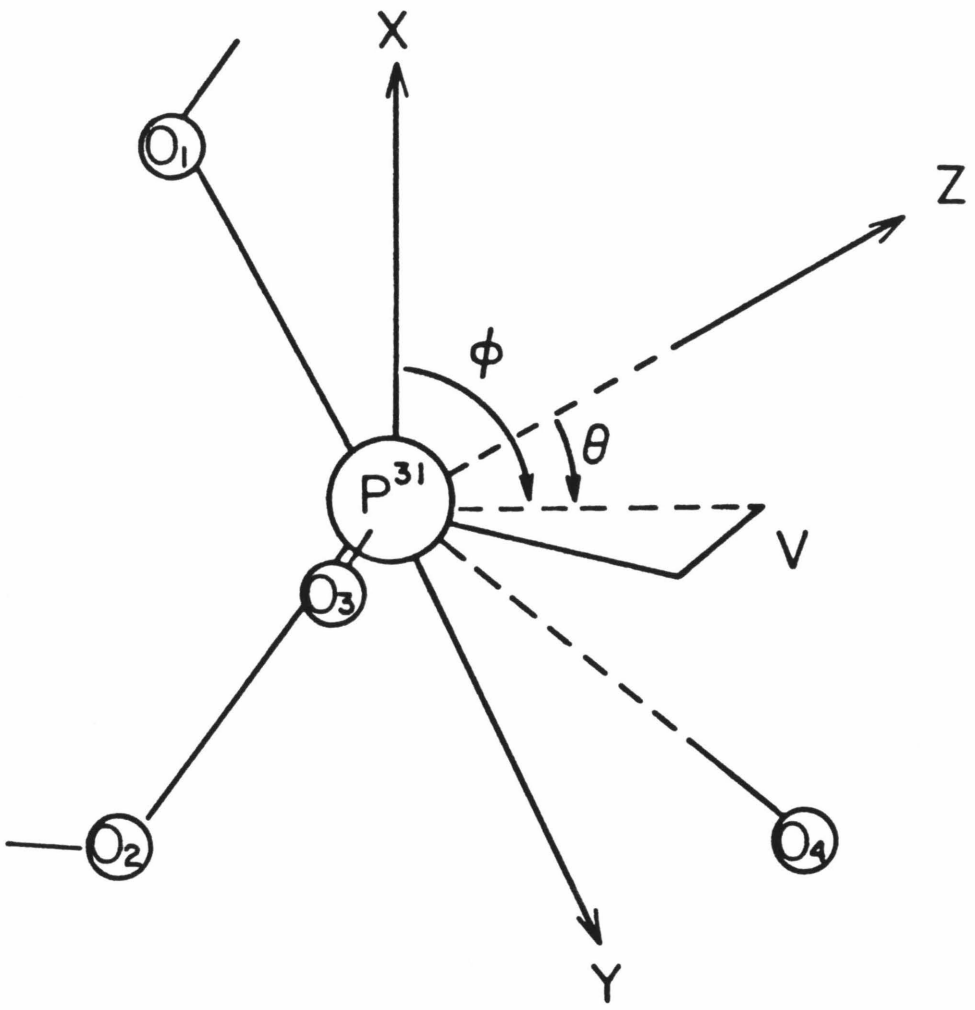
X
Z
Y
V
ϕ
θ
P^{31}
O_1
O_2
O_3
O_4

D. SIMULATION RESULTS AND DISCUSSION

Figure II.4a shows an experimental P31 spectrum of lipid head groups in an alamethicin lipid mixture at 4.7 tesla (200 MHz H1 and 80.45 MHz P31 frequency). The spectrum was acquired on a solid phase NMR instrument using a 200 watt amplifier for the observe channel and a 1000 watt amplifier connected to the H1 decoupler channel. The 90^{o} pulse for the observing nucleus is about 5 μsec and that for protons is 4 μsec. The higher power greatly improves the line shape of the spectra compared to the ones presented in the previous section that were acquired on a conventional spectrometer albeit at a higher field. It may be noted that the $\Delta\sigma$ is not affected significantly by this change in line shapes.

The spectrum shown in Fig. II.4a is fitted very well by the simulation shown in Fig. II.4b. The best fit was obtained with $D_I = 1 \times 10^{10}$ sec^{-1}, $D_{II} = 1 \times 10^{7}$ sec^{-1}, $D_{\perp} = 1$ sec^{-1}, $T_2^{-1} = 0.05g$, $\theta = 79^{o}$ and $\phi = 78^{o}$. The best fit parameters for a regular DML $\Delta\sigma$ above phase transition temperature were found to be $D_I = 1 \times 10^{10}$ sec^{-1}, $D_{II} = 1 \times 10^{7}$ sec^{-1}, $D_{\perp} = 1$ sec^{-1}, $T_2^{-1} = 0.1$ g and θ, $\phi = 83,75$.

Table II.1 shows the expected effect on the value of $\Delta\sigma$ when these parameters are changed over reasonable ranges. The corresponding spectra are presented in Fig. II.5.

The most signficant observation from this study is that $\Delta\sigma$ is very sensitive to the tilt angles θ and ϕ even with motional parameters that correspond to high temperature spectra. This was not commented upon in the original discussion of the problem by Freed and co-workers mainly because these authors were investigating gross changes in line shapes in the spectrum that is not observed with a small change in the tilt angles. Some

Figure II.4a High power (~ 200W) proton decoupled P31 NMR spectrum at 80.97 MHz. Temperature, 25°C

Figure II.4b Theoretical spectrum obtained from a density matrix calculation to simulate the P31 line shape of the spectrum shown in Figure II.4a.

Input parameters are: θ =79°, ϕ = 78°, $D_{\parallel}$= 1 x 10^{7} sec^{-1}, $D_{\perp}$= 1 sec^{-1}, D_I= 1x 10^{10} sec^{-1}, and T_2^{-1} = 0.05 gauss.

(see text for explanation of symbols). Ringing due to overtruncation has been eliminated by smoothing.

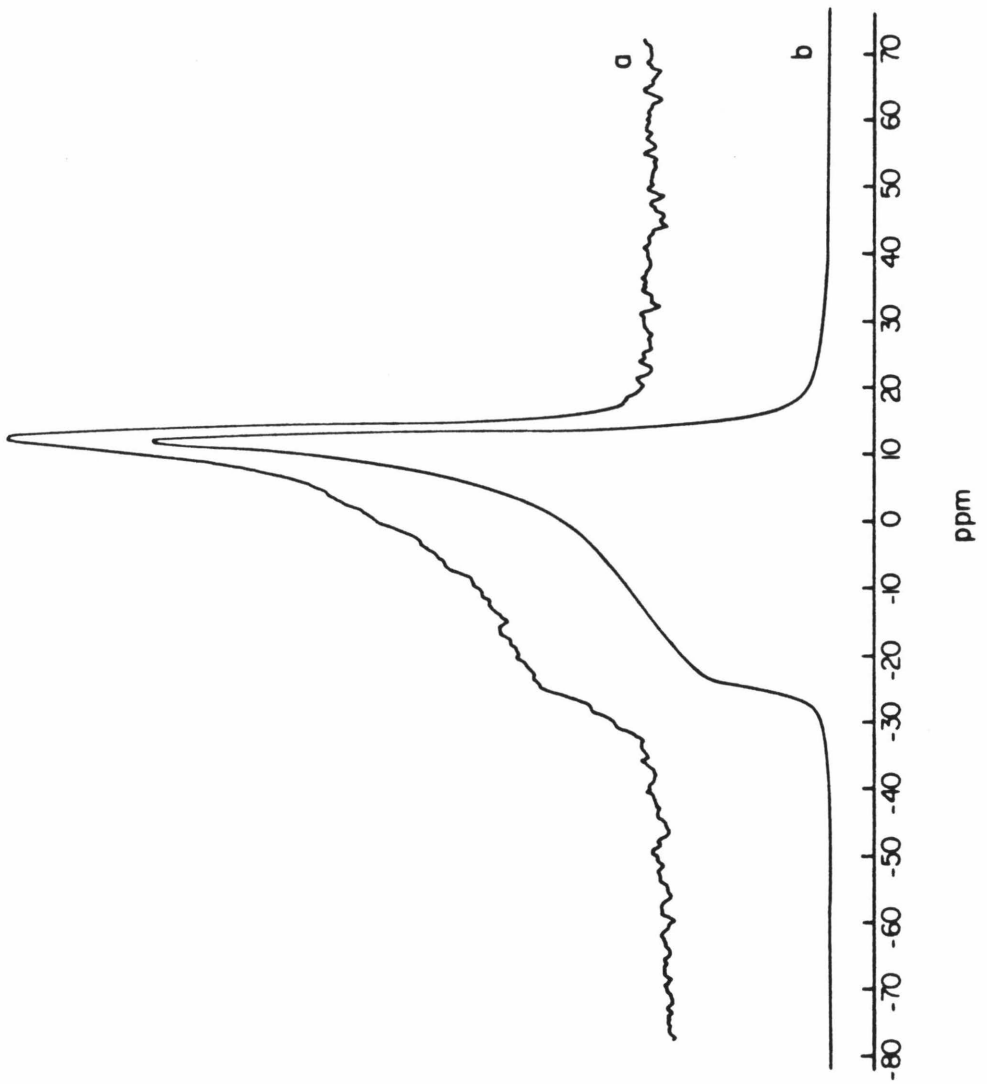
a
b
-80 -70 -60 -50 -40 -30 -20 -10 0 10 20 30 40 50 60 70
ppm

investigators have earlier discussed the importance of "torsional angles" (Skarjune and Oldfield, 1979; Grally et al., 1975) in determining the value of $\Delta\sigma$; however, lack of proper ab initio simulation methods have usually rendered such studies qualitative or incomplete. The angles θ and ϕ as defined in Figure II.3 are not expected to be unique. Many sets of angles as well as large fluctuations are suggested from an inspection of a scale model of a phospholipid. The flexible configuration of the head group combined with the sensitivity of this configuration to $\Delta\sigma$ indicates that the change in chemical shift anisotropy with temperature below the phase transition temperature as well as the change observed on adding peptides and proteins may actually be caused by a cooperative change in the average tilt angles of the lipid molecules in the bilayer. This will be further discussed in the next chapter where data on the interaction of alamethicin with bilayers is presented.

Table II.1 also shows that the value of $\Delta\sigma$ is insensitive to $D_{\parallel}$ and D_I for all values of $D_I \geq 1 \times 10^6$ sec^{-1} and $D_{\parallel} \geq 1 \times 10^4$ sec^{-1}. Beyond these limits, changes in $\Delta\sigma$ accompanied by large changes in the line shape are noted. At high temperatures, the expected values for the diffusion coefficients are $D_I \sim 10^{10}$ sec^{-1} and $D_{\parallel} \sim 10^8$ sec^{-1}. Any change in $\Delta\sigma$ would therefore necessitate a change in these diffusion constants by 3-4 orders of magnitude. Also, any further increase in these diffusion constants does not affect $\Delta\sigma$. In the previous section a large increase in $\Delta\sigma$ has been reported when the lipid multilayer undergoes a phase transition. If this increase were caused only by a decrease in D_I and $D_{\parallel}$ by over four orders of magnitude, the line shape would then be very grossly distorted (Fig. II.5). Since this is next observed (Fig. II.1), it is expected that tilt

angles and T_2^{-1} are also responsible for the observed changes in the spectrum below phase transition temperature.

Figure II.5 shows that the line shape of the spectrum is very strongly dependent on T_2^{-1}. In an experimental spectrum, T_2 is primarily determined by the residual P31-H1 coupling. This explains the differences in the line shape between spectra acquired with and without decoupling especially below the phase transition temperature. The low field "foot" is more prominent in the proton coupled spectra. This increase in "foot" height is also observed with a longer line width (αT_2^{-1}). The dependence of $\Delta\sigma$ on T_2^{-1} is minor, a change of only 4 ppm is seen, for example, when T_2^{-1} is changed by one order of magnitude (.01 gauss to .1 gauss). In the Freed formalism used in this study, T_2^{-1} is orientation independent. This assumption is not entirely justified although the orientation dependence of T_2^{-1} has been shown to have only minor effects on the spectrum (Seelig, 1978).

In summary, simulation of NMR line shapes for the P31 spectrum of phosphilipids in multilayers has been presented. The formalism developed by Freed and co-workers has been used for this purpose and a computer program from the same group has been employed to compute the spectra. A study of the dependence of the spectrum on several physically relevant input parameters has highlighted the importance of tilt angles in determining the chemical shift anisotropy. $\Delta\sigma$ has been shown to be less sensitive to diffusion constants and line width although the line shape changes considerably with changes in these parameters.

Table II.1

Corresponding Figure	T_2^{-1} gauss	$D_{\parallel}$ sec^{-1}	$D_{\perp}$ sec^{-1}	D_I sec^{-1}	θ degrees	ϕ degrees	$\Delta\sigma$ ppm	Inferences
II.5A j	0.1	1×10^7	1.0	1×10^{10}	33	75	54	
i						83	49	
h						73	56.5	$\Delta\sigma$ is highly sensitive to angles θ and ϕ. $\Delta\sigma$ decreases when θ decreases and/or ϕ increases.
g						63	69.5	
f						53	86.5	
e					90	75	58.5	
d					85		56.5	
c					75		40.5	
a					65		(0)	
b					55		(-34)	
II.5B a	0.1	1×10^7	1.0	1×10^{10}	83	75	54	
b		1×10^5					54.5	For high D_I, no effect on $\Delta\sigma$ is seen with change in $D_{\parallel}$.
c		1×10^3					54	
d		10					54	
e		0.1					54.5	

Table II.1 (cont.)

Corresponding Figure	T_2^{-1} gauss	$D_{\parallel}$ sec^{-1}	$D_{\perp}$ sec^{-1}	D_{I} sec^{-1}	θ degrees	ϕ degrees	$\Delta\sigma$ ppm	Inferences
II.5C a	0.1	1×10^4	1.0	1×10^{10}	83	75	54	
b	↓	↓	↓	1×10^8	↓	↓	54.5	
c				1×10^6			55	
d				1×10^4			undefined	
e				1×10^2			undefined	$\Delta\sigma$ is sensitive to $D_{\parallel}$ only when the latter is changed by ~4 orders of magnitude.
f				8×10^5			56	
g				4×10^5			56.5	
h				1×10^5			59.5	
i				6×10^4			66.5	
j				2×10^4			undefined	

Table II.1 (cont.)

Corresponding Figure	T_2^{-1} gauss	$D_{\parallel}$ sec^{-1}	$D_{\perp}$ sec^{-1}	$D_{\mathbb{T}}$ sec^{-1}	θ degrees	ϕ degrees	$\Delta\sigma$ ppm	Inferences
II.5D a	0.01	1×10^7	1.0	1×10^{10}	83	75	50	
b	0.02	↓	↓	↓	↓	↓	50.5	
c	0.03						51	
d	0.05						52	
								T_2^{-1} affects "foot height"; only a small effect on $\Delta\sigma$ is seen.
II.5B a	0.1						54	
II.5D e	0.15						56	
f	0.2						57	
g	0.3						61	
h	0.5						undefined	
i	1.0						undefined	

Figure II.5A Theoretical spectra illustrating the sensitivity of $\Delta\sigma$ and the P31 line shape to the values of θ and ϕ, for $D_{\parallel} = 1 \times 10^{7}$ sec^{-1}, $D_{\perp} = 1$ sec^{-1} and $T_2^{-1} = 0.1$ gauss. $D_I = 1 \times 10^{10}$sec^{-1}

a. $\theta = 65°$ $\phi = 75°$

b. $\theta = 55°$ $\phi = 75°$

c. $\theta = 75°$ $\phi = 75°$

d. $\theta = 85°$ $\phi = 75°$

e. $\theta = 90°$ $\phi = 75°$

f. $\theta = 83°$ $\phi = 53°$

g. $\theta = 83°$ $\phi = 63°$

h. $\theta = 83°$ $\phi = 73°$

i. $\theta = 83°$ $\phi = 83°$

j. $\theta = 83°$ $\phi = 75°$

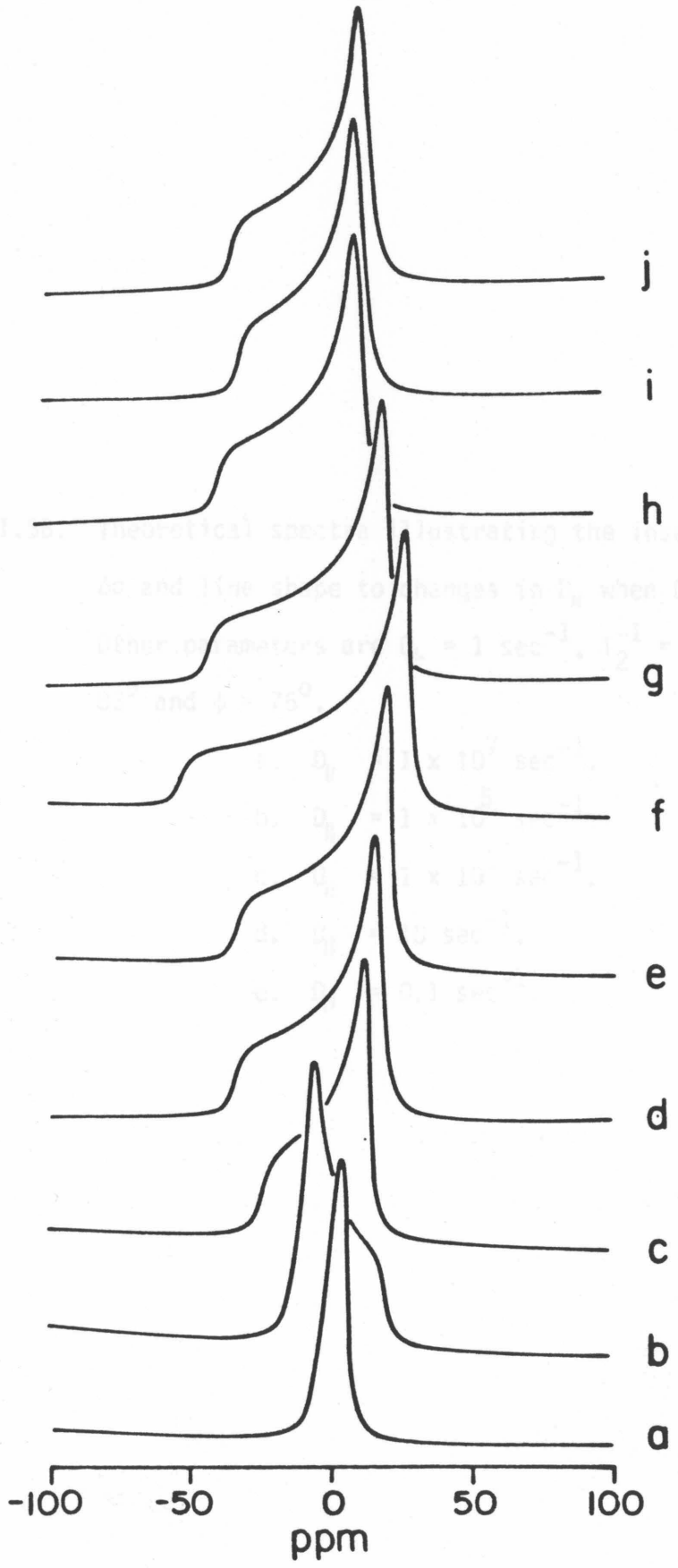
j
i
h
g
f
e
d
c
b
a
-100
-50
0
50
100
ppm

Figure II.5B. Theoretical spectra illustrating the insensitivities of $\Delta\sigma$ and line shape to changes in $D_{\parallel}$ when $D_I = 1 \times 10^{10}$ sec^{-1}. Other parameters are $D_{\perp} = 1$ sec^{-1}, $T_2^{-1} = 0.1$ gauss, $\theta = 83^{o}$ and $\phi = 75^{o}$.

a. $D_{\parallel} = 1 \times 10^{7}$ sec^{-1}.

b. $D_{\parallel} = 1 \times 10^{5}$ sec^{-1}.

c. $D_{\parallel} = 1 \times 10^{3}$ sec^{-1}.

d. $D_{\parallel} = 10$ sec^{-1}.

e. $D_{\parallel} = 0.1$ sec^{-1}.

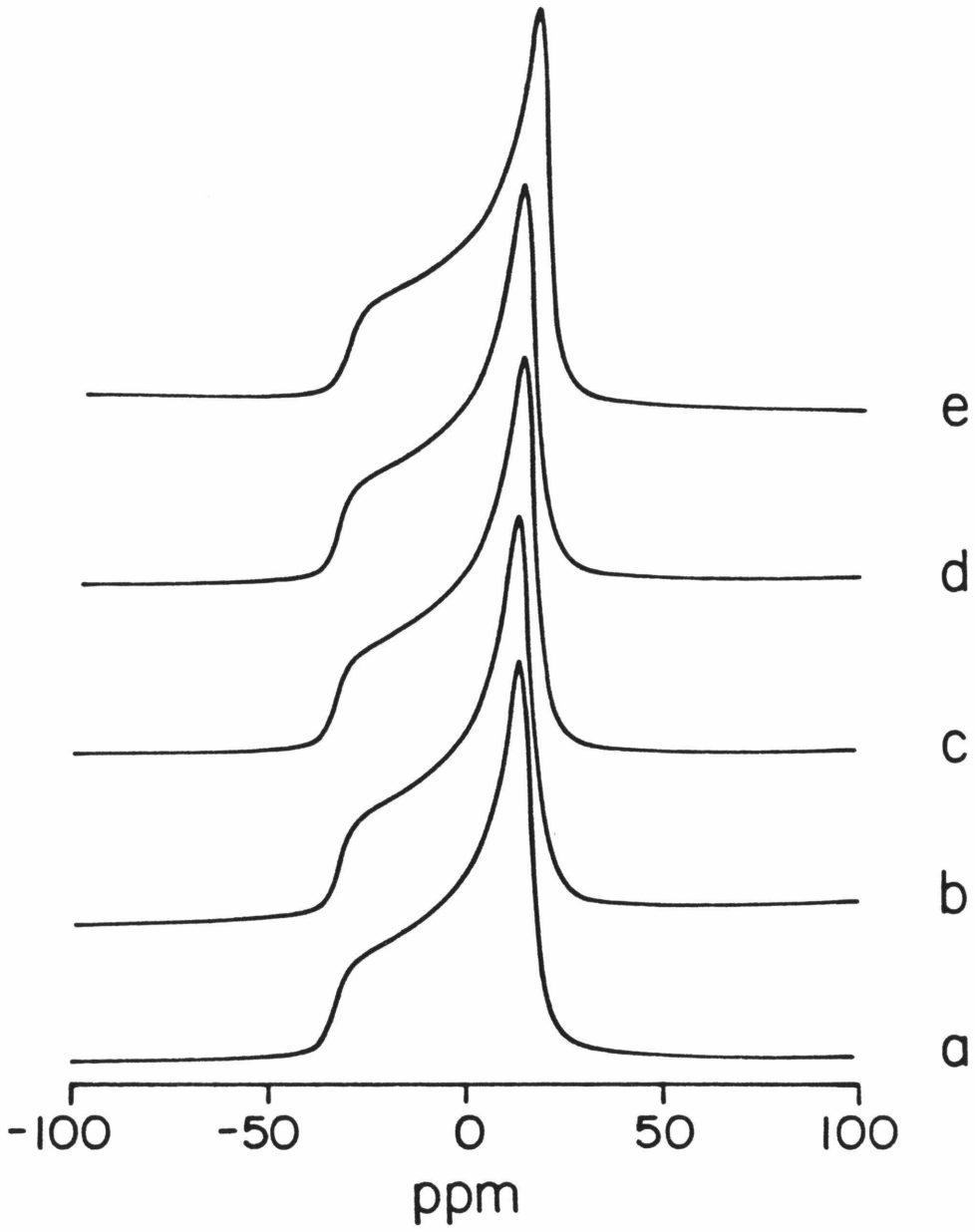
e
d
c
b
a
-100
-50
0
50
100
ppm

Figure II.5C. Theoretical spectra calculated with different values of D_I. For all spectra, $D_\perp = 1\ sec^{-1}$, $D_\parallel = 1 \times 10^4\ sec^{-1}$, $\theta = 83^o$, $\phi = 75^o$ and $T_2^{-1} = 0.1$ gauss.

a. $D_I = 1 \times 10^{10}\ sec^{-1}$

b. $D_I = 1 \times 10^{8}\ sec^{-1}$

c. $D_I = 1 \times 10^{6}\ sec^{-1}$

d. $D_I = 1 \times 10^{4}\ sec^{-1}$

e. $D_I = 1 \times 10^{2}\ sec^{-1}$

f. $D_I = 8 \times 10^{5}\ sec^{-1}$

g. $D_I = 4 \times 10^{5}\ sec^{-1}$

h. $D_I = 1 \times 10^{5}\ sec^{-1}$

i. $D_I = 6 \times 10^{4}\ sec^{-1}$

j. $D_I = 2 \times 10^{4}\ sec^{-1}$

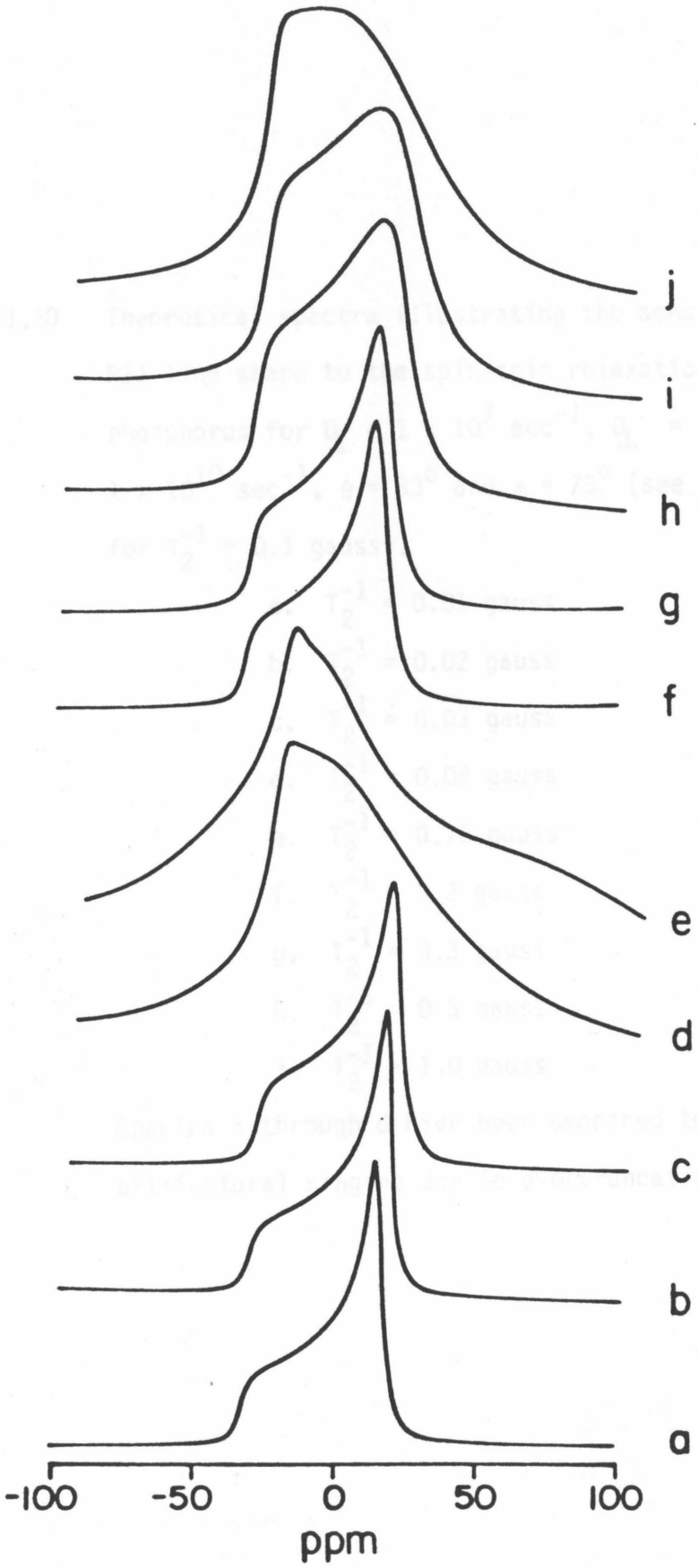
j
i
h
g
f
e
d
c
b
a
-100
-50
0
50
100
ppm

Figure II.5D Theoretical spectra illustrating the sensitivity of the P31 line shape to the spin-spin relaxation time of the phosphorus for $D_{\parallel} = 1 \times 10^{7}$ sec^{-1}, $D_{\perp} = 1$ sec^{-1}, $D_I = 1 \times 10^{10}$ sec^{-1}, $\theta = 83^{o}$ and $\phi = 75^{o}$ (see Figure II.5Ba for $T_2^{-1} = 0.1$ gauss).

a. $T_2^{-1} = 0.01$ gauss

b. $T_2^{-1} = 0.02$ gauss

c. $T_2^{-1} = 0.03$ gauss

d. $T_2^{-1} = 0.05$ gauss

e. $T_2^{-1} = 0.15$ gauss

f. $T_2^{-1} = 0.2$ gauss

g. $T_2^{-1} = 0.3$ gauss

h. $T_2^{-1} = 0.5$ gauss

i. $T_2^{-1} = 1.0$ gauss

Spectra a through d have been smoothed to eliminate artifactural ringing due to overtruncation.

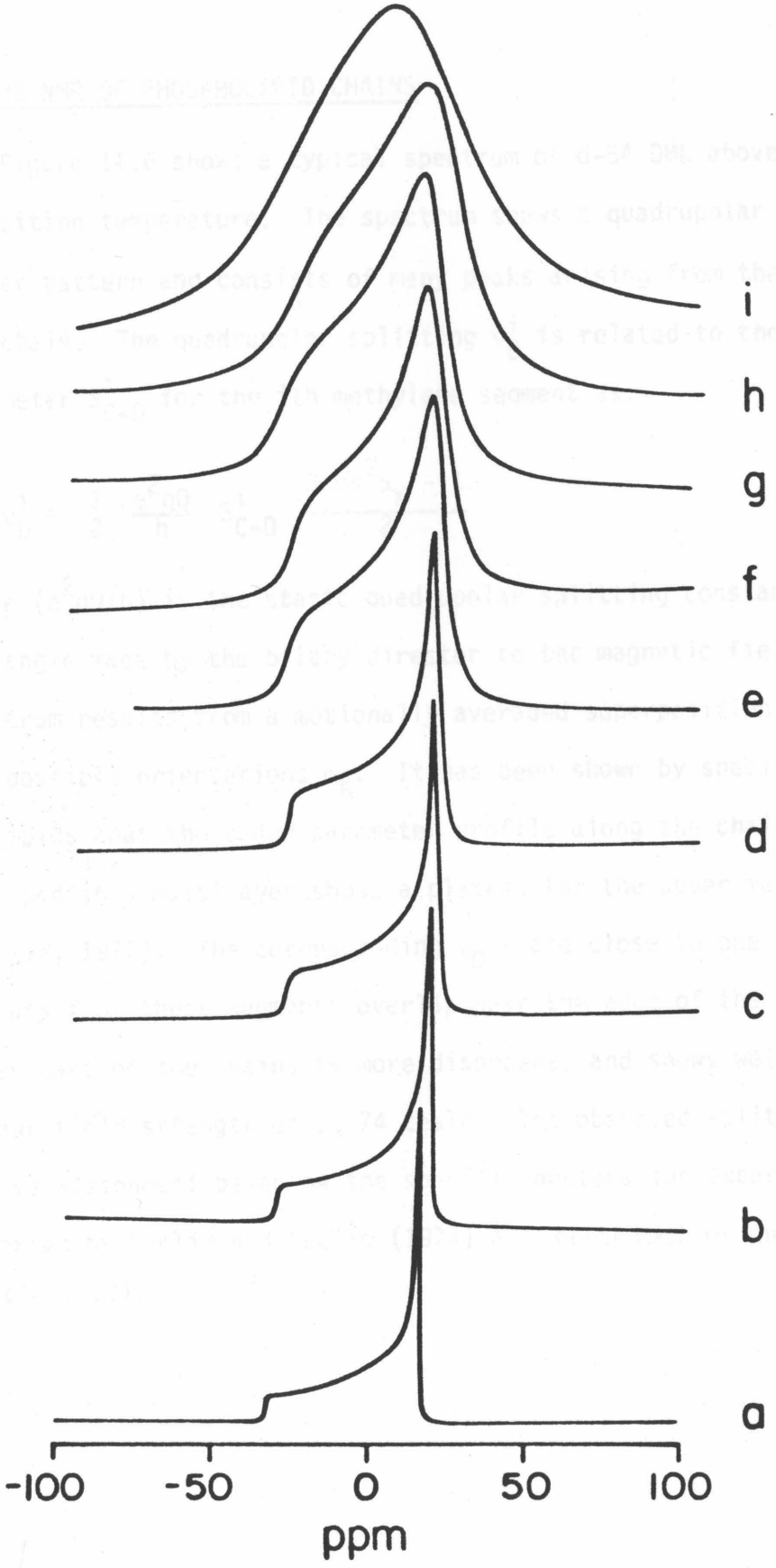
i
h
g
f
e
d
c
b
a
-100
-50
0
50
100
ppm

E. H2 NMR OF PHOSPHOLIPID CHAINS

Figure II.6 shows a typical spectrum of d-54 DML above the phase transition temperature. The spectrum shows a quadrupolar axially averaged powder pattern and consists of many peaks arising from the deuterons along the chain. The quadrupolar splitting ν_D^i is related to the C-D bond order parameter S_{C-D}^i for the ith methylene segment as:

$$\nu_D^i = \frac{3}{2} \frac{e^2qQ}{h} S_{C-D}^i \frac{3\cos^2\alpha_K - 1}{2} \qquad \text{II.7}$$

where (e^2qQ/h) is the static quadrupolar splitting constant and α_K is the angle made by the bilary director to the magnetic field. The multilayer spectrum results from a motionally averaged superposition of NMR lines for all possible orientations α_K. It has been shown by specific deuteration of lipids that the order parameter profile along the chain of a phospholipid in a multilayer shows a plateau for the upper methylene segments (Seelig, 1977). The corresponding ν_D's are close to one another and the signals from these segments overlap near the edge of the spectrum. The lower part of the chains is more disordered and shows well resolved peaks at our field strength of 11.74 tesla. The observed splittings and a tentative assignment based on the specific deuteration experiments on DPL reported by Seelig and Seelig (1974) are presented in the next chapter (Table II.2).

Chapter II.3

Interaction of Alamethicin with Phospholipid Multilayers

A. INTRODUCTION

Chapter II.2 describes two important NMR methods to probe phospholipid motional dynamics in multilayer membranes; in this chapter these methods are used to address an important controversy in the alamethicin literature. There has been much debate in recent publications over the position of alamethicin relative to phospholipid membranes in the absence of a field gradient. Earlier work on alamethicin-lipid vesicle interaction indicated surface activity (Lau and Chan, 1975,1976). Lis et al. (1976) have undertaken Raman spectroscopic investigation of the lipid-alamethicin system, and have agreed with the above notion of a primarily hydrophilic interaction of alamethicin at the lipid-water interface. Fringeli et al. (1979) on the other hand have proposed from an infrared attenuated total reflection study of alamethicin in the presence of thin films of lipid that the peptide is absorbed into the bilayer and is positioned parallel to the lipid chains. The photolabeling experiments of Latorre et al. (1981) have also suggested a similar result.

This work investigates the interaction of alamethicin with multilayer membranes using P31 NMR of the lipid head group phosphorus and H2 NMR of the lipid chain deuterons in a perdueterated lipid. Raman spectroscopy is also used to complement results from NMR measurements. These techniques have been shown to be sensitive tools in determining the nature of the bilayer phase, the order and the mobility of the lipids and the gel-liquid crystalline phase transition temperature not only for pure phospholipid

bilayers as indicated in Chapter II.2 but also in the presence of polypeptides and proteins. Experiments performed with alamethicin-DML mixtures were repeated with gramicidin-S and chlorophyll-A to provide contrasting examples that supplement the conclusions. The measurements of the chemical shift anisotropy for phosphorus and quadrupolar splitting of deuterium and a study of these NMR line shapes indicates that alamethicin maintains the lamellar bilayer phase of Dimyristoyl phosphatidyl choline (DML) and produces and insignificant change in the phase transition temperature at a rather high alamethicin to lipid ratio of 1:15. The peptide interacts strongly with the phospholipid head groups but not with lower parts of the lipid chains. These conclusions are further substantiated by the results from studies on gramicidin-S and chlorophyll-A. Taken together, the observations are all consistent with an interaction of alamethicin with lipid bilayers at the water-lipid interface.

B. MATERIALS AND METHODS

Alamethicin used in this study is a generous gift of Dr. G. B. Whitfield Jr. and Dr. J. E. Grady of the Upjohn Company and was used without further purification. Gramicidin-S was purchased from Sigma Co. chlorophyll-A was extracted and HPLC purified by Dr. Phoebe Dea. Multilayers containing alamethicin, gramicidin-S or chlorophyll-A were made by first dissolving a mixture of the components in methanol in an NMR tube, and then evaporating off this solvent with dry nitrogen. This ensured the proper mixing of the lipid with the nonlipid component. The tube was kept under vacuum for at least eight hours. The thin film formed was hydrated with 25 mM Tris buffer solution (PD 7.4) in D_2O by alternately vortexing on a mixer and gentle warming with a heat gun. The vortexing was continued for about five minutes

till a uniform white suspension was formed. For measurement at higher ionic strength, the buffer solution was made in 0.5 M NaCl. Samples for H2 NMR were made with a 2:1 mixture of normal DML with d-54 DML. Spectral parameters are identical to those mentioned in Chapter II.2. T1's were measured by the saturation recovery method as described in the standard Bruker software.

C INTERACTION OF ALAMETHICIN WITH DML MULTILAYERS

The characteristic features of P31 spectrum of DML multilayers have been described in Chapter II.2. The effect of alamethicin on these features will be discussed here. Samples for the study contained 15:1 or 2:1 mole ratio of lipid to the peptide. The principal observations from this study are the following:

a. As shown in Figure II.6 there is no qualitative change in the line shape of the spectrum even at very high concentration of alamethicin (2 moles of lipid per mole of peptide). This indicates that the integrity of the multilayer phase is maintained. Throughout the work we did not have evidence for any lipid polymorphism as a result of interaction of alamethicin with DML multilayers.

b. $\Delta\sigma$ decreases significantly when alamethicin is added to multilayers (Figure II.7). Above the phase transition temperature, the effect on the headgroups is maximal at the 15:1 lipid: alamethicin ratio, i.e. no further reduction in $\Delta\sigma$ is observed in the sample with the higher alamethicin ratio (2:1 lipid:alamethicin). Below the phase transition temperature, however, the lowering of $\Delta\sigma$ is more enhanced at the higher alamethicin ratio. This result

Figure II.6A. P31 NMR spectra of lipid head group phosphorus in DML-alamethicin mixtures, The spectra were recorded at 202.49 MHz P31 frequency. The temperature is 26^{o}C (above the phase transition temperature).

a. No alamethicin

b. 15:1 DML: alamethicin mole ratio

c. 2:1 DML: alamethicin mole ratio

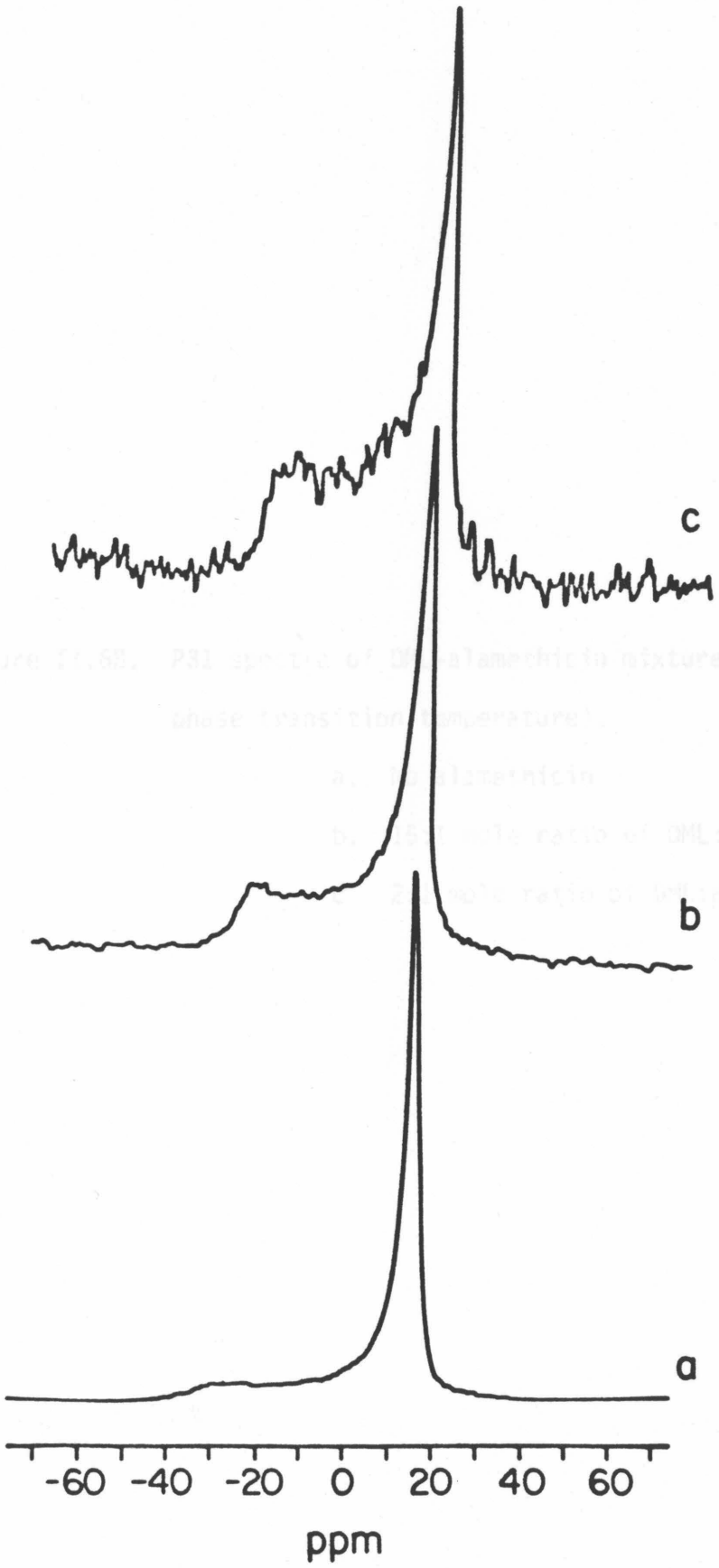
c
b
a
-60
-40
-20
0
20
40
60
ppm

Figure II.6B. P31 spectra of DML-alamethicin mixtures at 16° C (below phase transition temperature).

a. No alamethicin

b. 15:1 mole ratio of DML:alamethicin

c. 2:1 mole ratio of DML:alamethicin

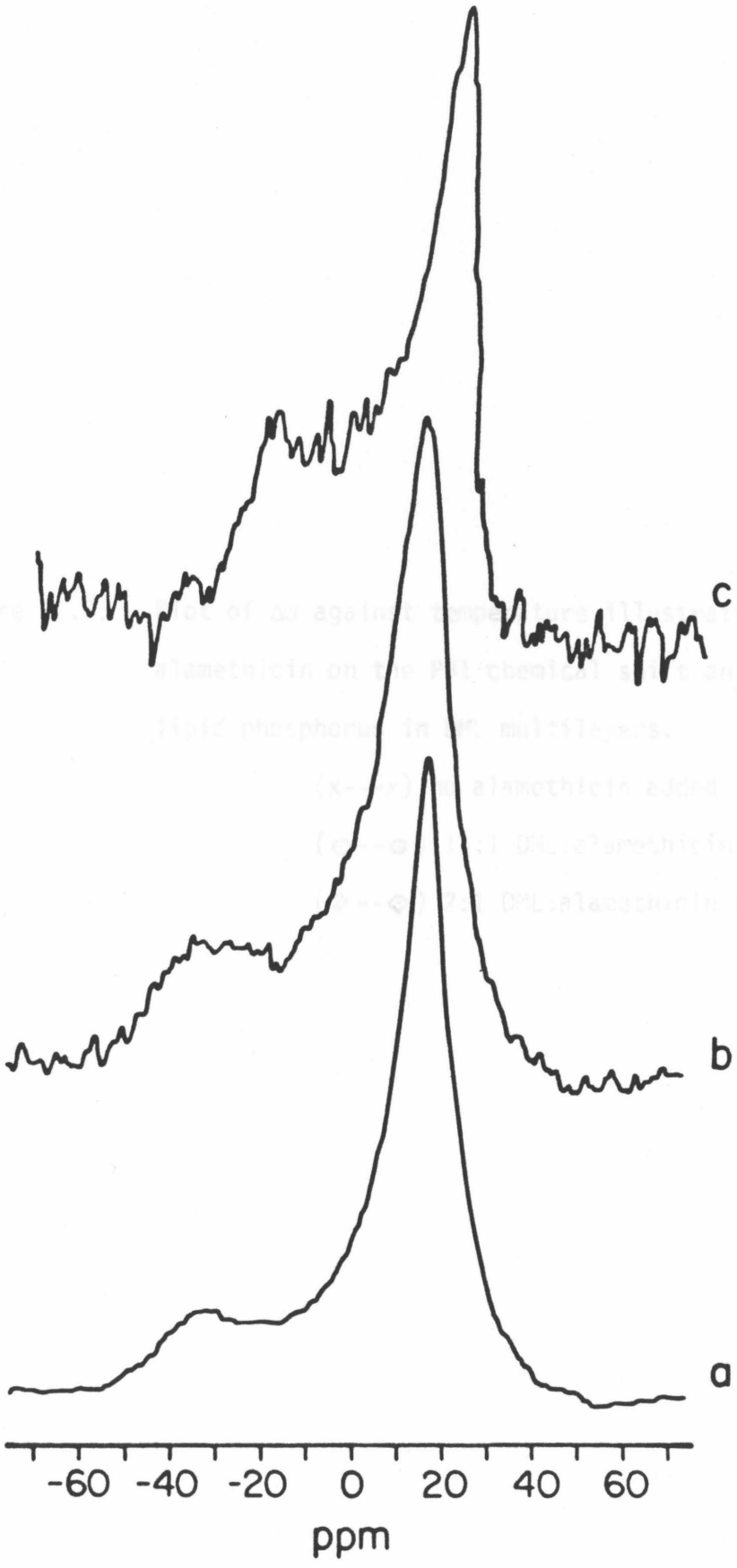
c
b
a
-60
-40
-20
0
20
40
60
ppm

Figure II.7. Plot of $\Delta\sigma$ against temperature illustrating the effect of alamethicin on the P31 chemical shift anisotropy of the lipid phosphorus in DML multilayers.

(x---x) no alamethicin added

(⊙--⊙) 15:1 DML:alamethicin (mole ratio)

(◈--◈) 2:1 DML:alamethicin (mole ratio)

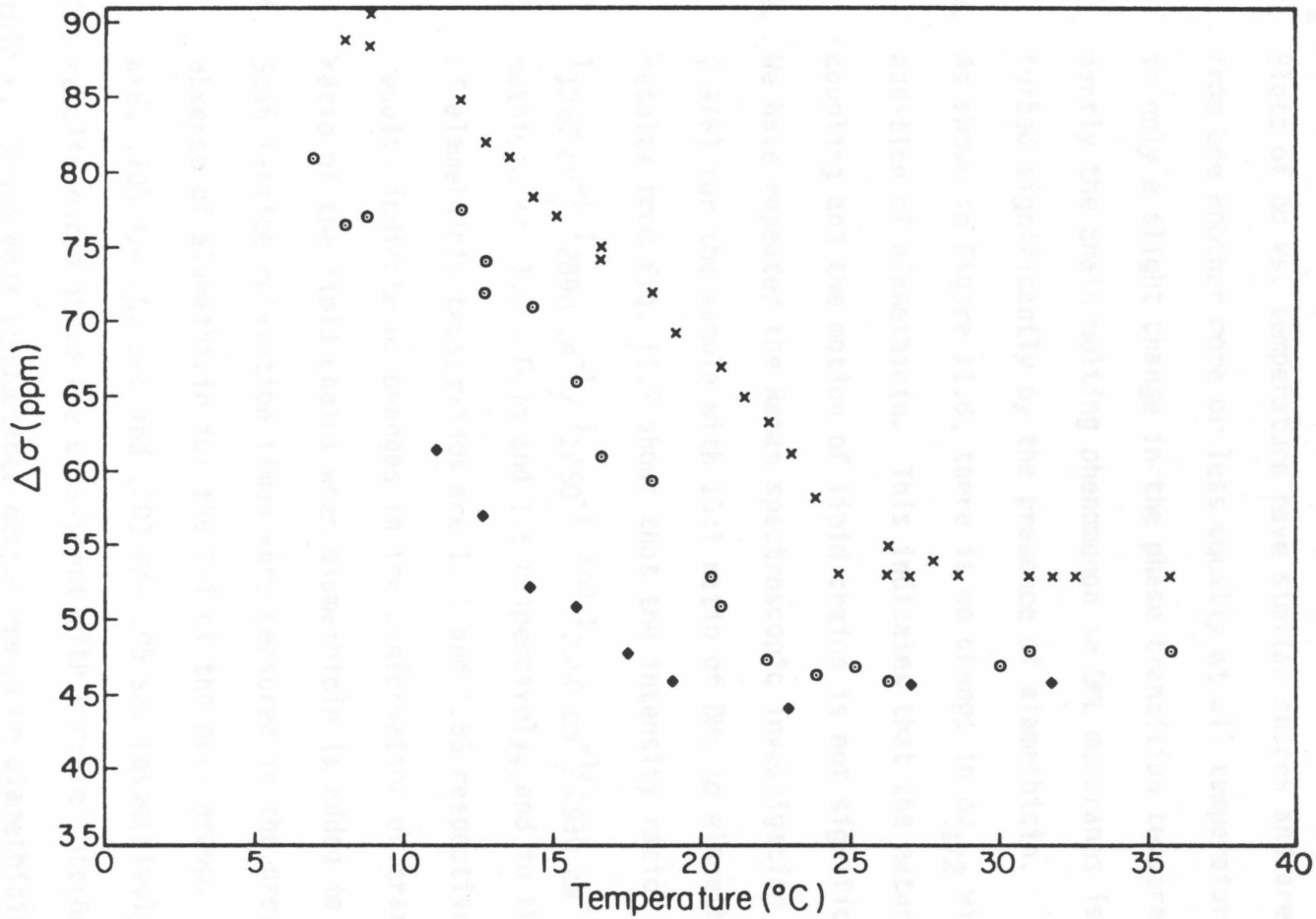
90
85
80
75
70
65
60
55
50
45
40
35
Δσ(ppm)
0
5
10
15
20
25
30
35
40
Temperature (°C)

indicates a strong interaction of the peptide phosphate head groups at the surface of multilayers.

c. Plots of $\Delta\sigma$ vs. temperature have similar shapes and are displaced from one another more or less equally at all temperatures. There is only a slight change in the phase transition temperature. Evidently the chain melting phenomenon in DML membranes is not perturbed significantly by the presence of alamethicin.

d. As shown in Figure II.8, there is no change in $\Delta\nu_{1/2}$ with the addition of alamethicin. This indicates that the nature of P31-H1 coupling and the motion of lipid chains is not significantly affected.

e. We have repeated the Raman spectroscopic investigation of Lis et al. (1976) for the sample with 15:1 ratio of DML to alamethicin. The results from Fig. II.9 shows that the intensity ratios $I_{1065\ cm^{-1}}/I_{1087\ cm^{-1}}$, $I_{2890\ cm^{-1}}/I_{2850^{-1}}$ and $I_{2850\ cm^{-1}}/2930\ cm^{-1}$ without alamethicin are 1.07, 0.95 and 1.5 respectively, and in the presence of alamethicin these ratios are 1, 1 and 1.35 respectively. These results indicate no changes in the conformation or trans-gausch ratio of the lipid chains when alamethicin is added to multilayers.

f. Spin lattice relaxation times were measured in the presence and absence of alamethicin for the P31 of the head group. The values are, .700 +/- .05 sec and .702 +/- .05 sec respectively.

The results noted above are consistent with surface interaction of alamethicin. Since most conductance measurements on alamethicin have been undertaken in the presence of salts, these experiments were repeated in a .5 M NaCl solution. A comparison of the temperature dependence of $\Delta\sigma$ in alamethicin-lipid mixtures in the presence and absence of salt is shown in

Figure II.8. Plot of $\Delta\nu_{1/2}$ against temperature for alamethicin containing DML multilayers.

(+--+) no alamethicin, with decoupling

(*--*) no alamethicin, no decoupling

(⊙ --⊙) 15:1 lipid:alamethicin mole ratio, with decoupling

(◈ --◈) 15:1 lipid:alamethicin mole ratio, no decoupling

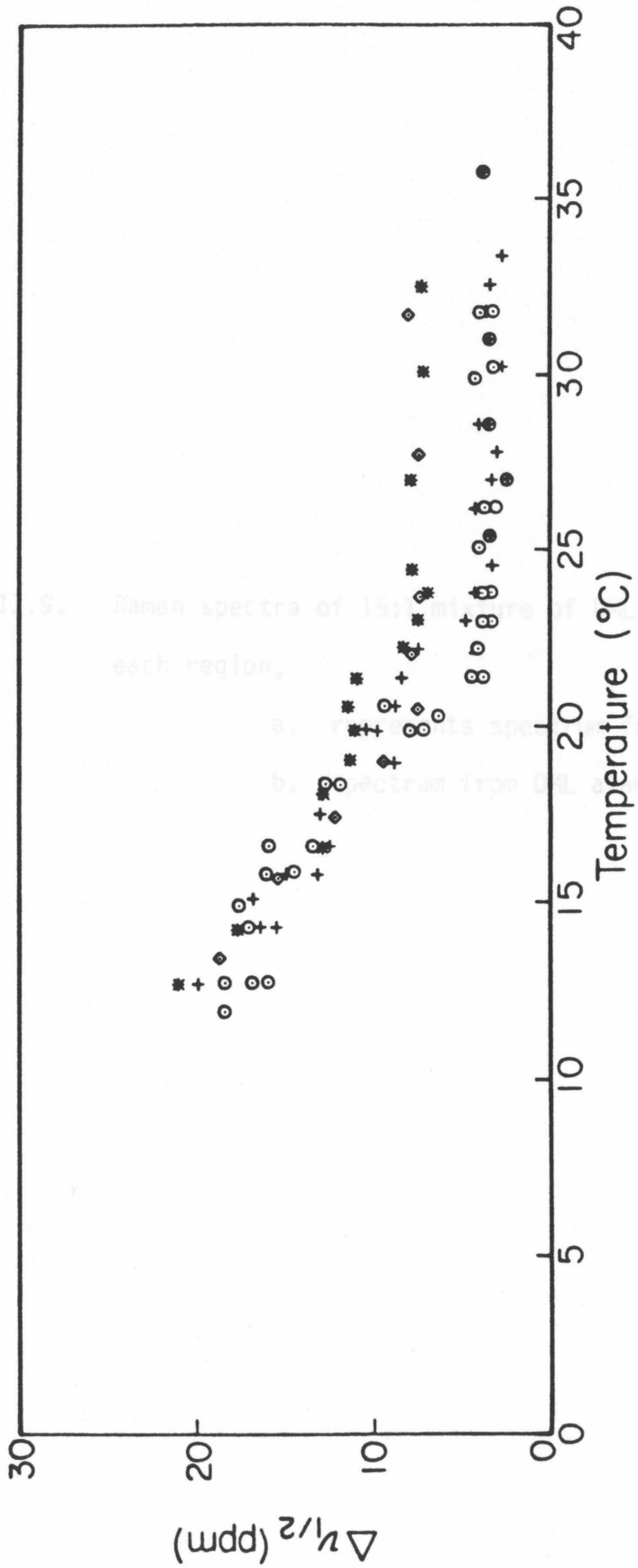
Δν1/2 (ppm)
30
20
10
0
0
5
10
15
20
25
30
35
40
Temperature (°C)

Figure II.9. Raman spectra of 15:1 mixture of DML and alamethicin. For each region,

a. represents spectrum for DML only, and

b. spectrum from DML alamethicin mixed system.

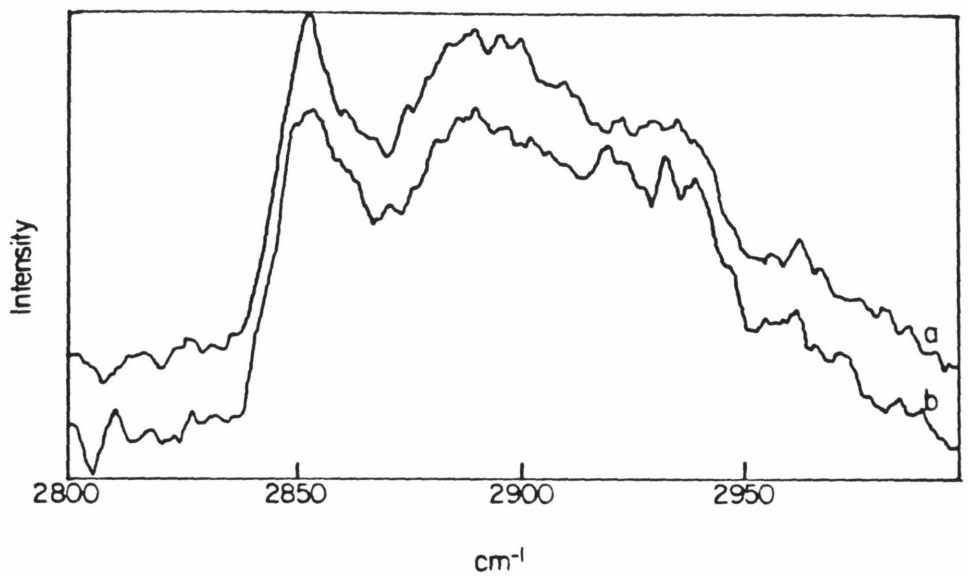
Intensity
a
b
2800
2850
2900
2950
cm-1

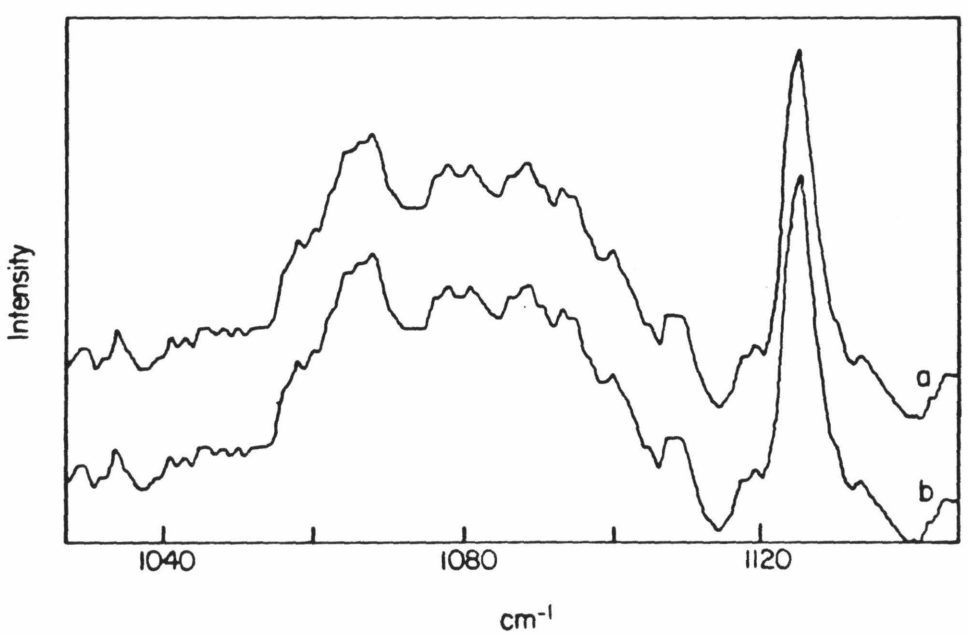
Intensity
a
b
1040
1080
1120
cm-1

Figure II.10. At 15:1 lipid to alamethicin ratio, there is no change in $\Delta\sigma$ with the addition of salt. At the higher alamethicin ratio however, the value increases above the phase transition temperature on adding salt. This suggests that at this concentration, the higher ionic strength is decreasing the affinity of alamethicin to the bilayer.

D. H2 MNR OF PHOSPHOLIPID CHAINS IN ALAMETHICIN-LIPID MIXTURE

Figure II.11 shows the H2 quad-echo spectrum from a sample of DML mixed with a high concentration of alamethicin (1 mole of alamethicin/15 moles of lipid). The powder pattern is identical to the reference spectrum except by a loss of intensity at the extreme edges (Fig. II.11) and within limits of experimental error, no change in ν_D of any peak is observed (table II.2). Below the phase transition temperaure (T_c) the H2 spectrum is broad. The peaks shown in Fig. II.11 are no longer resolved. This technique is inadequate in predicting the position of the peptide relative to the bilayer below the phase transition temperature. The combined H2 and P31 results show that above T_c alamethicin does not perturb the lipid chains in the absence of an applied electric field, but it interacts strongly at the surface of the membrane. The likely nature of this interaction is discussed later in this chapter.

E. INTERACTION OF GRAMICIDIN S AND CHLOROPHYLL A WITH DML MULTILAYERS: A STUDY IN CONTRAST

In the previous section the effect of alamethicin on the features of P31 and H2 NMR of phospholipids in multilayer membranes was described. In order to establish the significance of these results, two other systems were chosen and were subjected to similar experiments; the results from

Figure II.10. Plot of $\Delta\sigma$ vs. temperature at different ionic strengths. The sample has 15:1 mole ratio of DML:alamethicin.

(⊙ --⊙) no salt added

(◈ --◈) with 0.5 M NaCl

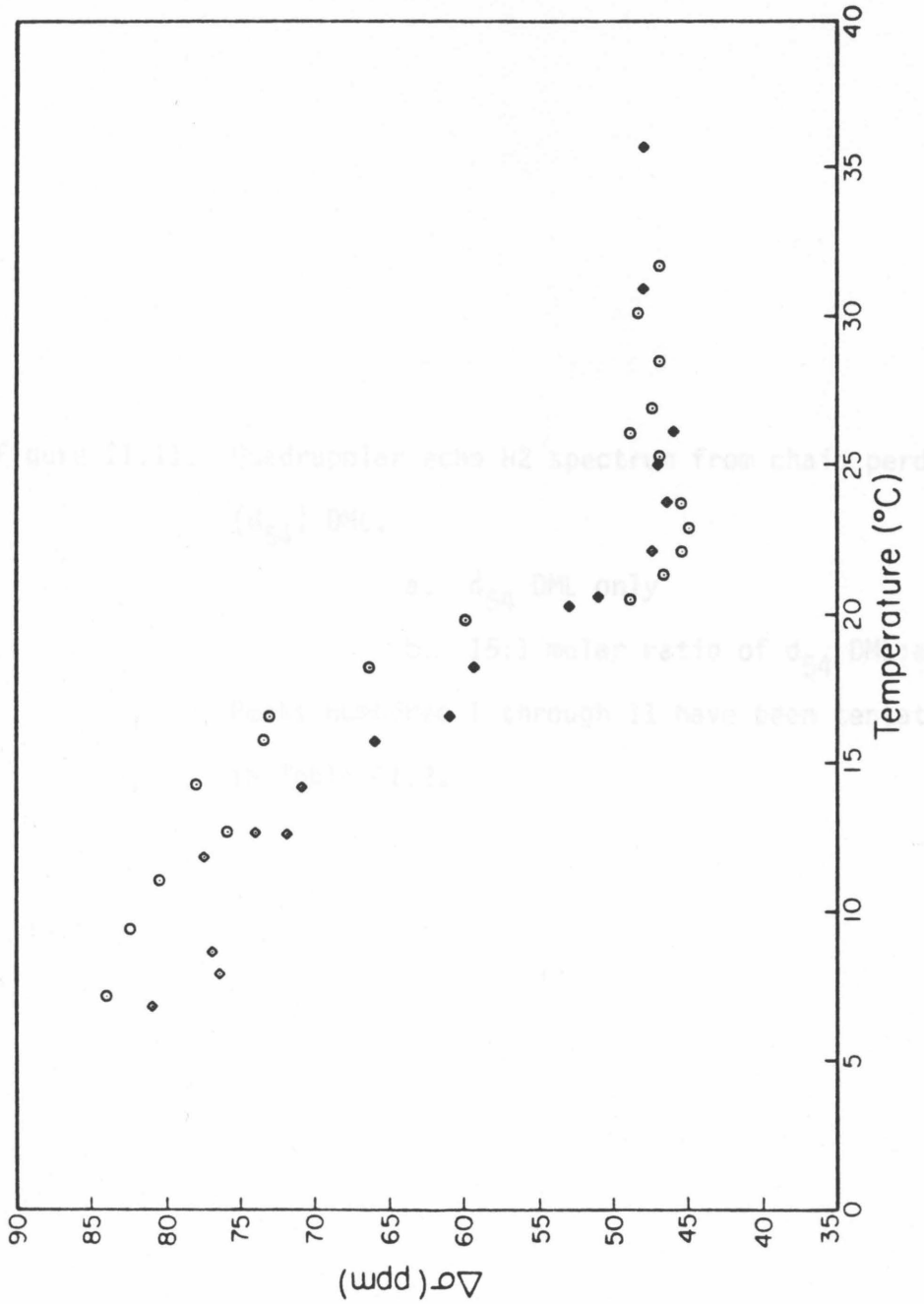
Δσ (ppm)
Temperature (°C)
90
85
80
75
70
65
60
55
50
45
40
35
0
5
10
15
20
25
30
35
40

Figure II.11. Quadrupolar echo H2 spectrum from chain perdeuterated (d_{54}) DML.

a. d_{54} DML only

b. 15:1 molar ratio of d_{54} DML:alamethicn

Peaks numbered 1 through 11 have been tentatively assigned in Table II.2.

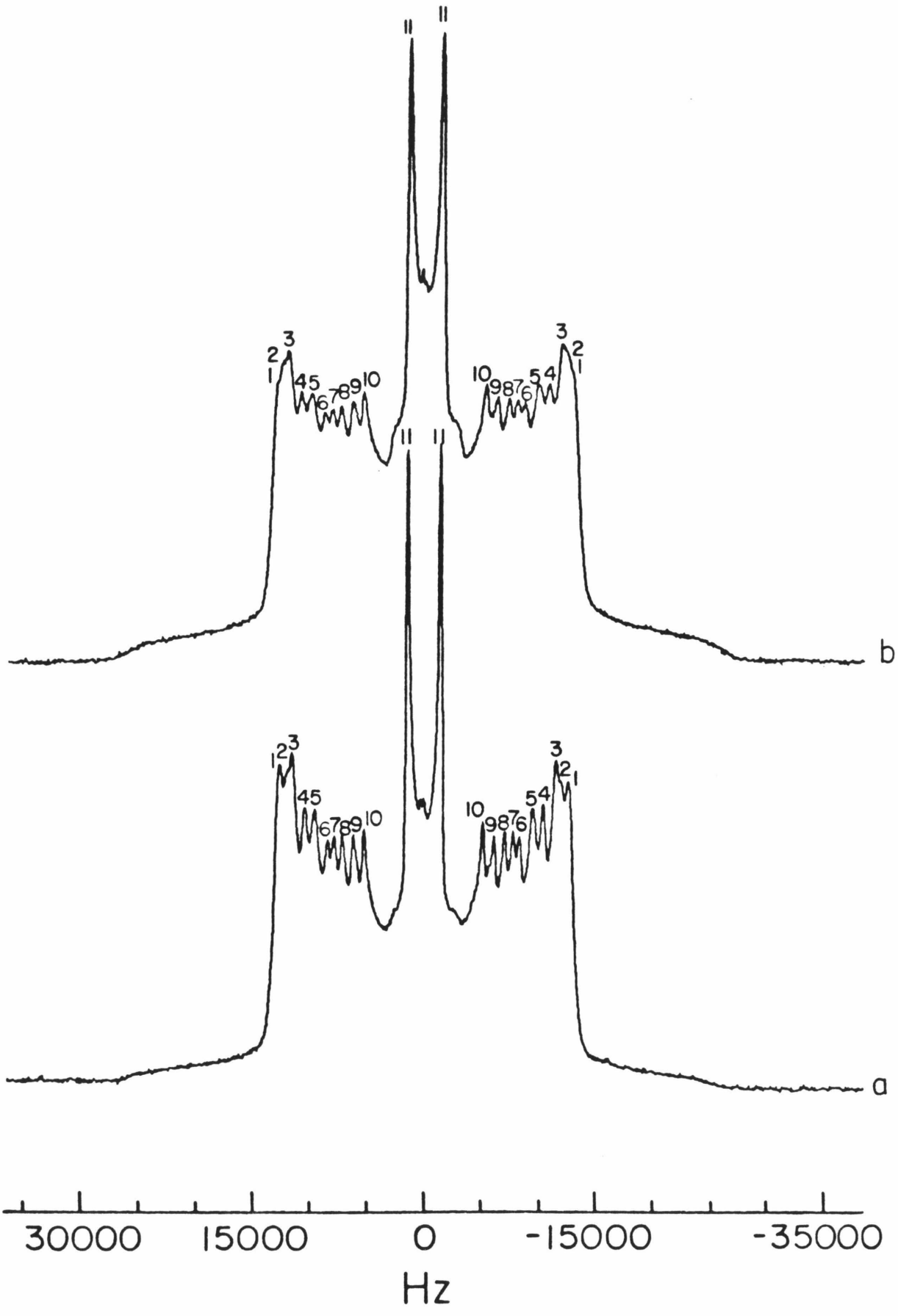
11
11
2
1
3
4
5
6
7
8
9
10
11
11
10
9
8
7
6
5
4
3
2
1
b
1
2
3
4
5
6
7
8
9
10
11
11
10
9
8
7
6
5
4
3
2
1
a
30000
15000
0
-15000
-35000
Hz

Table II.2

Peak	Tentative assignment chain deuteron on carbon #(a and b represent the two chains)	ν_D without alamethicin KHz	ν_D with alamethicin (15:1 lipid: alamethicin)	% difference
1	2a, 3-5	25.3	25.9	2.4
2	7b, 6a, 6b	24.0	25.2	5
3	8b, 7a, $2b_1$	23.0	23.9	3.9
4	9b, 8a	20.8	21.8	4.8
5	10b, 9a	19.0	19.8	4.2
6	10a	16.7	17.5	4.8
7	11b	15.6	16.3	4.5
8	11a	14.2	14.6	2.8
9	12b, $1b_2$	12.3	12.7	3.2
10	12a	10.5	10.8	2.8
11	13	2.9	2.9	(1.4)

these experiments can then be compared and contrasted with those of the previous section and would aid in establishing the nature of alamethicin-lipid interaction. The two molecules chosen for this purpose are gramicidin-S and chlorophyll-A. Gramicidin-S is a cyclic decapeptide antibiotic with an antiparallel β sheet conformation. The antibiotic action may be due to cell lysis, although it has been shown recently that the peptide binds strongly to nucleotides and phase transfers them into organic solvents (Krauss and Chan, 1983). It is proposed by these authors that gramicidin S is responsible for nucleotide depletion in a cell. Chlorophyll-A has a unique lipid-like structure. It consists of a porphyrin ring system attached to a phytol chain. This long hydrocarbon chain has been shown to interchelate into the lipid bilayer with the polar "head group" positioned at the interface (Eigenberg et al., 1982b). The lysing action of gramicidin-S and the interchelating action of chlorophyll-A are expected to be reflected in the P31 spectra of multilayers containing those macromolecules. This was indeed found to be so. The P31 spectrum of gramicidin-DML mixture at a mole ratio of 1:15 shows the standard shape for bilayer phase much above the phase transition temperature (T_c). At around T_c, however, phase separation is indicated by the appearance of new peaks (Figure II.12A). The polymorphic behavior is seen only around T_c at this concentration. At 1:2 gramicidin-S to DML ratio the bilayer phase is completely disrupted; only an isotropic signal is seen (Figure II.12B) indicating micellization of the bilayer. With the lowering of temperature a new phase appears that gives rise to a broad signal (Figure II.12B) similar to that obtained from the gel phase in DML. Figure II.13 shows a plot of $\Delta\sigma$ for lipid head group phosphorus in a 1:15 gramicidin-S-DML mixture as a function of temperature.

Figure II.12A. Spectra of 15:1 (mole by mole) of DML and gramicidin S near the phase transition temperature.

a. $21^{o}C$

b. $20^{o}C$

c. $19^{o}C$

d. $18^{o}C$

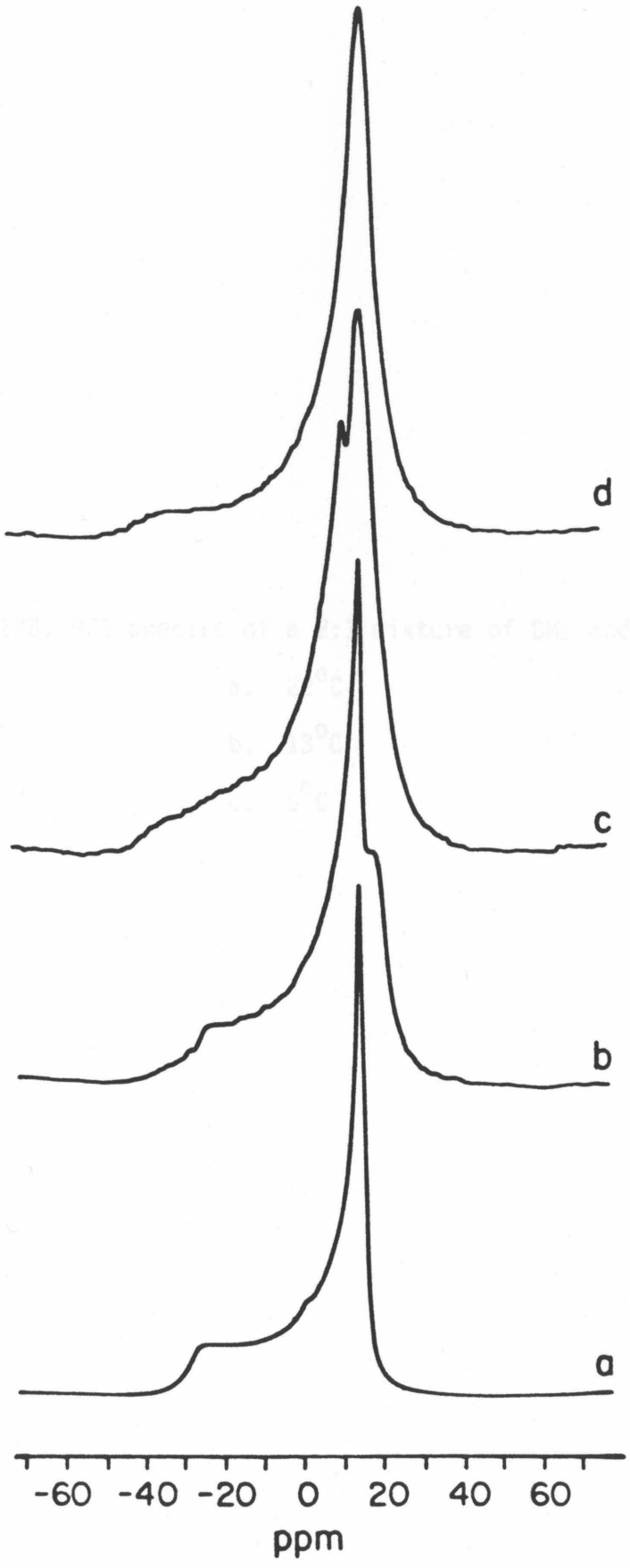
d
c
b
a
-60 -40 -20 0 20 40 60
ppm

Figure II.12B. P31 spectra of a 2:1 mixture of DML and gramicidin S.

a. $22^{o}C$

b. $13^{o}C$

c. $6^{o}C$

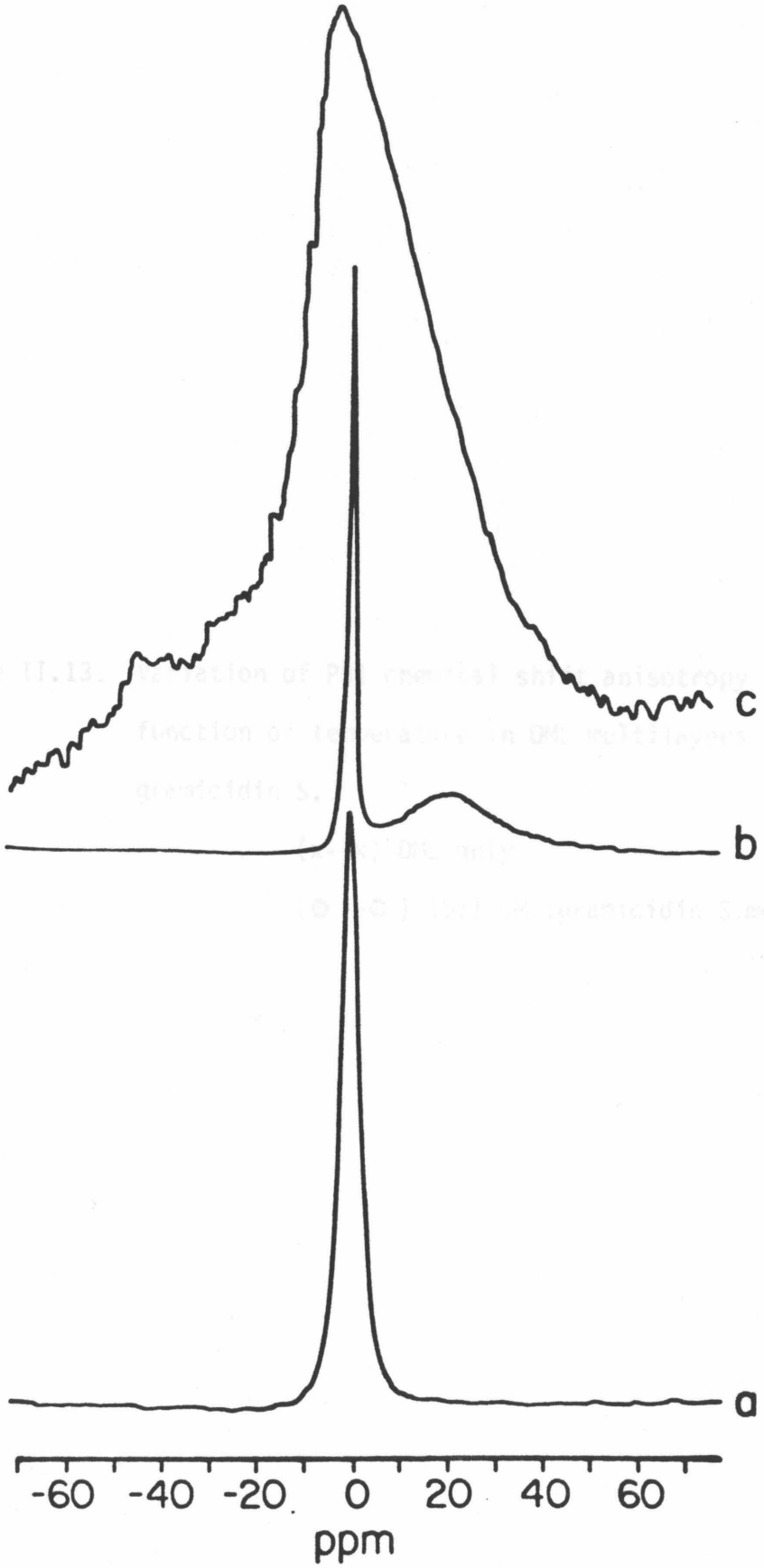
c
b
a
-60
-40
-20
0
20
40
60
ppm

Figure II.13. Variation of P31 chemical shift anisotropy ($\Delta\sigma$) as a function of temperature in DML multilayers containing gramicidin S.

(x--x) DML only

(⊙ --⊙) 15:1 DML:gramicidin S mole ratio

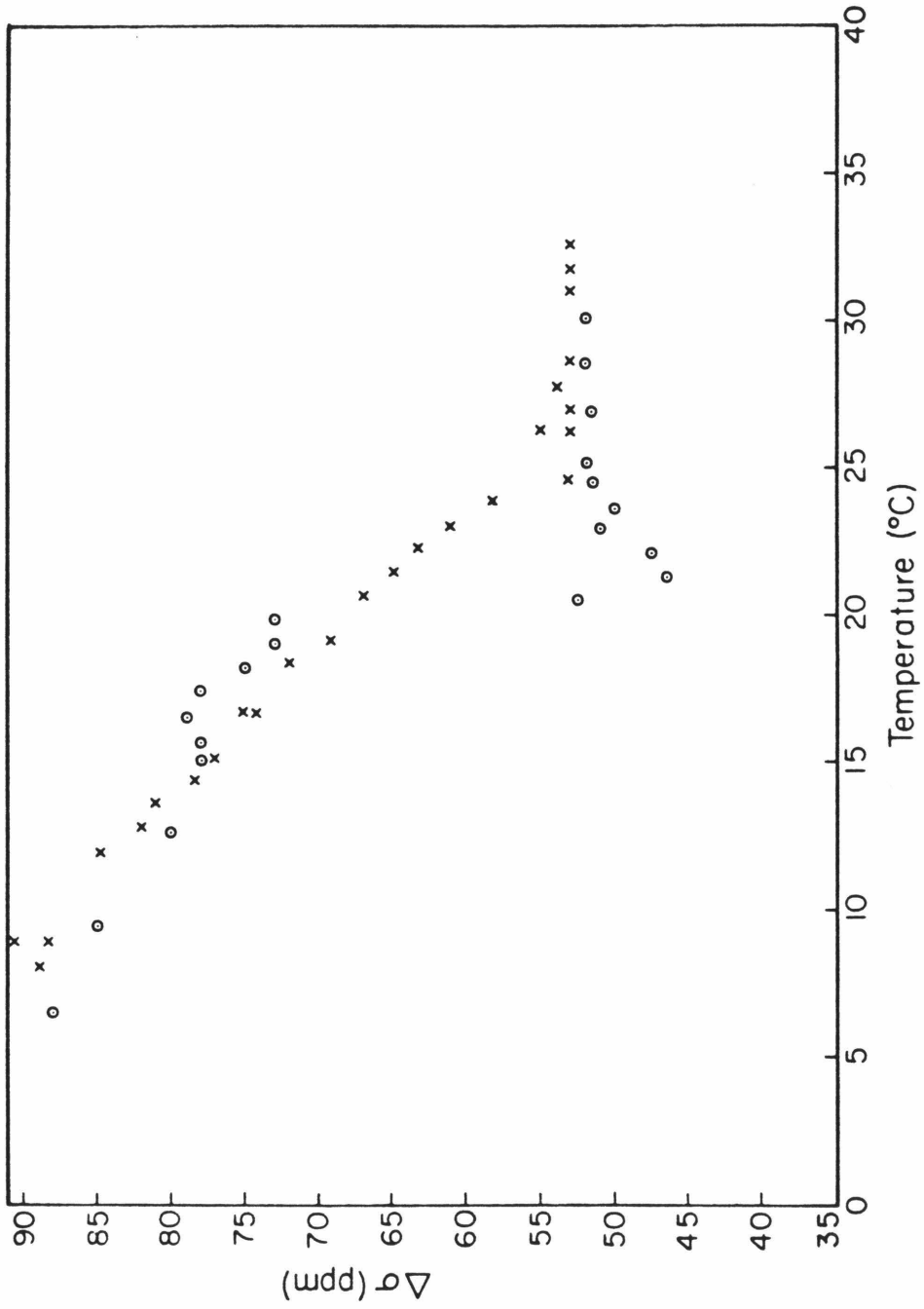
Δq (ppm)
Temperature (°C)
90
85
80
75
70
65
60
55
50
45
40
35
0
5
10
15
20
25
30
35
40

There is no noticable change in $\Delta\sigma$ of a multilayer when gramicidin-S is added except a sharp dip at the phase transition temperature where the spectrum (Figure II.12) shows definite signs of polymorphism. The appearance of the sharp peak at 0 ppm for gramicidin-S-DML mixtures is consistent with the observation that a lipid dispersion clarifies optically when gramicidin-S at a high concentration is added to it, indicating the formation of smaller (probably micellar) particles. These results are in sharp contrast to those observed for alamethicin where the axially averaged multilayer powder pattern is observed at all temperatures and at the low as well as high alamethicin to lipid ratio (1:15 and 1:2 respectively). There is no indication for lipid polymorphism. In addition, unlike the case of gramicidin-S, a large change in $\Delta\sigma$ is seen at all temperatures when alamethicin is added to multilayers indicating a strong interaction at the head group.

Chlorophyll-A introduces a minor difference in the shape of the P31 spectrum of multilayers (Figure II.14). The small low field shoulder is probably due to the reported compound formation at this concentration (Eigenberg et al., 1982a). No change in $\Delta\sigma$ is noted, but the phase transition temperaure is lowered by $7^{o}C$ (Figure II.15). This contrasts with the alamethicin/DML system at the same molar ratio (1:15) where no change in phase transition temperature or shape is seen, but a definite lowering of $\Delta\sigma$ is observed.

F. DISCUSSION

An important subject of discussion in the recent literature is the mode of interaction of alamethicin with membrane bilayers in the absence of electric field. Earlier reports on alamethicin proposed surface activity

Figure II.14. P31 spectra (202.49 MHz) of DML multilayers containing chlorophyll A. The sample contains 15:1 mole ratio of DML:chlorophyll A.

a. 22° C (above phase transition temperature)

b. 14° C (below phase transition temperature)

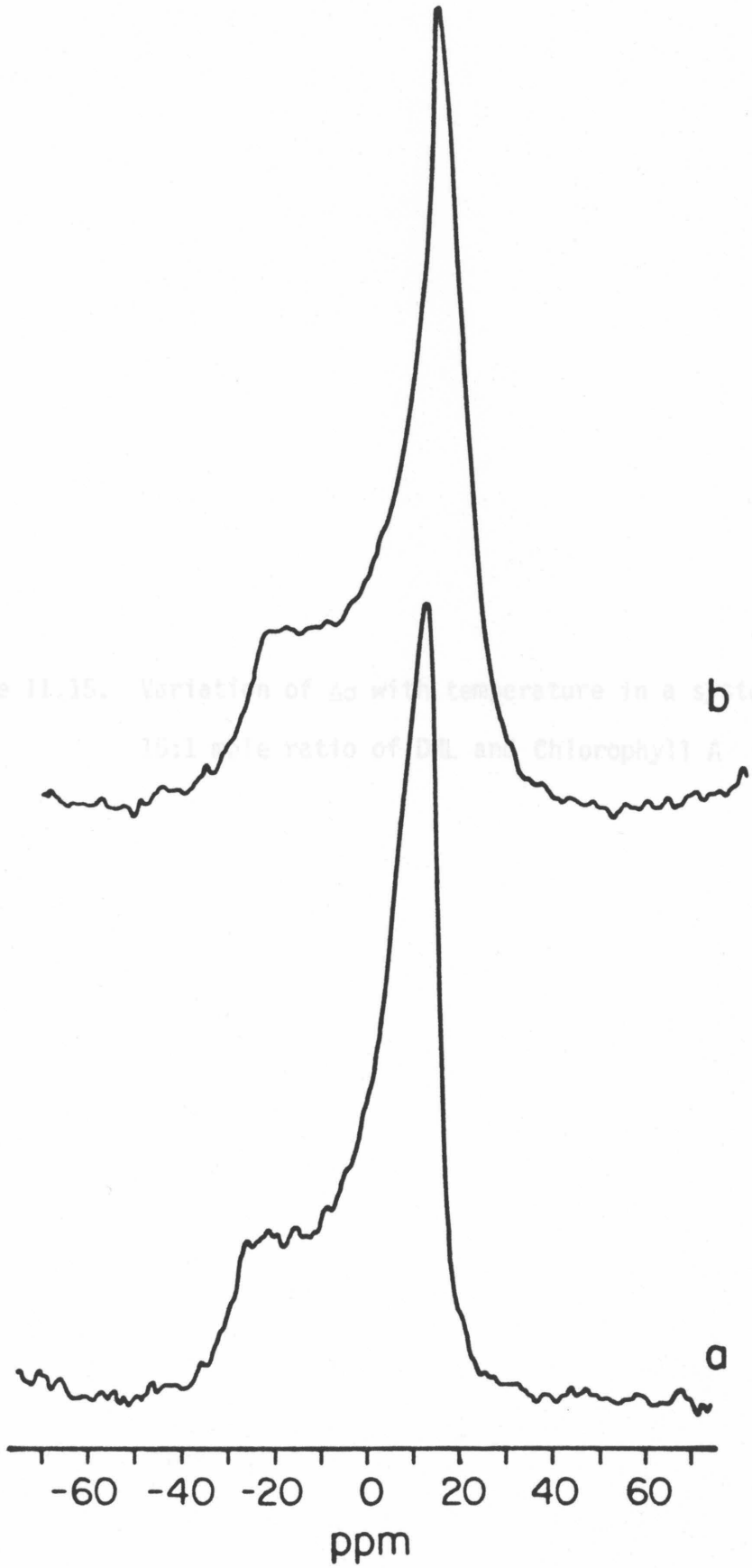
b
a
-60
-40
-20
0
20
40
60
ppm

Figure II.15. Variation of $\Delta\sigma$ with temperature in a system containing 15:1 mole ratio of DML and Chlorophyll A

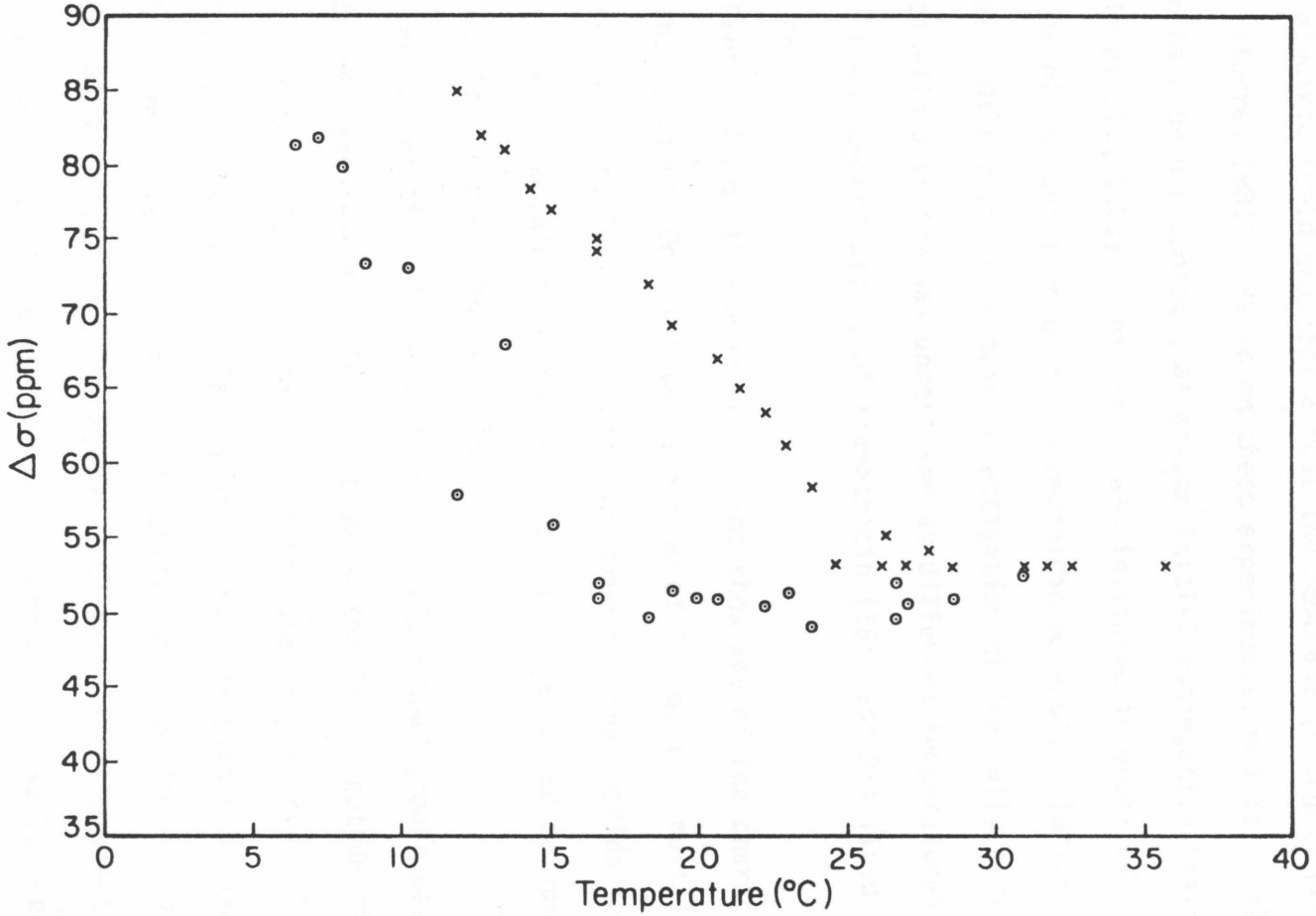
90
85
80
75
70
65
60
55
50
45
40
35
Δσ(ppm)
0
5
10
15
20
25
30
35
40
Temperature (°C)

(Lau and Chan, 1975, 1976); recently however, a number of investigators has claimed that the molecule is absorbed in the bilayer even when there is no electric field gradient across the membrane (Fringeli and Fringeli, 1979; Latorre, 1981). Based on these experiments, models of alamethicin action have been proposed that assume initial aggregation inside the membrane (Boheim et al., 1983). This study was initiated in order to resolve the question of the position of the alamethicin molecule relative to the lipid bilayer. Direct spectroscopic investigation of the fully hydrated alamethicin-lipid system was undertaken at different temperatures with relatively high concentrations of alamethicin (15:1 and 2:1 lipid :ala methicin molar ratio).

Proton NMR of this mixture did not show any of the characteristic peaks from the peptide. Only a broad spectrum of lipids in a multilayer is observed (not shown). The lack of a proton spectrum for the peptide indicates that in this system alamethicin is very strongly aggregated and motionally hindered; this results in broad NMR signals.

The interaction of alamethicin with lipid head groups was established by P31 NMR measurements. The spectrum of the lipid-peptide mixture is shown in Figure II.6. The pattern of the spectrum is typical of a multilamellar system that shows layers of essentially planar bilayers with complete axial motional averaging of the P31 shift tensor of the lipid head groups. Throughout the experiments, at all temperatures, even at the highest alamethicin-lipid ratio (1:2) and in the absence or presence of salt, the bilayer phase of DML is maintained. This is evidenced by the complete lack of all extra resonances that characterize lipid polymorphism (Cullis and DeKruijff, 1978).

No micelles, small vesicles or hexagonal phases result from the interaction of alamethicin with DML multilayers. This is unlike what has been seen for some gramicidin A-lipid systems by DeKruiff and coworkers (Van Echteld et al. 1981) and for gramicidin-S and chlorophyll-A (ibid Chapter II.3C). No major change in the DML bilayer structure is caused by alamethicin.

While no qualitative change in the shape of the spectrum is noted, the value of $\Delta\sigma$ is consistently lower at all temperatures in the presence of the peptide (Figure II.7). The observed lowering of $\Delta\sigma$ can be discussed now in the context of the simulation results noted in the previous chapter. Lowering of $\Delta\sigma$ has been commonly associated in the literature with increased motional disorder. It has been shown in the previous chapter, however, that changes in diffusion constants near the fast anisotropic diffusion limit do not affect the value of $\Delta\sigma$. The axially averaged bilayer spectrum of DML with alamethicin can only be obtained with rapid rotation of P-O bonds and fast rotational diffusion of the lipids. Increase in the rates of fast diffusion would not any further decrease the value of $\Delta\sigma$. The change in $\Delta\sigma$ is therefore interpreted to be caused by slight changes in the average tilt angle of the lipid head group in the presence of alamethicin. As is illustrated in table II.1, relatively minor changes in θ and ϕ ($\lesssim 5^{o}$) can explain the reduction of $\Delta\sigma$ seen in these studies. In fact $\theta = 79^{o}$ and $\phi = 78^{o}$ simulates the spectrum of the alamethicin/DML system exactly while the angles that fit the DML $\Delta\sigma$ best are $\theta = 83^{o}$ and $\phi = 75^{o}$. Since the head groups in DML are zwitterionic, a change in the average orientation in a few lipids is expected to propagate cooperatively through the bilayer by electrostatic interactions, resulting in the observed changes in $\Delta\sigma$.

The other change in the spectrum of DML seen on adding alamethicin to multilayers is an increase in the height of the low field "foot". This is expected to be caused by small changes in T_2^{-1} due to a change in the direct magnetic dipolar interaction of the protons on alamethicin with the phosphorus of the head group. $\Delta\nu_{1/2}$ does not change when alamethicin is added to bilayers. This parameter is a measure of inter and intra molecular H1-P31 coupling and is likely to be affected only by increased motion of the lipid molecule as a whole.

The gel-liquid crystalline phase transition temperature T_c changes very little upon addition of alamethicin to DML multilayers. As seen in Figure II.6, there is no measurable shift in T_c at alamethicin to lipid ratio of 1:15. At much higher ration (1:2), a shift of about 4^oC is seen. Only minor effects on T_c are expected by the action of surface active moeties. Larger effects on the phase transition temperature are seen at lower mole ratios, e.g., the case of chlorophyll A, where the phytol chain interchelates into the bilayer.

Conclusive evidence for the nonperturbation of the lipid chains by alamethicin comes from H2 NMR of chain perdeuterated lipid. In a deuterium quad-echo spectrum, the splitting ν_D^i due to each deuteron is a function of the order parameter (eqn. II.7). As has been shown in Fig. II.11, a broadening of the peak at the extreme edges of the spectrum is noted. This suggests an interaction near the bilayer interface. No other change in the pattern of the spectrum or in ν_D^i's is observed. Interaction of alamethicin with lipid membranes does not affect the order parameters and relaxation times (cf. Seelig and Seelig, 1978; Rice et al., 1979) of the side chain deuterons.

The results from H2 NMR have been further complemented by an investigation of the lipid chain conformation in the presence and absence of alamethicin

by Raman spectroscopy. The Raman intensity ratios I_{1065}/I_{1087}; I_{2890}/I_{2850} and I_{2850}/I_{2930} have been shown by Lis et al. (1976) to be sensitive to gauch-trans ratios and conformation of the phospholipid chains. In agreement with the NMR results, the Raman spectra show no change in the above ratios indicating that the presence of alamethicin does not change the conformation of the lipid side chains.

Since all ionic conductivity experiments are performed in the presence of salt, it was important for us to confirm whether the conclusions arrived at in the absence of salt are valid at higher ionic strengths. As shown in Fig. II.10, no change in $\Delta\sigma$ takes place in the 15:1 lipid to alamethicin sample when 0.5M NaCl is added. This indicates that the nature of perturbation is similar at the higher ionic strength. At the very high alamethicin concentration (2:1 lipid to alamethicin) the $\Delta\sigma$ actually goes up when salt is added. This points to the possible electrostatic nature of this lipid-peptide interaction at least above the phase transition temperature.

G. CONCLUSION

The interaction of alamethicin with fully hydrated DML multilayers has been investigated over a range of temperatures. The alamethicin molecule in this mixture is invisible to proton NMR; the P31 NMR of the lipid phosphate shows that the presence of alamethicin causes change in the average conformation headgroups without destroying the basic bilayer structure. No perturbation of the lower part of lipid side chains by alamethicin is noted by H2 NMR of chain perdeuterated lipids or by Raman spectroscopy.

The action of the alamethicin molecule in the presenceof an applied

field necessarily involves the formation of ion channels; the amphiphilic and aggregated secondary structure proposed Part I and the surface interaction demonstrated here is then consistent with micelles of alamethicin molecules aligning themselves at the interface of the bilayer in the absence of the field; channels would form when the aggregates enter the bilayer under the action of the field. In this final conducting state the hydrophobic faces would line up along the chains while the hydrophilic core would support a fluctuating higher dielectric channel.

Chapter III.1

The Phospholipid Arrangement in Small Bilayer Vesicles as Revealed by Proton Magnetic Resonance Studies at 500 MHz

A. INTRODUCTION

Phospholipid molecules in a biological membrane or in an aqueous dispersion undergo highly anisotropic motions (Bocian and Chan, 1978). The motional characteristics of the chains are naturally governed by the nature of packing of lipid molecules. It has been argued on geometric grounds (Sheetz and Chan, 1972; Huang and Mason, 1978) that the molecular packing in small unilamellar vesicles is dictated by the surface curvature and is highly asymmetric with respect to the inner and outer halves of the bilayer. Thus the motional freedom of chains in sonicated vesicles can be markedly different from that in multilamellar arrays. The first indication that there are motional differences in the chains between vesicles and multilayers came from nuclear magnetic resonance studies (Sheetz and Chan, 1972; Lichtenberg et al., 1975; Chan et al., 1973). Unfortunately, the analysis of NMR line shapes in terms of local segmental motion of the hydrocarbon chains and vesicle tumbling has been a controversial subject. It is now known from calorimetric data as well as NMR studies that the thermal phase transition behavior of saturated lipids is dramatically altered when lipid multilayers are sonicated to yield small unilamellar vesicles (Sheetz and Chan, 1972; Sturtevant et al., 1974; Gruenewald et al., 1979). Not only is the thermal transition broadened, the onset of the transition also occurs at a significantly lower temperature. Accompanying these effects is a corresponding decrease in the enthalpy and

entropy of the transition as well. Raman studies also suggest (Gaber and Peticolas, 1977) a significant difference in the "intermolecular order" of the chains between multilamellar dispersions and small single walled vesicles. Thus, surface curvature can have real effects on the structural and dynamical properties of a phospholipid bilayer membrane.

Since the two monolayers of a small bilayer vesicle exhibit curvature which is different in both magnitude and sign, it follows that one should expect structural and motional differences between them. Recent work on small vesicles has in fact emphasized such possible differences between the two halves of the bilayer. F19 NMR of vesicles comprised of lipids with fluorine substituted on the chain in fact showed chemical shift nonequivalence and resonance width difference between the fluorine labels located on the inside and outside chains of the vesicle (Longmuir and Dahlquist, 1976). Also choline methyl protons in the two halves of the bilayer exhibit different spin lattice relaxation times (Kroon et al., 1976) in addition to chemical shift nonequivalence (Eigenberg and Chan, 1980).

This chapter reports further characterization of small bilayer vesicles by H1 NMR at 500 MHz. At this frequency, one might expect the additional spectral dispersion to permit resolution of the hydrocarbon chain resonances from the two halves of the bilayer, given the packing arrangements and motional states that have been conjectured. This expectation is clearly borne out in the present study, as, in addition to the split head group resonances, two component peaks are also now observed for both the methylene and the methyl protons. Analysis of these spectra has provided additional insights into the effect of surface curvature on the structural and dynamical properties of bilayer vesicles.

B. MATERIALS AND METHODS

Synthetic lecithins were purchased from Calbiochem-Boehringer and found to be pure by thin-layer chromatography. Deuterium oxide (99.8 atom percent), all salts and EDTA were obtained from Aldrich Chemical Company.

Vesicles were prepared by ultrasonic irradiation of lipids dispersed in D_2O. The concentration of lipids used was 10 mg/ml in most experiments. Sonication was done with a model W-225R cell disrupter from Ultrasonics Inc. using a microtip at a power setting of 5-6 and a 50% duty cycle for 20-30 min. During this period the sample tube was immersed in a glycerol bath to prevent overheating. The resulting clear solution was then centrifuged for 5 min to remove any large particles.

The samples containing manganese ions were prepared by dilution of sonicated vesicles with appropriate solutions to maintain osmotic balance across the bilayer membrane (see figure legend for details).

Proton NMR spectra were recorded at various temperatures on a Bruker WM500 spectrometer operating at a field strength of 11.74 tesla (500.13 MHz proton frequency). The magnetization transfer experiments were performed by irradiating the acyl resonances until a steady state was reached. The amplitude of irradiation (γH_2) was kept at approximately 30 Hz to prevent spillovers. H_2 was then turned off and a strong nonselective 90^o pulse was applied to generate a free induction decay. The sequence was then repeated for signal enhancement.

C. RESULTS

The 500 MHz proton NMR spectra of dipalmitoyl phosphatidyl choline vesicles, recorded at various temperatures, are shown in Figure III.1. Throughout the temperature range examined, the choline N-methyl resonance (3.2 ppm) is resolved into two peaks. The larger, downfield component has been shown to arise from lipids located in the outer half of the bilayer, while the smaller peak is assigned to the inner-facing lipids (Sheetz and Chan, 1972). A similar inside-outside distribution with similar chemical shift differences is also seen for both the choline N-methylene signal (3.65 ppm) and the choline PO-methylene peak (4.25 ppm).

In a recent NMR study of distearoyl phosphatidyl choline vesicles it was reported that the inner monolayer choline methyl resonance undergoes an upfield shift of $\sim$0.04 ppm as the temperature is lowered through the thermal phase transition (T_c) (Eigenberg and Chan, 1980). The same phenomenon is observed for dipalmitoyl phosphatidyl choline with an identical upfield shift of the inner choline methyl resonance of 0.04 ppm, except that the shift begins at about 38^{o} C instead of 47^{o}C in the case of distearoyl phosphatidyl choline. In addition, both the inner N-methylene and the PO-methylene resonances display similar upfield shifts as the temperature is lowered through T_c.

The chain methylene protons alpha to the carbonyl give rise to a broad peak centered at 2.35 ppm which is made up of overlapping components. Below T_c, this signal as well as the β-position methylene centered at 1.55 ppm becomes extremely broad and is difficult to monitor. The remaining methylene protons give rise to a large asymmetric peak centered at $\sim$1.25 ppm. The composite peak appears to be made up of at least two overlapping components:

Figure III.1. 500 MHz proton NMR spectrum of dipalmitoyl phosphatidyl choline vesicles at various temperatures. Spectral assignments:

a. choline PO-methylene

b. glycerol CH

c. choline N-methylene

d. choline methyls

e. α-methylenes of the hydrocarbon chains

f. β-methylenes

g. bulk methylenes

g. terminal methyls


d
g'
g
d'
h
a
b
c
e
f
T(°C)
41.5
h'
h
37
36
35
34.5
4
3
2
1
PPM downfield from TMS

a broad downfield component and a narrower upfield component. Attempts to deconvolute this signal into two resonances yielded an apparent linewidth for the broad component that was two to three times larger than the narrow component. Both methylene components broaden and lose apparent intensity as the system is cooled below T_c. These spectral changes are accompanied by a downfield shift of the broad component with the lowering of temperature just above T_c, as illustrated for distearoyl lecithin vesicles in Figure III.2. Only the broad methylene component appears to have shifted ($\sim$30 Hz) over the range of temperature examined.

An analogous behavior is observed for the methyl resonance at 0.85 ppm. This peak is also split into two components. While the sharper component shows no detectable change in its chemical shift when the temperature is lowered, the broad resonance moves downfield by 19 Hz over the range of temperature investigated in the case of dipalmitoyl phosphatidyl choline.

Somewhat similar changes were observed for resonances of distearoyl lecithin and dimyristoyl lecithin (Figure III.3). In distearoyl lecithin, the bulk methylenes are better resolved and exhibit a temperature dependence in their chemical shifts similar to that for dipalmitoyl lecithin. The methyl signal for distearoyl lecithin, however, seems to be more symmetrical and shows no discernible chemical shift dispersion. In contrast, the methyl and bulk methylene signals of dimyristoyl lecithin are asymmetric over the full range of temperatures studied.

Assignment of Acyl Resonances

On the basis of the available data on lipid organization in vesicles, three alternative assignments for the split acyl resonances may be

Figure III.2. Variation of the resonance positions of the broad and sharp components of the chain methylene protons from distearoyl phosphatidyl choline vesicles vs. temperature. The chemical shifts have been corrected for the effect of temperature on the bulk magnetic susceptibility of the sample by referring them to the sharp component of the terminal methyl signal. Owing to the strong overlap of the two components, only the apparent positions of these resonances are plotted here. The experimental uncertainty in these measurements is ±1 Hz.

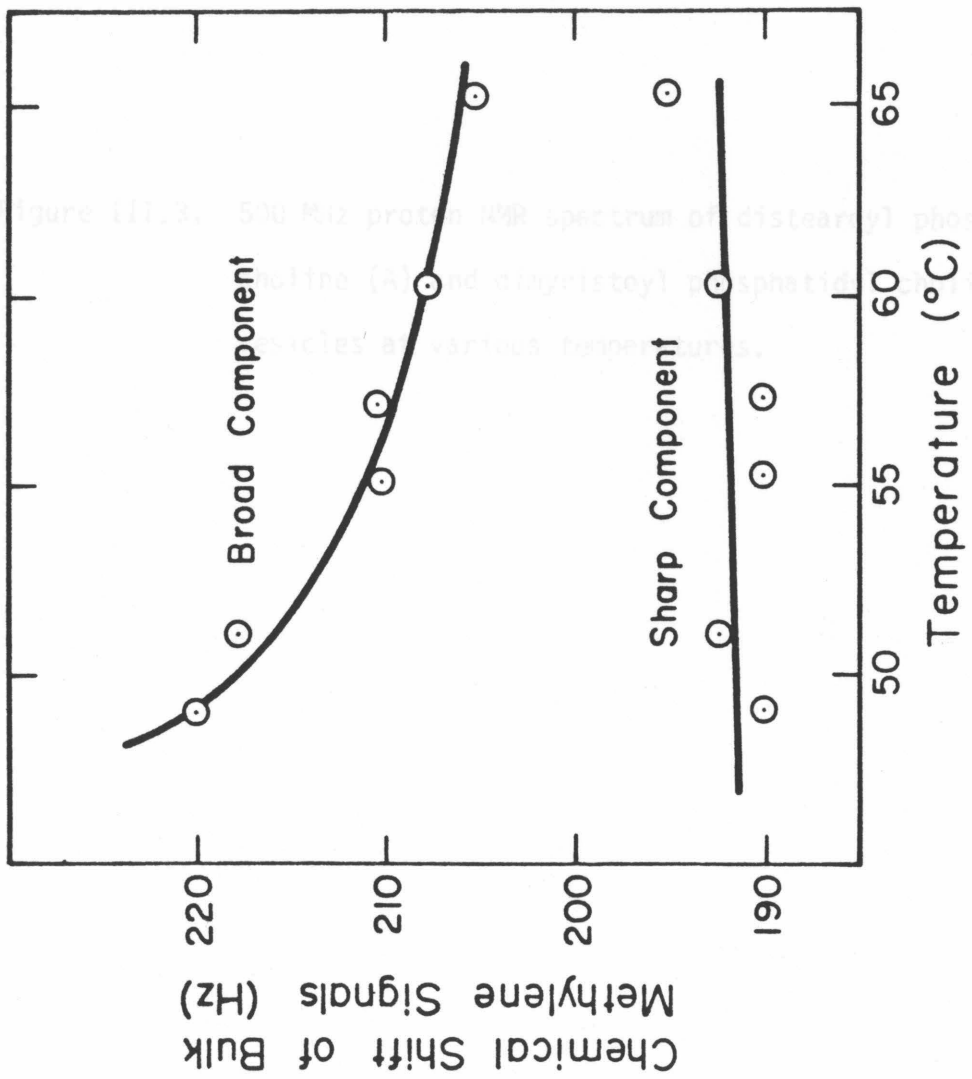
Chemical Shift of Bulk
Methylene Signals (Hz)
220
210
200
190
Broad Component
Sharp Component
50
55
60
65
Temperature (°C)

Figure III.3. 500 MHz proton NMR spectrum of distearoyl phosphatidyl choline (A) and dimyristoyl phosphatidyl choline (B) vesicles at various temperatures.

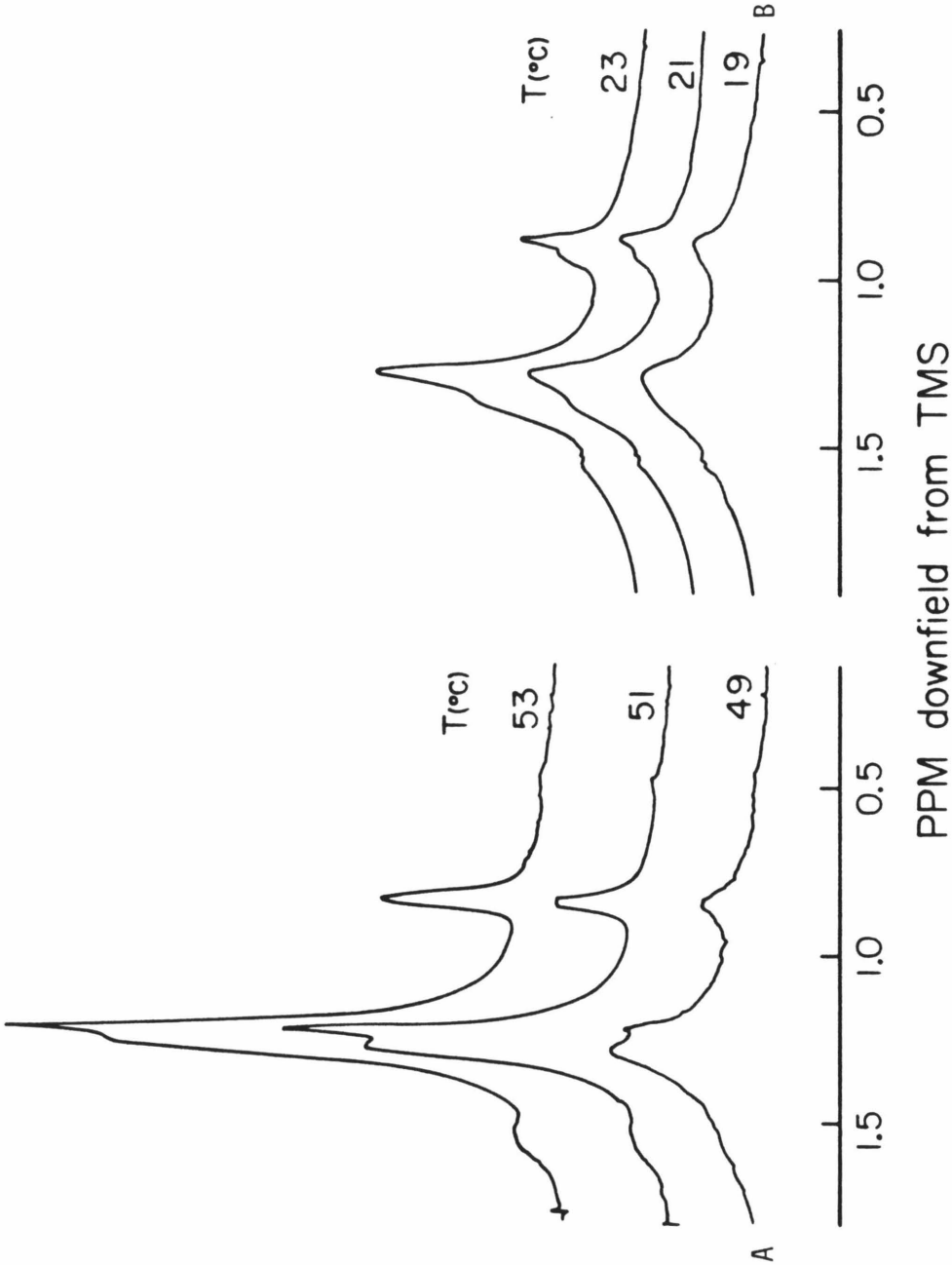
T(°C)
53
51
49
A
T(°C)
23
21
19
B
1.5
1.0
0.5
1.5
1.0
0.5
PPM downfield from TMS

considered. The possiblities are that the broad downfield and the narrow upfield components correspond to:

A a rigid upper segment and a more fluid lower segment of the hydrocarbon chain,

B the outside facing and inside facing lipid populations of the vesicle bilayer, or

C the acyl chains esterified to the 2-carbon and 3-carbon position of the lipid glycerol moiety.

In order to discriminate between these possibilities, the enhanced relaxation that a paramagnetic ion can have on a proton in its proximity is taken advantage of. In one series of experiments, isotonic vesicles with manganese ions in the external solution were prepared. In another, vesicles were prepared in manganese chloride and the potential effect of the broadening agent on the lipid molecules in the outer monolayer was quenched by chelating the manganese ions with EDTA. Since the vesicle bilayer is impermeable to the manganese ions under these conditions, the enhanced relaxation brought on by the presence of the paramagnetic ions result in preferential broadening of resonances arising from lipids in the monolayer directly in contact with them (Sheetz and Chan, 1982). As was expected, the downfield choline resonance is eliminated in the first series of experiments. In the second series of experiments, where both the inner and outer choline resonances were initially broadened beyond detection by the manganese, the outer choline resonance reappears when the external manganese is chelated with EDTA.

The effects of manganese, present only in the extravesicular medium, on the bulk methylene signal are shown in Figure III.4. External

Figure III.4. 500 MHz proton NMR spectrum of dipalmitoyl phosphatidyl choline vesicles at 36^{o}.

A. Vesicles prepared in 90 mM NaCl, diluted 1:1 (v/v) with 90 mM NaCl (control).

B. Vesicles prepared as in (A) but diluted 1:1 with 90 mM NaCl + 0.5 mM $MnCl_2$.

C. Vesicles prepared in 90 mM NaCl + 0.5 mM $MnCl_2$, diluted 1:1 with 60 mM EDTA.

D. Vesicles prepared as in (C) but diluted 1:1 with 90 mM NaCl + 0.5 mM $MnCl_2$.

Insert is a vertical expansion of the spectra in the region of the α-methylene resonances.

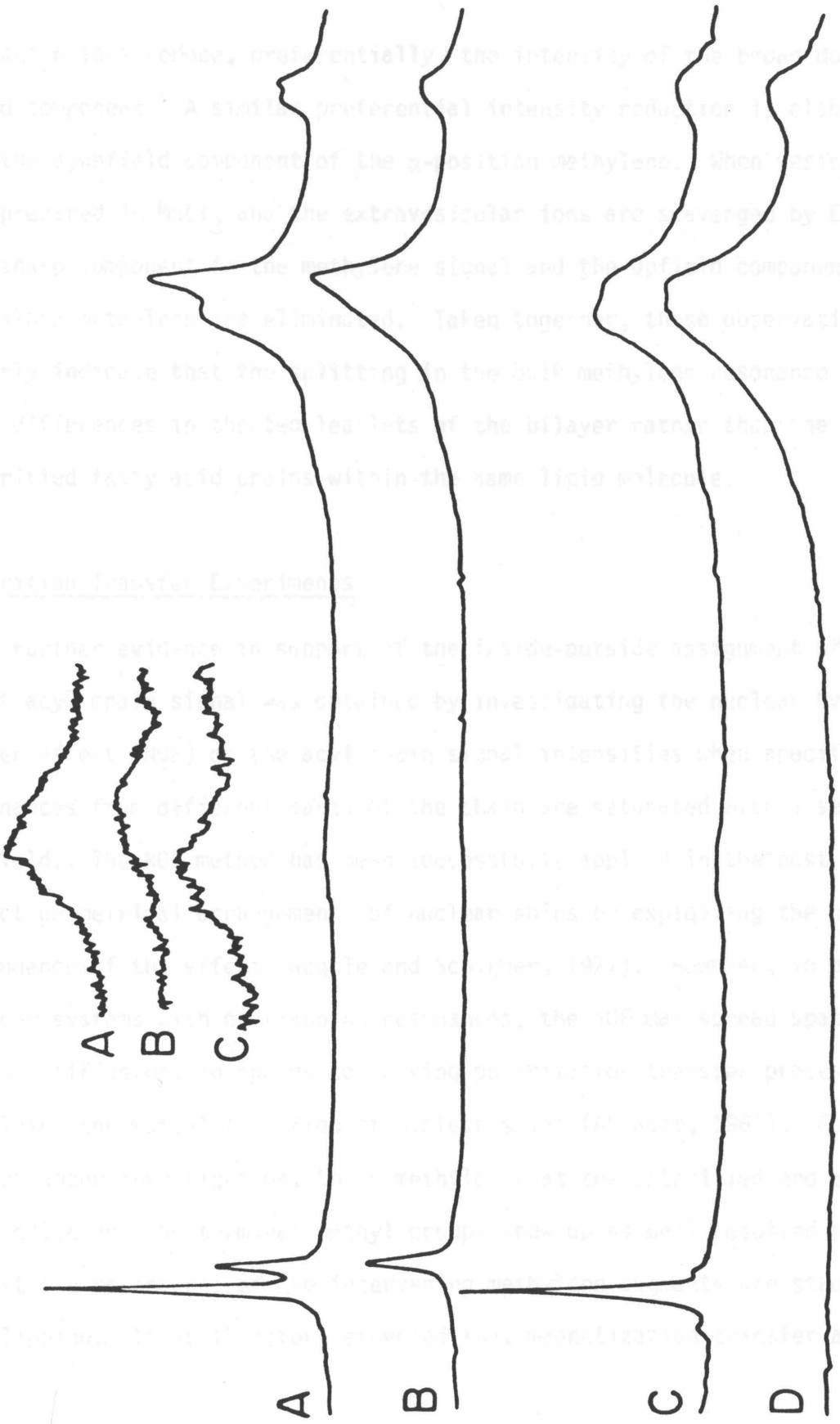
A
B
C
A
B
C
D

manganese ions reduce, preferentially, the intensity of the broad downfield component. A similar preferential intensity reduction is also seen for the downfield component of the α-position methylene. When vesicles are prepared in $MnCl_2$ and the extravesicular ions are scavenged by EDTA, the sharp component in the methylene signal and the upfield component of the alpha methylene are eliminated. Taken together, these observations clearly indicate that the splitting in the bulk methylene resonance arises from differences in the two leaflets of the bilayer rather than the two esterified fatty acid chains within the same lipid molecule.

Saturation Transfer Experiments

Further evidence in support of the inside-outside assignment of the split acyl chain signal was obtained by investigating the nuclear Overhauser effect (NOE) on the acyl chain signal intensities when specific resonances from different parts of the chain are saturated with a second rf field. The NOE method has been successfully applied in the past to detect geometrical arrangements of nuclear spins by exploiting the distance dependence of the effect (Noggle and Schirmer, 1971). However, in multinuclear systems with overlapping resonances, the NOE may spread spatially by spin diffusion, an energy conserving polarization transfer process involving the mutual flip-flop of nuclear spins (Abragam, 1961). For the system under investigation, the α-methylenes at the esterified end of the acyl chain and the terminal methyl groups show up as well resolved signals, whilst the resonances of the intervening methylene segments are strongly overlapping. It is therefore expected that magnetization transfer along

these hydrocarbon chains would occur chiefly by spin diffusion, particularly when the chain is sufficiently rigid that the dipolar coupling between CH_2 segments favors cross relaxation over T_1 relaxation at the various sites. Only at the ends of the hydrocarbon chains will magnetization exchange occur via the nuclear Overhauser mechanism.

The results of the saturation transfer experiments are presented in Figure III.5, where the effect of selective saturation of either the α-methylenes or the terminal methyls on the bulk methylene signal is seen. In both cases, one observes a negative NOE for the downfield component of the split bulk methylene signal. The narrower, upfield component is affected to a significantly lesser extent. The preferential saturation of the downfield component of the bulk methylene and the methyl signals, when the α-methylene protons are irradiated, as well as the preferential saturation of the downfield components of the bulk methylenes when the terminal methyls are saturated indicates clearly that the broader bulk methylene and terminal methyl components of the signals arise from one complete lipid chain along which transfer of saturation is quite efficient, while the sharp components arise from lipid chains that are less rigid and have a lower efficiency for saturation transfer. These results are consistent with the assignment of the two component peaks of the acyl resonances to the chains of the two leaflets of the bilayer. Inasmuch as the broad downfield resonance is assigned to the protons on the outer chains and the sharper upfield resonances to the protons on the inside chains, we infer from the apparently broader resonance widths and the preferential negative NOE observed for the lipids in the outer monolayer, that there is a greater degree of motional restriction for these chains in bilayer vesicles.

Figure III.5. Saturation transfer experiments on dipalmitoyl phosphatidyl choline vesicles at 37^{o}.

A. Normal proton spectrum of acyl chain resonances at 500 MHz.

B. Spectra obtained upon irradiation near the chain methyl resonances.

C. Resultant spectrum when the α-position methylene resonance is selectively saturated.

D. Resultant spectrum when the β-position methylene resonance is selectively saturated.

Arrows indicate the frequency at which saturating signals were applied.

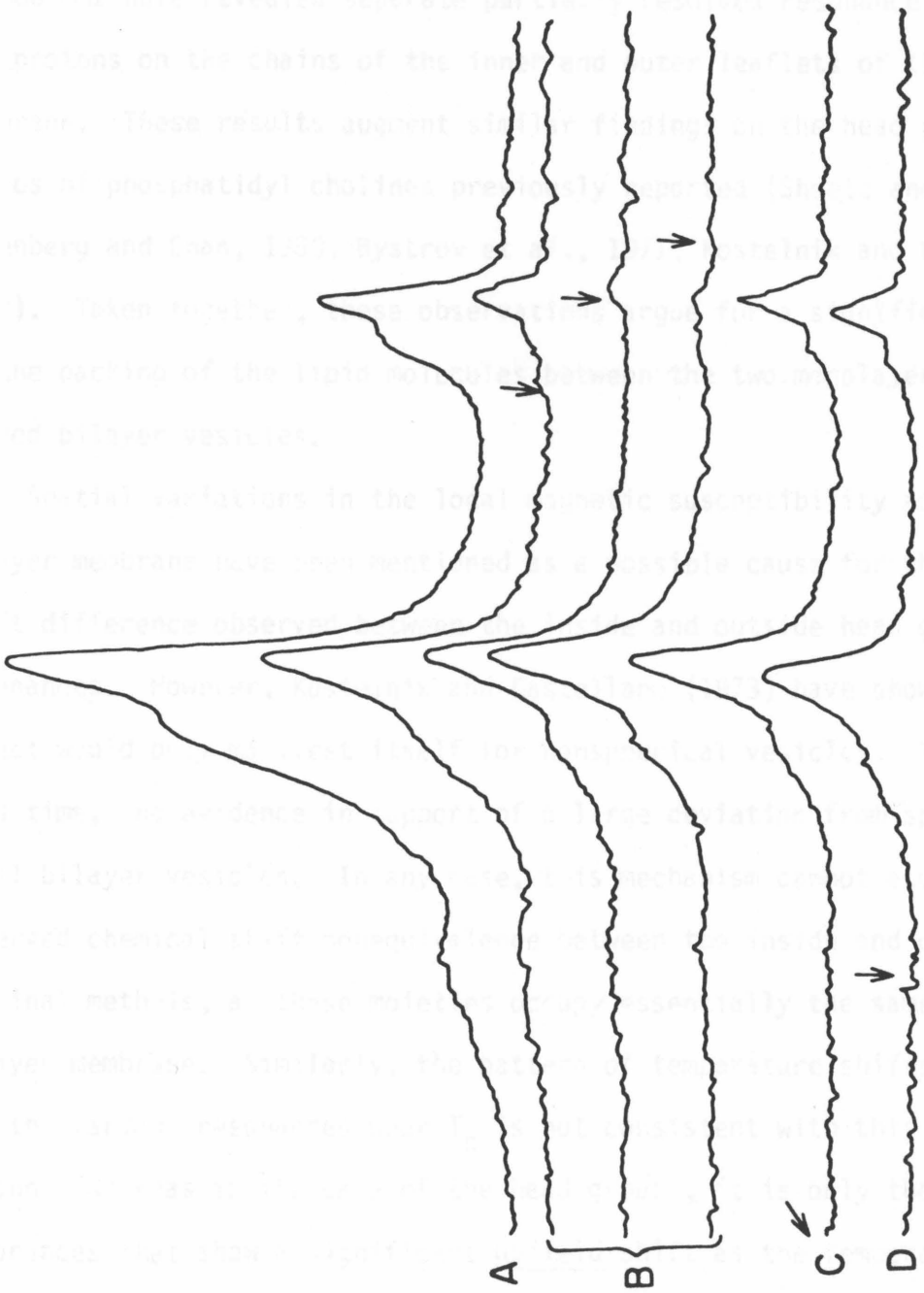
A
B
C
D

D. DISCUSSION

The present proton NMR studies of small unilamellar lecithin vesicles at 500 MHz have revealed separate partially resolved resonance peaks for the protons on the chains of the inner and outer leaflets of the bilayer membrane. These results augment similar findings on the head group resonances of phosphatidyl cholines previously reported (Sheetz and Chan, 1972; Eigenberg and Chan, 1980; Bystrov et al., 1971; Kostelnik and Castellano, 1973). Taken together, these observations argue for a significant difference in the packing of the lipid molecules between the two monolayers of a highly curved bilayer vesicles.

Spatial variations in the local magnetic susceptibility across the bilayer membrane have been mentioned as a possible cause for the chemical shift difference observed between the inside and outside head group resonances. However, Kostelnik and Castellano (1973) have shown that this effect would only manifest itself for nonspherical vesicles. There is, at this time, no evidence in support of a large deviation from sphericity for small bilayer vesicles. In any case, this mechanism cannot account for the observed chemical shift nonequivalence between the inside and outside terminal methyls, as these moieties occupy essentially the same part of the bilayer membrane. Similarly, the pattern of temperature shifts observed for the various resonances near T_c is not consistent with this interpretation. Whereas in the case of the head groups, it is only the inside resonances that show a significant upfield shift as the temperature is lowered through T_c, for the chain resonances, it is the outside chain protons that move as the temperature is varied near T_c. Unfortunately,

the methylene peaks become very broad near T_c and it was not possible to monitor them over the entire phase transition region. Nevertheless, it was possible to ascertain that the bulk methylene signal arising from the chains of the outer leaflet undergoes a displacement towards lower fields as the temperature is decreased towards T_c. These observations could only be rationalized in terms of intrinsic packing differences between the lipid molecules located in the two leaflets of the bilayer and concomitant variations in the packing characteristics that must necessarily accompany the thermal phase transition under the geometrical constraints imposed by the extreme surface curvature.

The temperature shifts observed for the chain protons on the outer leaflet and the inner head group resonances are readily understood on the basis of well documented chemical shift mechanisms (Emsley et al., 1966). With respect to chain packing, it is now generally accepted that the major forces of interaction between two lipid chains at short ranges ($\sim$5 Å) are those of the van der Waals type. This interaction causes expansion of the electronic cloud around the protons of the methylene segments, which in turn leads to a reduction in the contribution of these electrons to the magnetic shielding of the protons from the applied magnetic field. It then follows that the more tightly packed the hydrocarbon chains become, the greater the deshielding of the protons associated with these chains. For the problem at hand, since the two leaflets exhibit surface curvature differing in both magnitude and sign, the outer hydrocarbon chains are necessarily on the average more tightly packed than the inner chains (Huang and Mason, 1978; Chrzeszczyk et al., 1977). This packing difference would explain their intrinsically lower field position in the proton NMR

spectrum as well as the additional shift toward lower field as the bilayer is condensed into the gel phase. In contrast, electrostatic effects must dominate the intermolecular shifts of the resonances from the switterionic head groups. Again, because of the "wedge" effect, the packing of the inner head groups must more closely resemble that in a flat bilayer, whereas the head groups located at the vesicle surface must be quite loosely packed. Accordingly, one expects a more substantial electrostatic contribution to the chemical shift of the inner head groups as well as a greater sensitivity of these resonances to the packing changes brought about by the thermal phase transition of the lipid.

The intrinsic asymmetry of a highly curved bilayer vesicle is manifested not only as a chemical shift nonequivalence between the protons from the two halves of the bilayer but also differences in resonance widths. While it is not clear to what extent the different linewidths of the inner and outer bulk methylene peaks reflect different chemical shift dispersion of the various methylene segments along the hydrocarbon chains between the two leaflets rather than different relaxation rates arising from motional differences, the observed linewidth nonequivalence observed for the inner and outer terminal methyl resonances most certainly arises from different degrees of motional restriction and rates of segmental motions between the two types of chains. It is evident from the saturation transfer experiments that the hydrocarbon chains located on the outer leaflets are indeed motionally more restricted than their counterparts in the opposing leaflet.

The motional state of the lipid molecules in a small vesicle is highly complex not only because of the intrinsic bilayer asymmetry, but also because

of the multiplicity of motions that can occur. On the local level, in addition to fast bond isomerizations along the hydrocarbon chains, there exist bulk motions corresponding to fluctuations of the hydrocarbon chains about the bilayer normal. On the more global scale, the lipid molecules can undergo lateral diffusion along the plane of the vesicle surface, flip-flop exchanges between the two leaflets and in addition, the entire bilayer unit can experience slow Brownian type overall tumbling motions in the medium it is suspended. Generally speaking, the local segmental motions are rapid whereas the global motions are slow. Those specific motions that are primarily effective in averaging the magnetic dipolar interactions among the spins in the vesicle may be inferred from the results of our saturation transfer experiments. According to the theory of Balaram et al. (1973), the NOE's obtained under the conditions of our experiment (11.7 Tesla) should be negative if all the above motional processes contribute to the motional averaging. In fact, if the dipolar averaging is dominated by vesicle tumbling and lateral diffusion of the lipid molecules, as has been assumed in a number of treatments, the NOE factor would be -1, i.e. the resonance peaks would be completely saturated. In actuality, only an incomplete transfer of saturation is observed even in the steady state irradiation experiments.

In conclusion, the present work confirms the general picture on vesicles structure and lipid chain packing and dynamics that was put forward originally by Sheetz and Chan (1972) and elaborated by others (Huang and Mason, 1978; Chrzeszczyk et al., 1977). It is evident that surface curvature can affect the packing of the lipid molecules in bilayer membranes in subtle and important ways.

References

Abragam, A. (1961) The Principles of Nuclear Magnetism, Oxford University Press, London.

Anil Kumar, Ernst, R. R. and Wüthrich, K. (1980) Biochem. Biophys. Res. Commun. 95, 1.

Aue, W. P., Bartholdi, E. and Ernst, R. R. (1976) J. Chem. Phys. 64, 2229.

Balaram, P., Bothner-By, A. A. and Breslow, E. (1973) Biochemistry, 12, 4695.

Balasubramanian, T. M., Kendrick, N. C. E., Taylor, M., Marshall, G. R., Hall, J. E., Vodyanoy, I. and Reusser, F. (1981) J. Am. Chem. Soc. 103, 6127.

Banerjee, U., Tsui, F. P., Balasubramanian, T. N., Marshall, G. R., and Chan, S. I. (1983) J. Mol. Biol. 165, 757.

Bean, R. C., Sheppard, W. C., Chan, M., and Eichner, J. (1969) J. Gen. Physiol. 53, 741.

Bloch, F., Hausen, W. W. and Packard, M. (1946) Phys. Rev. 69, 127.

Bocian, D. F. and Chan, S. I. (1978) Ann. Rev. Phys. Chem. 29, 307.

Boheim, G. (1974) J. Membr. Biol. 19, 277.

Boheim, G. and Kolb, H. A. (1978) J. Membr. Biol. 38, 99.

Boheim, G., Hanke, W. and Jung, G. (1983) Biophys. Struct. Mech. 9, 187.

Bystrov, W. F., Dubrovina, N. I., Barsukov, L. I. and Bergelson, L. D. (1971) Chem. Phys. Lipids, 6, 343.

Bystrov, V. F. (1976) Progress in NMR Spectroscopy, 10, 41.

Calahan, M. and Hall, J. E. (1982) J. Gen. Physiol. 79, 411.

Campbell, R. F., Meirovitch, E. and Freed, J. H. (1979) J. Phys. Chem. 83, 525.

Chan, S. I., Sheetz, M. P., Seiter, C. H. A., Feigenson, G. W., Hsu, M., Lau, A. and Yau, A. (1973) Ann. N.Y. Acad. Sci. 222, 499.

Chrzeszczyk, A., Wishnia, A. and Springer, C. S. (1977) Biochim. Biophys. Acta, 470, 161.

Cullis, P. R. (1976) FEBS Lett. 68, 173.

Cullis, P. R. and DeKruijff, B. (1978) Biochim. Biophys. Acta. 507, 207.

Davis, D. G. and Gisin, B. F. (1981) FEBS Lett. 133, 247.

DeKruijff, B., Cullis, P. R., Radda, G. K. and Richards, R. E. (1976) Biochim. Biophys. Acta, 419, 411.

Den Hollander, J. A., Brown, T. R., Ugurbil, K. and Shulman, R. G. (1979) Proc. Natl. Acad. Sci. U.S.A. 76, 6096.

Dickerson, R. E. and Geis, I. (1969) The structure and action of proteins, W. A. Benjamin, Inc. 27.

Donovan, J. J. and Latorre, R. (1979) J. Gen. Physiol. 73, 425.

Eigenberg, K. E. and Chan, S. I. (1980) Biochim. Biophys. Acta, 599, 330.

Eigenberg, K. E., Croasmun, W. R. and Chan, S. I. (1982a) Biochim. Biophys. Acta, 679, 353.

Eigenberg, K. E., Croasmun, W. R. and Chan, S. I. (1982b) Biochim. Biophys. Acta, 679, 361.

Eisenberg, M., Hall, J. E. and Mead, C. A. (1973) J. Membr. Biol. 14, 143.

Emsley, J. W., Feeney, J. and Sutcliffe, R. H. (1966) High Resolution Nuclear Magnetic Resonance Spectroscopy, Pergamon Press, London, 841.

Ernst, R. R. (1975) Chimia, 79, 179.

Farrar, T. C., and Becker, E. D. (1971) Pulse and Fourier Transform NMR, Academic Press Inc., NY., 22.

Fox, R. O. and Richards, F. M. (1982) Nature, 300, 325.

Fox, R. O. and Richards, F. M. (1982) Biophys. J. 37, 179a.

Freed, J. H., Bruno, G. V. and Polnaszek, C. F. (1971) J. Phys. Chem. 75, 3385.

Freeman, R., Morris, G. A. and Turner, D. L. (1977) J. Magn. Reson. 26, 373.

Fringeli, U. P. and Fringeli, M. (1979) Proc. Natl. Acad. Sci. U.S.A., 76, 3852.

Gaber, B. P. and Peticolas, W. L. (1977) Biochim. Biophys. Acta, 465, 260.

Gally, H. U., Niederberger, W. and Seelig, J. (1975) Biochemistry, 14, 3647.

Gisin, B. F., Kobayashi, S. and Hall, J. E. (1977) Proc. Natl. Acad. Sci. U.S.A., 74, 115.

Gisin, B. F., Davis, D. G. Borowska, Z. K., Hall, J. E. and Kobayashi, S. (1981) J. Am. Chem. Soc., 103, 6376.

Gordon, L. G. M. and Haydon, D. A. (1976) Biochim. Biophys. Acta, 436, 541.

Gruenewald, B., Stankowski, S. and Blume, A. (1979) FEBS Lett. 102, 227.

Hall, J. E. (1981) Biophys. J. 33, 373.

Hauser, H., Finer, E. G. and Chapman, D. (1970) J. Mol. Biol. 53, 419.

Hodgkin, A. L. and Huxley, A. F. (1952) J. Physiol. 117, 500.

Hoult, D. I. and Lauterbur, P. C. (1979) J. Magn. Reson. 34, 425.

Huang, C. and Mason, J. T. (1978) Proc. Natl. Acad. Sci. U.S.A. 75, 308.

Irmscher, G. and Jung, G. (1977) Eur. J. Biochem. 80, 165.

Israelachvili, J. N., Marčelja, S. and Horn, R. G. (1980) Quart. Rev. Biophys. 13, 121.

Jeener, J., Meier, B. H., Bachman, P. and Ernst, R. R. (1979) J. Chem. Phys. 71, 4546.

Jones, L. R., Maddock, S. W. and Besch, H. R. (1980) J. Biol. Chem. 255, 9971.

Kohler, S. J. and Klein, M. P. (1976) Biochemistry, 15, 967.

Kohler, S. J. and Klein, M. P. (1977) Biochemistry, 16, 519.

Kolb, H. A. and Boheim, G. (1978) J. Membr. Biol. 38, 151.

Kostelnik, R. J. and Castellano, S. M. (1973) J. Magn. Reson. 9, 291.

Krauss, E. M. and Chan, S. I. (1983) Biochemistry, in press.

Kroon, P. A., Kainosho, M. and Chan, S. I. (1976) Biochim. Biophys. Acta, 433, 282.

Kumar, A., Wagner, G., Ernst, R. R. and Wüthrich, K. (1980a) Biochem. Biophys. Res. Commun. 96, 1156.

Kumar, A., Ernst, R. R. and Wüthrich, K. (1980b) Biochem. Biophys. Res. Commun. 95, 1.

Latorre, R., Miller, C. G. and Quay, S. (1981) Biophys. J. 36, 803.

Latorre, R. and Alvarez, D. (1981) Physiol. Rev. 61, 77.

Lau, A. L. Y. and Chan, S. I. (1975) Proc. Natl. Acad. Sci. U.S.A. 72, 2170.

Lau, A. L. Y. and Chan, S. I. (1976) Biochemistry, 15, 2551.

Leibfritz, D., Haupt, E., Dubischar, N., Lachman, H., Oekonomopulos, R. and Jung, G. (1982) Tetrahedron, 38, 2165.

Lichtenberg, D., Petersen, N. O., Girardet, J., Kainosho, M., Kroon, P. A., Seiter, C. H. A., Feigenson, G. W. and Chan, S. I. (1975) Biochim. Biophys. Acta, 382, 10.

Lis, L. J., Kauffman, J. W. and Shriver, D. F. (1976) Biochim. Biophys. Acta, 436, 513.

Longmuir, K. J. and Dahlquist, F. W. (1976) Proc. Natl. Acad. Sci. U.S.A. 73, 2716.

Marshall, G. R. and Balasubramanian, T. M. (1979) Pept. Struct. Biol. Funct. Proc. Am. Pept. Symp. 6th, 639.

Marshall, G. R. and Balasubramanian, T. M. (1979) Peptides: Structure and Biological Function (Proc. Sixth Am. Pept. Symp.) (Gross, E. and Meiehofer, J., eds.), Pierce Chem. Co., 639.

Martin, D. R. and Williams, R. J. P. (1976) Biochem. J. 153, 181.

Mason, R. P., Polnaszek, C. F. and Freed, J. H. (1974) J. Phys. Chem. 78, 1324.

Mathew, M. K., Nagaraj, R. and Balaram, P. (1981) Biochem. and Biophys. Res. Comm. 98, 548.

Mantsch, H. H., Hazime, S., Smith, I. C. P. (1977) Prog. NMR Spectr. 11, 211.

McLaughin, A. C., Cullis, P. R., Berden, J. A., Richards, R. E. (1975) J. Magn. Res. 20, 146.

McMullen, A. I., Marlborough, D. I. and Bayley, P. M. (1971a) FEBS Lett. 16, 278.

McMullen, A. I. and Stirrup, J. A. (1971) Biochim. Biophys. Acta, 241, 807.

Mohr, M. and Kleinkauf, M. (1978) Biochim. Biophys. Acta, 526, 375.

Mueller, P. and Rudin, D. O. (1968) Nature 217, 713.

Nagaraj, R. and Balaram, P. (1981) Acc. Chem. Res. 14, 356.

Nagaraj, R. and Balaram, P. (1981a) Biochemistry 20, 2828.

Nagaraj, R. and Balaram, P. (1981b) Tetrahedron 37, 1263.

Nagayama, K. (1981) Adv. Biophys. 14, 139.

Nagayama, K., Wuthrich, K., Bachmann, P. and Ernst, R. R. (1977) Biochem. Biophys. Res. Commun. 78, 99.

Nagayama, K., Wuthrich, K. and Ernst, R. R. (1979a) Biochem. Biophys. Res. Commun. 90, 305.

Nagayama, K., Bachman, P., Ernst, R. R. and Wuthrich, K. (1979) Biochem. Biophys. Res. Commun. 86, 218.

Nagayama, K. and Wuthrich, K. (1981) Eur. J. Biochem. 114, 365.

Noggle, J. H. and Schirmer, R. E. (1971) The Nuclear Overhauser Effect; Chemical Applications, Academic Press, New York.

Oekonomopulos, R., Jung, G., and Leibfritz, D. (1982) Tetrahedron 38, 2157.

Pandey, R. C., Cook, J. C. and Rinehart, K. L. (1977) J. Am. Chem. Soc. 99, 8469.

Payne, J. W., Jakes, R. and Hartley, B. S. (1970) Biochem. J. 117, 757.

Perrin, F. (1934) J. Phys. Radium, 5, 497.

Peterson, N. O. and Chan, S. I. (1977) Biochemistry 16, 2657.

Pulla Rao, C., Nagaraj, R., Rao, C. N. R. and Balaram, P. (1980) Biochemistry, 19, 425.

Purcell, E. M., Torrey, H. C. and Pound, R. V. (1946) Phys. Rev. 69, 37.

Rice, D. M., Hsung, J. C., King, T. E. and Oldfield, E. (1979) J. Am. Chem. Soc. 18, 5885.

Seelig, A. and Seelig, J. (1974) Biochemistry, 13, 4839.

Seelig, J. and Gally, H. U. (1976) Biochemistry, 15, 5199.

Seelig, J. (1977) Quart. Rev. Biophys. 10, 353.

Seelig, J. (1978) Biochim. Biophys. Acta, 515, 105.

Seelig, A. and Seelig, J. (1978) Z. Physiol. Chem. 359, 1747.

Seiter, C. M. A. and Chan, S. I. (1973) J. Am. Chem. Soc. 95, 7541.

Sheetz, M. P. and Chan, S. I. (1972) Biochemistry 11, 4573.

Skarjune, R. and Oldfield, E. (1979) J. Am. Chem. Soc. 18, 5903.

Smith, D. G., Pletnev, V. Z., Duax, W. L., Balasubramanian, T. M., Bosshard, H. E., Czerwinski, E. W., Kendrick, N. E., Mathews, F. S. and Marshall, G. R. (1981) J. Am. Chem. Soc. 103, 1493.

Sturtevant, J. M. (1974) Stud. Natl. Sci. N.Y. Vol. 4 (Quant. Stat. Mech; Natl. Sci., Coral Gables Conf. 1973), 63.

Van Echteld, C. J. A., Van Stigt, R., DeKruijff, B., Heunissen-Bijvelt, J., Verkleij, A. J. and DeGier, J. (1981) Biochim. Biophys. Acta, 648, 287.

Vodyanoy, I., Hall, J. E., Balasubramanian, T. M. and Marshall, G. R. (1982) Biochim. Biophys. Acta 684, 53.

Wagner, G., Anil Kumar and Wüthrich, K. (1981) Eur. J. Biochem. 114, 375.

Wagner, G. and Wüthrich, K. (1982) J. Mol. Biol. 155, 347.

Woessner, D. E. (1962) J. Chem. Phys. 37, 647.

Woessner, D. E., Snowden, B. S. and Meyer, G. H. (1969) J. Chem. Phys. 50, 719.

Wüthrich, K., Wider, G., Wagner, G. and Braun, W. (1982) J. Mol. Biol. 155, 311.

Yantorno, R. E., Takashima, S. and Mueller, P. (1977) Biophys. J. 17, 87.

Proposition I

Towards Neurospecificity, with Fluorescence Energy Transfer

1. Neurospecificity

During the development of the nervous system, nerves form synaptic connections with other cells in a precisely accurate and predetermined manner. The mechanism for this recognition process that sets up the neural network over rather long distances is unknown and constitutes the problem of neurospecificity. Dramatic experimental demonstration of neurospecificity is provided in leech where an individual severed nerve cell can grow back and selectively restore functional connections with identified target cells (Zipser and McKay, 1981). In amphibians and fish, rotations and transplantation of sensory structures such as the eyes have shown that input cells (i.e. retinal ganglion cells that will send axons to the brain) which are put in the ectopic positions can still send axons to the correct targets in the optic tectum (Jacbson, 1978). In drosophila, homeotic mutants exemplify neurospecificity. In the Antp and ss^a mutants, the antenna of the fly is in part converted into a leg. Stimulation of the ectopic leg still leads to probosis extension: a normal tarsus response but not an antenna response (Deak, 1976; Stocker, 1977). The transplanted sensory axons can therefore still make appropriate connections even though they enter the central nervous system by an anomalous route. The neurons seem somehow labeled so as to be found by the correct counterpart supporting Sperry's suggestion that chemical gradients exist across the nervous system (Sperry, 1945). The concept of chemical recognition or chemospecificity in neural recognition has been a topic of recurring discussions

over the years; and while growth molecules such as nerve growth factor (Levi-Montalcini, 1964; Levi-Montalcini and Cohen, 1960) and "glue molecules" such as N-CAM and L-CAM (Buskirk et al., 1980) have been shown to promote cell division and adhesion, respectively, no specificity in molecular recognition in the brain has been unraveled. It is proposed here that fluorescence labeled monoclonal antibodies to specific molecules in the nervous system be used in energy transfer experiments to derive information about the possible existence of molecular recognition processes that might trigger the feedback signal to terminate growth and form synaptic junctions.

2. Fluorescence Energy Transfer

Electronic excitation energy can be efficiently transferred over 10-60 Å. According to Förster (1948,1966), the rate of energy transfer K_T and the efficiency E are given by

$$K_T = r^{-6}K^2Jn^{-4}K_f \times 8.71 \times 10^{23} \text{ sec}^{-1}$$

$$E = r^{-6}/(r^{-6} + R_o^{-6})$$

Ro is the distance at which transfer efficiency is 50%, given by

$$R_o = (JK^2Q_on^{-4})^{1/6} \times 9.7 \times 10^3 \text{ Å}$$

r: distance between centers of the donor and acceptor chromophore.

K^2: orientation factor in the dipole-dipole interaction.

J: spectral overlap integral.

n: refractive index of medium between donor and acceptor.

K_R: rate constant for emission by the energy donor.

Q_o: quantum yield of fluorescence of the energy donor in the absence of acceptor.

For efficient energy transfer, the fluorescence emission spectrum of the donor must overlap the absorption spectrum of the acceptor (this gives a high J). The experimental technique typically requires two separate sets of intrinsically fluorescent or fluorescence labeled molecules that constitute the donor-acceptor pair. The donor is excited, usually with a laser, at its fluorescence excitation frequency; if the acceptor is within tens of angstroms over a reasonable time scale (microseconds at low temperatures in proteins), energy transfer follows. The fluorescence from the acceptor molecules is monitored using a steady state fluorimeter, a microscope, a flow cytometer or a fluorescence activated cell sorter. Usual steady state energy transfer techniques give an average value of the measured data over the whole sample. This is disadvantageous when the scattering intensity is high and when cell populations are heterogeneous. A newer flow technique (Tron et al., 1983) makes it possible to detect energy transfer on a cell by cell basis. Many donor-acceptor pairs are available (Stryer, 1978); fluorescein isothiocyanate and tetramethyl rhodamine is a good example of such a pair.

3. Fluorescence Energy Transfer as a Tool to Detect Chemically Induced Neurospecificity

Fluorescence energy transfer has been used as a "spectroscopic ruler" (Stryer, 1978) for measurement of distances between acceptor-donor pairs usually attached on different sites of protein or nucleotide molecules. Hahn and Hammes (1978) used this technique, for example, to obtain a structural map of acetyl transcarbonylase and have deduced the distance between catalytic sites of different subunits. Other systems investigated

have included Rhodopsin (Wu and Stryer, 1972) cytochromeC oxidase (Dockter et al., 1977) ribosomes (Huang et al., 1975) and transfer RNA (Beardsley and Cantor, 1970). More relevantly to our problem, intermolecular singlet energy transfer has been used by Gennis et al. (1972) for measuring distance between Trypsin, α chymotrypsin and their protein inhibitors.

Fluorescence labeling of individual molecular components in the nervous system would have been an impossible task but for the recent developments in hybridoma technology (Kohler and Milstein, 1975) that enable one to generate monoclonal antibodies of predefined specificity. Using this technique, Zipser and McKay (1981) were able to identify a large number of molecules that are specific to individual types of cell in the nervous system of leech. The method has also been applied successfully to Drosophila (Fujita et al., 1982).

The leech system is perhaps the simplest and most attractive for initial investigation of neurospecificity. Here the distribution of nerves and their connectivities are well understood. In addition, Zipser and McKay (1981) report that screening of 475 hybridomas have yielded about 300 nervous tissue reactive antibodies. Of these, about 40 make antibodies that identify single kinds of cells or small sets of cells. While many of these molecules are probably responsible for the general functions of the nervous system, a few, especially the ones that show up during development are expected to be responsible for neuronal recognition. Regeneration studies on nerves (Muller, 1979) are expected to provide useful hint about the molecules that are candidates for neurospecificity. In accordance with the principles of the fluorescence energy transfer technique, it will be necessary to make monoclonal antibodies against these proposed molecules, labeled with at

least two separate fluorophores to serve as the donor-acceptor pair. A complex formation between molecules that brings them closer than ~70 Å can then be detected by this technique as an indication of chemospecificity in neuronal recognition. The staining due to fluorescence labeled molecules can be easily observed over a light microscope, hence a photomultiplier tube assisted detection system should be sufficient to overcome the sensitivity problem in the detection of the energy transfer fluorescence signal.

The study can be repeated at different stages of development of the nervous system and linked with sequencing and gene cloning experiments (more likely in Drosophila) for a better understanding of the problem.

References

Beardsley, K. and Cantor, C. R. (1970) Proc. Natl. Acad. Sci. U.S.A. 65, 39.

Buskirk, D. R., Thiery, J. P., Rotishauser, U. and Edelman, T. M. (1980) Nature, 285, 488.

Deak, I. I. (1976) Nautre, 260, 252.

Dockter, M. E., Steinemann, A. and Schatz, G. (1977) J. Biol. Chem.

Fujita, S. C., Zipursky, S. L., Benzer, S., Ferrus, A. and Shotwell, S. L. (1982) Proc. Natl. Acad. Sci. U.S.A. 79, 7929.

Gennis, L. S., Gennis, R. B. and Cantor, C. R. (1972) Biochemistry, 11, 2517.

Hahn, L. H. E. and Hammes, G. G. (1978) J. Am. Chem. Soc. 17, 2423.

Huang, K. H., Fairclough, R. H. and Cantor, C. R. (1975) J. Mol. Biol. 97, 443.

Jacobson, M. (1978) Developmental Neurobiology, Plenum: New York and London, 562.

Köhler, G. and Milstein, C. (1975) Nature, 256, 495.

Levi-Montalcini, R. (1964) Science, 143, 105.

Levi-Montalcini, R. and Cohen, S. (1960) Ann. N.Y. Acad. Sci. 85, 324.

Muller, K. J. (1979) Biol. Rev. 54, 99.

Sperry, R. W. (1945) J. Physiol. 8, 15.

Stocker, R. F. (1977) J. Comp. Physiol. 115, 351.

Stryer, L. (1978) Ann. Rev. Biochem. 47, 819.

Trőn, L., Szöllősi, J., Damjanovich, S. H., Helliwell, S. H., Arndt-Jovin, D. J. and Jovin, T. M. (1983) Biophysical J., in press.

Wu, C. W., and Stryer, L. (1972) Proc. Natl. Acad. Sci. U.S.A. 69, 1104.

Zipser, B. and McKay, R. (1981) Nature, 289, 549.

Jacobson, M. (1978) Developmental Neurobiology, Plenum: New York and London, 562.

Proposition II

High Field PMR of Small Lipid Vesicles in Biomembrane Studies

An important aspect of research in membrane biology is the organization of nonlipid components or other membrane active molecules in the lipid bilayer matrix. Commonly asked questions include the position of these molecules relative to the bilayer, the nature of their interaction with lipids, the time scales of interaction and the dynamics and packing of these membrane components. The tools for such investigations generally require labeling the lipids or the interacting molecules with paramagnetic ESR spin labels, NMR labels such as C13, F19 or H2 or fluorescence active chromophores. Conventional proton NMR of lipid chains hardly affords any information since the large dipolar couplings between the protons in the chains give rise to broad and overlapping resonances. With the advent of high field NMR it is now possible to obtain more information from NMR of lipid side chains in small vesicles. It has been described in Part III of this thesis that the bulk methylene protons from the outside facing lipids show up as a peak distinctly separated and differently broadened from the peak arising from the methylene protons on the outside facing lipid chains (Figure P.1). The same is true of the terminal methyl group resonances. The distinction is due to the difference in the packing characteristics of the two leaflets of the bilayer.

This report proposes that this newly observed feature of the proton NMR spectrum that is observable at (or above) a field strength of 11.7 Tesla (500 MHz proton resonance frequency) can be used to study several molecular interactions in membranes. This is best illustrated by choosing a few

Figure P.1a H1 NMR spectrum of the chain methylene and methyl regions from small (125 Å radius) DPL vesicles. Temperature, 58°C (above phase transition temperature. The broad and sharp components in the methylene envelope arise from chains of outside facing and inside facing lipids respectively (ibid Chapter III.1).

Figure P.1b H1 spectrum similar to that in Figure P.1a for lipid vesicles with 10% cholesterol.
Note that the sharper component is preferentially broadened.

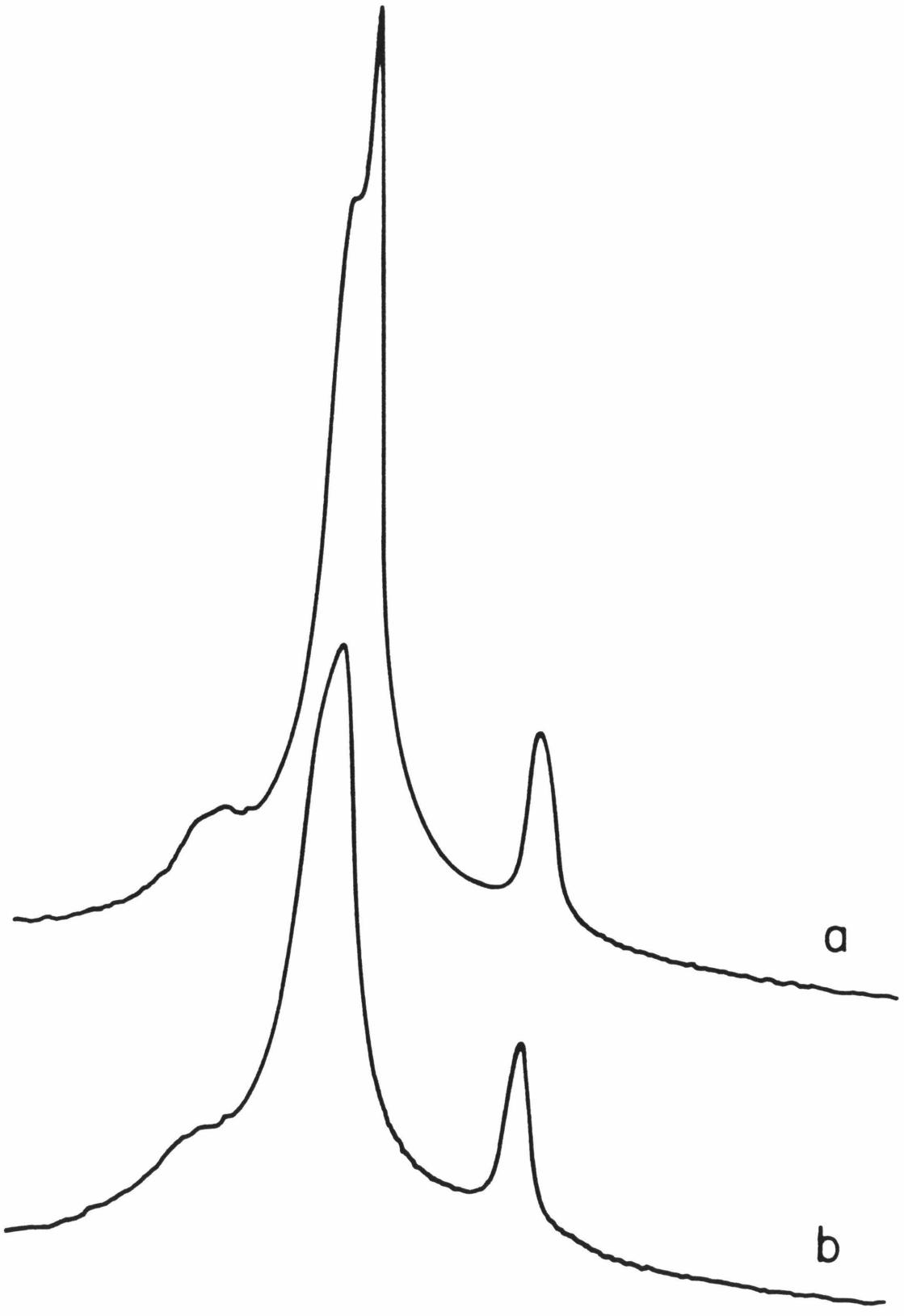
a
b

important problems from the current literature where this method can be applied with sufficient advantages.

(a) Cholesterol-lipid interaction

It has been proposed that cholesterol incorporated into vesicles aligns itself more or less parallel to the membrane director (Rothman and Engleman, 1972). This would cause an ordering of the chains, but is expected to maintain the rotational freedom of the methyl groups (Stockton et al., 1972). A direct verification of the above may be obtained and further insight into the packing of cholesterol into bilayers derived by studying the effect of this molecule on the proton resonances from the outside facing and inside facing lipid chains. Preliminary experiments on this system have been undertaken. Figure P.1 shows that addition of 10% cholesterol to lipid vesicles causes a preferential broadening of the sharp upfield peak that arises from the inside facing lipid chains. At higher concentrations (40%) both halves of the bilayer are affected. It is also observed that the methyl group resonance sharpens up, particularly below the phase transition temperature (not shown). These observations are consistent with a preferential absorption of cholesterol in the inside facing lipid leaflet. This is expected in view of the looser packing of this half of the bilayer (Huang and Mason, 1978; Schuh et al., 1981). This also results in greater separation of the terminal methyl groups resulting in higher disorder and a sharper signal particularly below the gel-liquid crystalline phase transition temperature. A detailed temperature and concentration dependent study, as well as relaxation measurements would provide

further information on the packing and interaction of this important molecule in cell membranes.

(b) Peptide-lipid interaction

Peptide antibiotics and peptide ionophones like valinomycin, alamethicin, gramicidin-A and gramicidin-s exhibit important membrane active functional characteristics. Valinomycin is a carrier of K^+ ions across membranes. Finer et al (1969) have proposed incorporation of the peptide into bilayer vesicles. Hsu and Chan (1973) have found that the peptide interacts differently with Dipalmitoyl lecithin and Dimyristoyl lecithin bilayers. Preliminary studies with H2 NMR indicate that the nature of interaction of valinomycin with bilayers is determined by the presence or absence of K^+ ions (Zidovetzki and Banerjee unpublished results). The action of valinomycin can be better characterized with the method proposed here and its exact position in the vesicle can be determined in the presence and absence of K^+ ions.

Gramicidin-A has been shown to be a transmembrane channel former and may be used as a standard for calibration of the method, it has been shown, however (Van Echteld et al., 1981) that this peptide exhibits lipid polymorphism with negatively charged lipids; the formation of the second phase has been proposed to affect one leaflet of the monolayer more than the other (Van Echteld et al., 1981). This hypothesis can be experimentally tested using this technique.

The interaction of alamethicin with multilayers has been discussed in detail in this thesis. Earlier, Lau and Chan (1976) reported that alamethicin causes extensive fusion in vesicles. These experiments were undertaken with

samples containing 0.4% alamethicin. It has been shown recently, however, that fusion is almost nonexistent when the concentration of alamethicin is lower by about one order of magnitude (Hunt and Jones, 1982). Proton NMR at high field of small vesicle-alamethicin mixtures can therefore indicate the disposition of alamethicin relative to the bilayer. This would be an independent confirmation of the data on multilayers presented in part II. In addition, voltage gradients can be created across the bilayer of vesicles by maintaining an ionic gradient (Lau and Chan, 1976). A study of vesicle spectrum inside and outside chains can be used then to address the important question regarding the nature of alamethicin pores and the position of the molecule in the presence of a potential gradient across the bilayer.

(c) lipid-protein interaction

The applicability of the proposed method to lipid-protein systems is best illustrated with the example of cytochrome-c oxidase interaction with lipid vesicles. It has been proposed (Nicholls et al., 1980) and counter-proposed (Racker et al., 1979) that the enzyme shows orientation preference in membranes. Casey et al. (1982) have investigated the vesicle-oxidase system by monitoring heme reduction with membrane-permeant and membrane-impermeant reagents, and also by kinetic analysis of reduction of attached spin labels to conclude that the proposition of relative orientation is 85% and 50% depending upon whether the vesicles are generated by cholate dialysis or sonication, respectively. A direct observation of the extent of orientation preference (if any) may be achieved by using the proton NMR technique for separate observation of outer and inner chains proposed here. This method is especially suitable for this system since screening on

cytochrome-c oxidase vesicles show that the enzyme is reconstituted only into small (110 Å radius) vesicles. This size is ideal for observation of separate chain resonances from the "inner" and "outer" leaflets of the bilayer.

In conclusion the packing difference of the inner and outer leaflets of the bilayer that manifests itself as separate peaks in high field NMR can be used in regular spectral or relaxation measurements in vesicles reconstituted with different kinds macromolecules to obtain important information regarding the disposition of the above molecules in relation to the bilayers and the nature of interaction between lipids and the macromolecules.

References

Casey, R. P., Ariano, B. H. and Azzi, A. (1982) Eur. J. Biochem. 122, 313.

Finer, E. G., Hauser, H., and Chapman, D. (1969) Chem. Phys. Lipids, 3, 386.

Hsu, M. C. and Chan, S. I. (1973) Biochemistry, 12, 3872.

Huang, C. and Mason, J. T. (1978) Proc. Natl. Acad. Sci. U.S.A. 75, 308.

Hunt, G. R. A. and Jones, I. C. (1982) Bioscience Rep. 2, 921.

Lau, A. L. Y. and Chan, S. I. (1976) Biochemistry, 15, 2551.

Nicholls, P., Hildebrand, V. and Wrigglesworth, J. M. (1980) Arch. Biochem. and Biophys. 204, 533.

Racker, E., Violand, B., O'Neal, S., Alfonzo, M., Telford, J. (1979) Arch. Biochem. and Biophys. 198, 470.

Rothman, J. E. and Engleman, D. M. (1972) Nature, 237, 42.

Schuh, J. R., Banerjee, U., Mueller, L. and Chan, S. I. (1982) Biophys. Biochim. Acta, 687, 219.

Stockton, G. W., Polnaszek, C. F., Tulloch, A. P., Hasan, F. and Smith, I. C. P. (1976) Biochemistry, 15, 954.

Van Echteld, C. J. A., Van Stigt, R., DeKruijff, B., Heunissen-Bijvelt, J., Verkleij, A. J. and DeGier, J. (1981) Biochim. Biophys. Acta, 648, 287.

Proposition III

Two-Dimensional Electron Nuclear Correlated (ENCORE) Spectroscopy: A New Spectroscopic Technique

Specific hyperfine couplings between nuclei and electrons are traditionally investigated using double resonance techniques such as ENDOR and ELDOR (Kevan and Kispert, 1976) or by the recently developed spin echo modulation methods (Kevan and Schwartz, 1979). A two-dimensional pulse technique is proposed, which in its two versions discussed here, will help unravel small dipolar couplings between an electron and a nucleus created by an interaction over long distances, and is also expected to serve as a "spin ruler" in estimating distances between such spins in solids, solutions and for macromolecular systems.

This proposed method uses pulse sequences similar to those established for heteronuclear shift correlation spectroscopy (Maudsley and Ernst, 1977), however, additional problems are encountered here due to the high gyromagnetic ratio (γ_e) and small spin-spin relaxation time (T_{1e}) for the electron and the large spin-spin coupling between the electron and the nucleus. These issues will be addressed later.

For simplicity, a nucleus with spin 1/2 is chosen. The energy diagram of the two spin electron-nuclear system contains four levels. The splittings for weak dipolar coupling are shown in Figure P.2. The weak coupling can be realized only with a large interspin distance (several angstroms). The method relies on a coherent transfer of transverse magnetization between the electron and the nucleus. The basic scheme for the experiment is shown in Figure P.3. Two versions are presented as Figure P.3A and P.3B. The first

Figure P.2 Energy levels for a two spin electron-nucleus system. Arrows indicate allowed transitions.

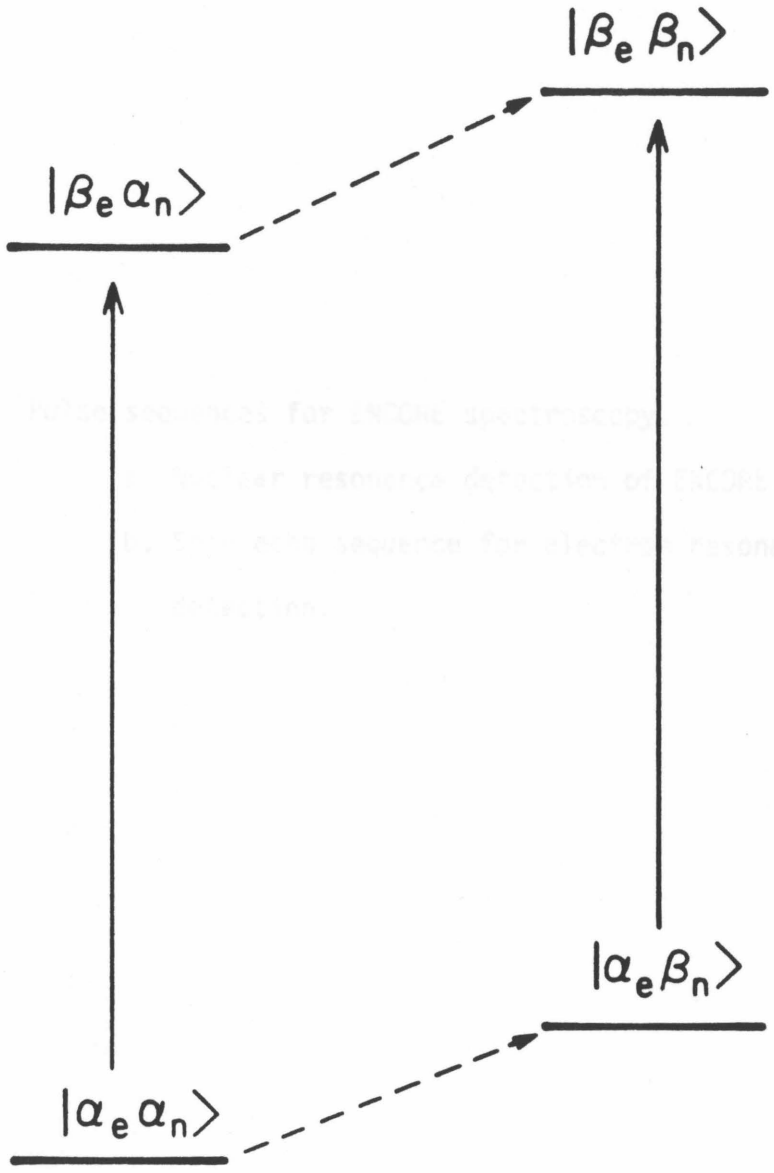
$|\beta_e \beta_n\rangle$
$|\beta_e \alpha_n\rangle$
$|\alpha_e \beta_n\rangle$
$|\alpha_e \alpha_n\rangle$

Figure P.3 Pulse sequences for ENCORE spectroscopy.

a. Nuclear resonance detection of ENCORE.

b. Spin echo sequence for electron resonance detection.

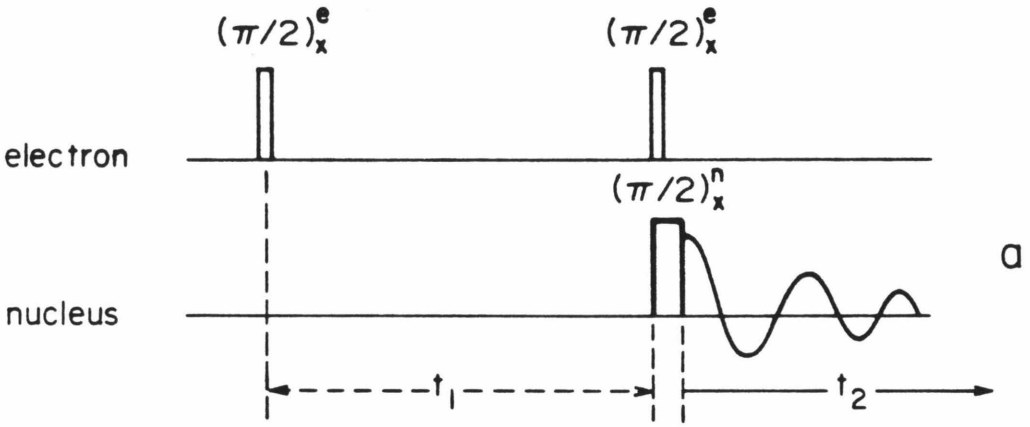
$(\pi/2)^e_x$
$(\pi/2)^e_x$
electron
$(\pi/2)^n_x$
nucleus
t_1
t_2

a

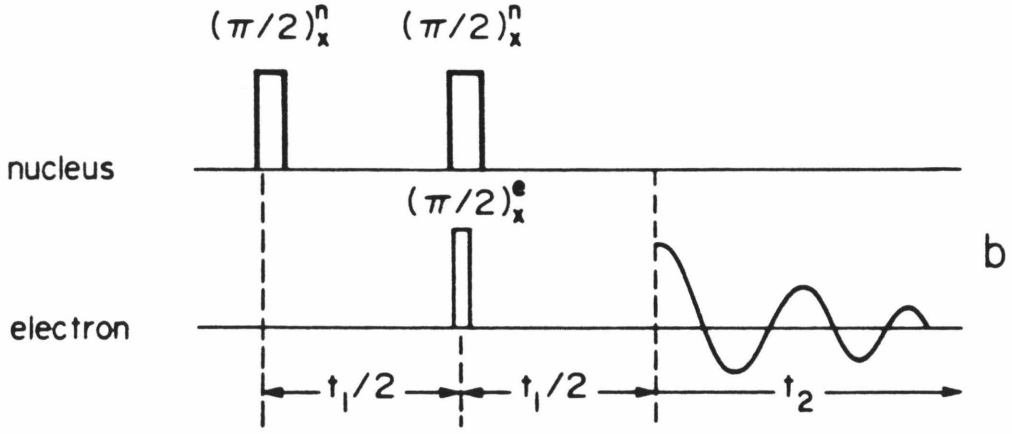
$(\pi/2)^n_x$
$(\pi/2)^n_x$
nucleus
$(\pi/2)^e_x$
electron
$t_1/2$
$t_1/2$
t_2

b

version of the method requires an NMR detection system. A saturating string of random pulses destroys all previous traces of magnetization in the nucleus. A $\pi/2$ microwave pulse is then applied to excite all electronic spins to the transverse plane in the rotating frame. After an evolution period t_1, two simultaneous $\pi/2$ pulses, one microwave to cause electronic transitions generating a longitudinal magnetization, and a radio frequency pulse to excite the nuclei are applied. In accordance with the principles of two-dimensional NMR (Nagayama, 1981) this causes a transfer of magnetization from the electrons to the nuclei due to an intermixing of the transitions only if the nuclear spin is coupled to the electronic spin. The magnetization of the precessing nucleus is then measured as a function of t_2. The experiment is repeated for a large number of t_1's. For signal averaging the pulse sequence may be repeated several times. Since electrons are being used to "pump" the nuclei, the repetition rate is only determined by the spin lattice relaxation time of the electron and may therefore be very fast. The set of FID's thus acquired constitutes a data matrix $s(t_1,t_2)$. A two-dimensional Fourier transformation gives the "spectrum" $F(\omega_1,\omega_2)$ containing the coupling information between the two spins. A particular representation of the spectrum is indicated in Figure P.4. The two one-dimensional axes correspond to frequencies for NMR and ESR observation, respectively. The convectivity of the two transitions due to a weak dipolar coupling will show up as a cross peak indicated by X. The intensity of the peak can be calibrated for the strength of coupling and therefrom to the interspin distance or the coupling constant.

In the second version of the experiment one could ostensibly reverse the pulse sequences i.e. a $\pi/2$ nuclear pulse followed by a pair of

Figure P.4 A possible Fourier transformed representation of the correlated spectrum. X represents the cross peak arising from the dipolar coupling between the nuclear and the electronic spins.

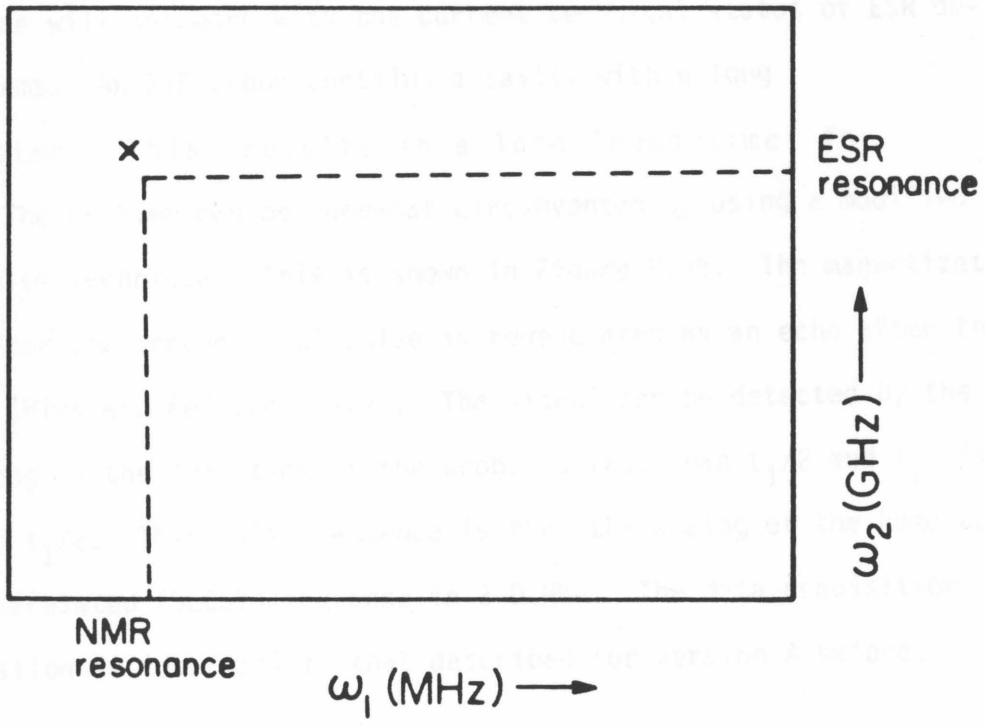
ESR
resonance
ω_2 (GHz)
NMR
resonance
ω_1 (MHz)

simultaneous nuclear and electronic pulses. An ESR detection of the signal as a function of t_1 would constitute a two-dimensional spectrum. The major advantage of this method is the enormous gain in sensitivity due to the high magnetogyric ratio of the electron ($\gamma_e/\gamma_N \sim 1000$). The increased sensitivity derives from the fact that the electronic transitions are now "pumped" by the nuclear transitions. Unfortunately, however, this reversed pulse sequence will not work with the current technical status of ESR detection systems. An ESR probe contains a cavity with a long ringing time. This results in a long 'dead time' for the probe. The problem can be somewhat circumvented by using a modified spin echo pulse technique. This is shown in Figure P.3B. The magnetization generated after the second ($\pi/2$) pulse is regenerated as an echo after the time $(t_1)/2$ (Mims and Peisach, 1979). The signal can be detected by the cavity as long as the dead time of the probe is less than $t_1/2$ and T_{1e} is greater than $t_1/2$. This pulse sequence is then the analog of the homonuclear spin echo correlated (SECSY) sequence in 2-D NMR. The data acquisition and manipulation is identical to that described for version A before.

Problem Areas

1. The spin lattice relaxation time

T_{1e} for an electron is usually very short. For this method to work, the pulse separation t_1 is required to be much shorter than the relaxation time. It is therefore desirable to perform the experiments with slow relaxing spin species (such as nitroxide radicals) and at low temperatures ($\sim$4 K) so that the T_{1e} is long enough for the realization of the experiment. T_{1e} of the order of 1msec is available, pulse repetition rates of 1KHz are practical and one million FID's in 20 minutes is remarkable

(Weissman, 1982).

2. The ESR version of this method requires uniform pulses separated by very short delays and probes with very small ringing time. While current workers in pulsed ESR (Weissman, 1982) claim these conditions can be met [5KW coherent microwave power has been used in some experiments (Semenov et al., 1980), and 100nsec dead time probes have been discussed in the lieterature (Trifunac and Lawler, 1981)], pulse fourier transform ESR is still a technical challenge.

3. The hyperfine coupling between electrons and nuclei can be very large if the nuclei are very close to the electrons. Under these conditions, the nuclear spin is completely saturated and since the usual Zeeman quantization fails, so will this method. On the other hand, if the dipolar coupling between the spins is weak due to large separations (many examples of $0\text{-}10^5$ Hz couplings are available, see for example LaMar et al., 1973), this technique (version A) would accurately exhibit the couplings since the detection system is identical to that in high resolution NMR.

Applications

Many applications of the technique can be readily found. To cite a few examples, it would be useful in determining spin distribution in solids, in studies of inorganic complexes to determine interaction of metal site electrons with the ligand nuclei, in biophysical studies of electron transfer sites in metalloproteins and in determining position of a labeled protein for example, relative to a spin labeled lipid in a biological membrane.

References

Kevan, L. and Schwartz, R. N. eds (1979) Time Domain Electron Spin Resonance John Wiley & Sons, N.Y., 280

Kevan, L. and Kispert, L. D. (1976) in Electron Spin Double Resonance Spectroscopy John Wiley & Sons, N.Y., 1

LaMar, G. N., Horrocks , W. DeW. Jr., and Holm, R. H. (1973) NMR of Paramagnetic Molecules, Academic Press, N.Y.

Maudsley, A. A. and Ernst, R. R. (1977) Chem. Phys. Lett. 50, 368

Mims, W. B. and Peisach, J. (1979) Biological Applications of Magnetic Resonances, Shulman R. G. ed., Academic Press, N.Y., 221

Nagayama, K. (1981) Adv. Biophys. 14, 139

Semenkov, A. G., Schirov, M. D., Zhidkov, V. D., Khmelinskii, V. E., Dvornikov, Z. V. (1980) Inst. Chem. Kinet. Combust., Novosibersk, Preprint 3

Trifunac, A. D. and Lawler, R. G. (1981) Chem. Phys. Lett. 84, 515

Weisman, S. I. (1982) Ann. Rev. Phys. Chem. 33, 301

Proposition IV

Molecular Dissection of Behavior.

The title of this proposition is reminiscent of a popular article published in Scientific American a decade ago, entitled Genetic Dissection of Behavior (Benzer 1973). In the last twenty years, advances in molecular neurogenetics have aided in a one-to one mapping of the genetics of simple organisms with the development of the nervous system and the sense organs (Hall and Greenspan 1979). Interesting results have been obtained with the fruit fly Drosophila, where genetics is simple enough to be well understood and the nervous system is complicated enough to make its study meaningful.

Very recently, developments in the generation of monoclonal antibodies have made it possible to identify surface molecules in the nervous system (Zipser and McKay 1981; Fujita et al. 1982). These help distinguish one nerve from another and from other components in the nervous system. More importantly, progress has been made in isolating these surface molecules with an aim towards identifying their function in the nervous system and linking them with behavior (Zipursky and Venkatesh 1983). This is a step farther from a genetic dissection of behavior towards understanding of the molecular interactions in the brain. The approach currently in use is first described, and an alternative approach is proposed that is expected to address more specific problems relating to the organization of the nervous system in Drosophila.

The current approach.

A large number of hybridomas that produce monoclonal antibodies to specific antigens in the Drosophila nervous system has been isolated by injection of Drosophila brains into mice and hybridization of the host spleen cells with myeloma cell lines (Fujita et al. 1982). These hybridomas have been used to identify polypeptides arising in the developing brain and visual system of Drosophila. Immunoaffinity columns are used to isolate several micrograms of the molecules that are specific to axons (corresponding to monoclonal antibody 22C10), photoreceptor cells (Mab 24B10), sensory hairs in antenna (Mab 21A6) and rhabdomeres (Mab 28H9). The N-termini of these molecules are sequenced, and probe molecules corresponding to the sequence are synthesized. These are used to screen Drosophila DNA libraries to identify the genes corresponding to the surface molecule. Chemical modification of this gene is expected to block the synthesis of the antigen, as well as exhibit behavioral or anatomical malfunction. The isolated molecule can thus be linked to this defect, indicating its functional importance in the animal. In this approach, the judicial selection of one of the many available surface molecules is of prime importance. A laborious isolation procedure could, otherwise, produce a molecule with little or trivial function in the brain.

An alternative approach.

Mutations causing defects in the Drosophila nervous systems and connected sense organs have been very well studied (Pak, 1975). Hundreds of mutants of the nervous system have been isolated, showing for example, defects like lack of optical pigments, irregular development of the compound eye, or poorly formed axon to axon synaptic connections. It is proposed, that

a mutant strain be selected that shows an organizational or behavioral defect in the nervous system or the sense organs. The brain of the mutant fly is then subjected to the antibody screening procedure to identify specific antigen molecules. A comparison with the wild type chemical map of the brain will help identify the particular molecules that are responsible for the deficiencies in the mutant. The appearance of the chemical can be traced through development in a normal fly, and probed genetically, to obtain a clearer understanding of its function in the nervous system. Unlike the previous approach, this method of identification proceeds from an 'interesting' physiological and behavioral characteristic and the results from the investigation are expected to be easier to interpret. This is made clearer with an example:

The compound eye of Drosophila is made up of approximately 700 ommatidia. Each of these has eight photoreceptor cells (Ready et al. 1976). Cells 1 through 6 occupy the periphery of the ommatidium. Their rhabdomeres, the light sensitive part of the membrane, are long structures extending the whole length of the ommatidium. The axons from these cells terminate and synapse in the second order optic lobe, the lamina (Braitenberg,1972). The cells 7 and 8, on the other hand, have narrower and shorter rhabdomeres and their axons do not terminate or synapse in the lamina, but project through it, terminating in the next optic lobe, the medulla. What molecular interaction prompts cells 7 and 8 not to form connections at the lamina, but to penetrate through to the medulla? Purification of surface antigens and identifying their genetic precursors would hardly afford an answer, since it is not known which of the many molecules may be responsible. the approach suggested

here can, however, be used. A Drosophila mutant that lacks the seventh cell (sev) has been identified (Harris et al. 1976). Flies lacking all cells but the eighth can also be made (double mutant sev rdgB) (Hall et al. 1982). The "sevenless" can be screened against monoclonal antibodies molecules that are lacking since they belong to cell 7 only. Similarly, molecules that are specific to cell eight can be identified by screening the double mutant. The molecules can be probed genetically and identified at different stages of development of the visual system to provide crucial answers to the nature of organization and specificity in the nervous system.

References

Benzer, S. (1973) Scientific American, 233, 24.

Braitenberg, V. (1972) Information Processing in the Visual System of Arthropods. Wehner, R.,ed. Springer Verlag, Berlin., 3.

Fujita, S.C., Zipursky, S.L., Benzer, S., Ferrus, A. and Shotwell, S.L. (1982) Proc. Natl. Acad. Sci. 79, 7929.

Hall, J.C., Greenspan,R.J. and Harris, W.A. (1982) Genetic Neurobiology, MIT press, Cambridge, MA., 75.

Hall, J. and Greenspan, R.J. (1979) Ann. Rev. Genet. 13, 127.

Harris, W.A., Stark, W.S. and Walker, J.A. (1976) J. Physiol. 256, 415.

Pak, W.L. (1975) Handbook of Genetics, King, R.C. ed., Plenum press, NY, 3, 703.

Ready, D.F., Hanson, T.E. and Benzer, S. (1976) Developmental Biol. 53, 217.

Zipursky, S.L., Venkatesh, T.R. and Benzer, S. (1983) CALTECH Biol. Divn. Ann. Rep. in press.

Zipser, B. and McKay,R. (1981) Nature, 289, 549.

Proposition V

Laser Raman Investigation of The Secondary Structure of Alamethicin.

Although the Raman effect was discovered in 1928 (Raman and Krishnan, 1928), the usefulness of this technique as a spectroscopic tool in elucidating biochemical structures was not realized until the 1970's (for a general review see Yu, 1977). Most investigations involving structure determination by Raman spectroscopy are qualitative;attempts towards quantitation of the data have been made by Lippert et al. (1976; 1975) who have shown that empirical equations can be constructed that relate the intensities of amide vibrations to the relative ratios of α helical, β sheet and random coil structures in a protein. In essence, the study claims that the intensities of the 1240 cm^{-1}, 1632 cm^{-1} and 1660 cm^{-1} Raman bands from a protein are linear combinations of the corresponding intensities from purely α helical, β sheet and random coil proteins weighted by the proper fractions of these conformations in the protein under investigation; i.e.,

$$C\, I^{p}_{1240} = f_{\alpha} I^{\alpha}_{1240} + f_{\beta} I^{\beta}_{1240} + f_{R} I^{R}_{1240} \qquad 1$$

$$C\, I^{p}_{1632} = f_{\alpha} I^{\alpha}_{1632} + f_{\beta} I^{\beta}_{1632} + f_{R} I^{R}_{1632} \qquad 2$$

$$C\, I^{p}_{1660} = f_{\alpha} I^{\alpha}_{1660} + f_{\beta} I^{\beta}_{1660} + f_{R} I^{R}_{1660} \qquad 3$$

$$f_{\alpha} + f_{\beta} + f_{R} = 1 \qquad 4$$

where, I^{p}_{x} represents intensity of the band at x cm^{-1} for the protein

while, I_x^{α}, I_x^{β} and I_x^{R} are the intensities of the bands at x cm^{-1} for purely α helical, β sheet and random coil conformations respectively. C is a scaling factor that depends on the particular protein. f_{α}, f_{β}, and f_R are the fraction of the protein in α helical,β sheet and random coil conformations respectively. The quantities I_x^{α}, I_x^{β} and I_x^{R} have been determined from studies on model compounds like poly-L-lysine which exhibit a single conformation along the entire length of the molecule depending on the pH and temperature. Lippert and co-workers have used this technique to examine the conformation of many common proteins in solution (Lippert et al. 1976), as well as in membranes (Lippert et al. 1975). Peptide chemists have used the method to probe the conformations of gramicidin A (Iqbal and Weidekamm, 1980).

In part I of this thesis, the secondary structure of alamethicin has been discussed as a partly helical and partly extended conformation . This can be confirmed with the technique described here. As a first step towards this goal, the Raman spectrum of solid alamethicin was acquired. The major bands were identified based on the assignments of Raman modes in proteins described by Spiro and Gaber (1977). This is shown in Figure P.5. Sharp peaks at 1275 and 1650 cm^{-1} indicate at least partially helical structures. Non-helical regions are characterized by bands at 1002 cm^{-1} and 1685 cm^{-1}. Conformationally sensitive amide II, amide III and C-C stretches can be used to quantitate the fraction of helical and nonhelical regions in the molecule. Using reported values of I_x^{α}, I_x^{β} and I_x^{R} (Lippert et al. 1976) and substituting the measured values of $I_{1240}^{\text{alamethicin}}$, $I_{1632}^{\text{alamethicin}}$ and $I_{1660}^{\text{alamethicin}}$ into equations 1,2, 3 and 4, one obtains,

Figure P.5 Raman spectrum of solid alamethicin.

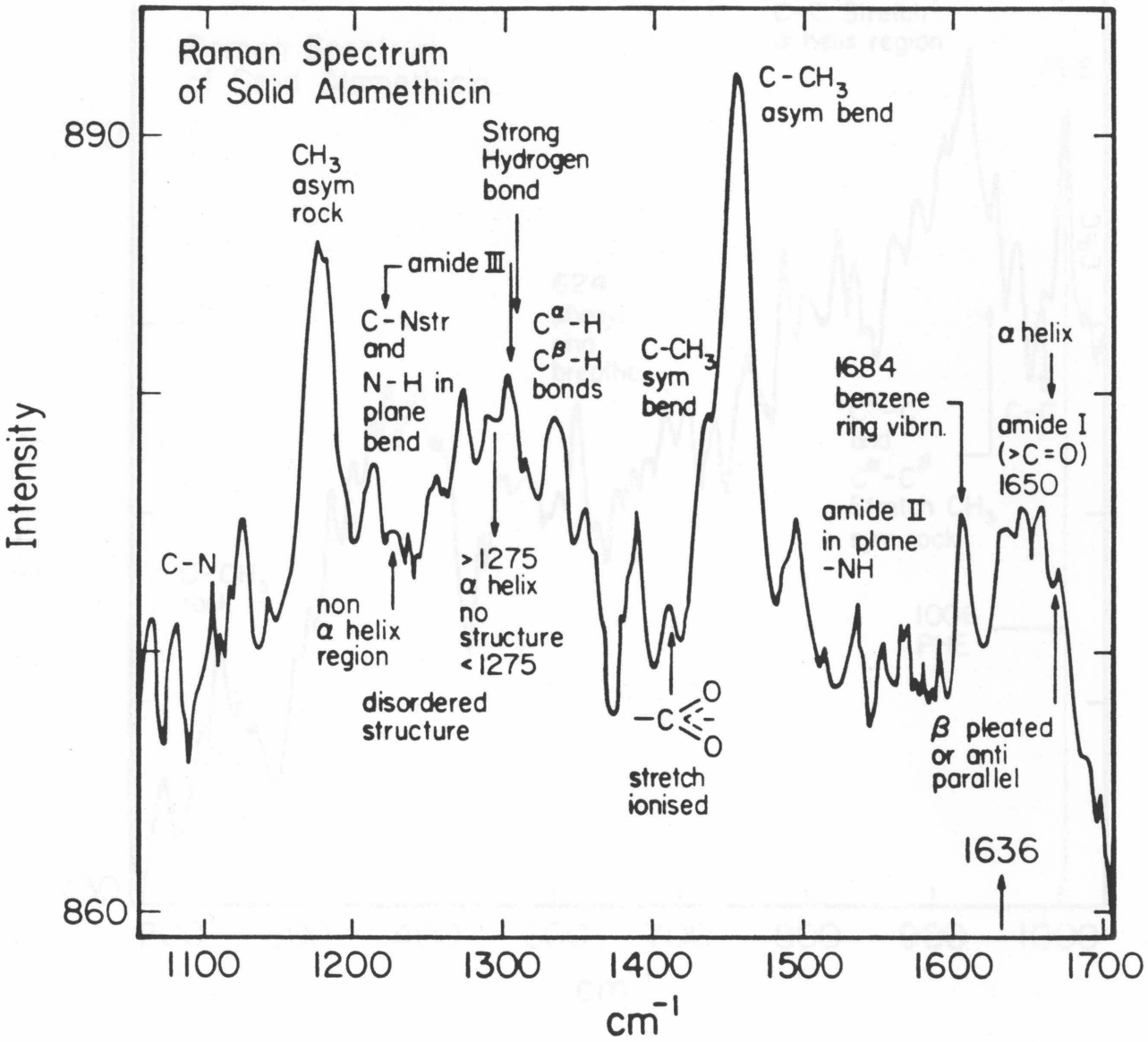
Raman Spectrum
of Solid Alamethicin
890
860
Intensity
CH3
asym
rock
Strong
Hydrogen
bond
amide III
C-Nstr
and
N-H in
plane
bend
Cα-H
Cβ-H
bonds
C-CH3
sym
bend
C-CH3
asym bend
1684
benzene
ring vibrn.
α helix
amide I
(>C=O)
1650
amide II
in plane
-NH
C-N
non
α helix
region
>1275
α helix
no
structure
<1275
disordered
structure
stretch
ionised
β pleated
or anti
parallel
1636
1100
1200
1300
1400
1500
1600
1700
cm-1

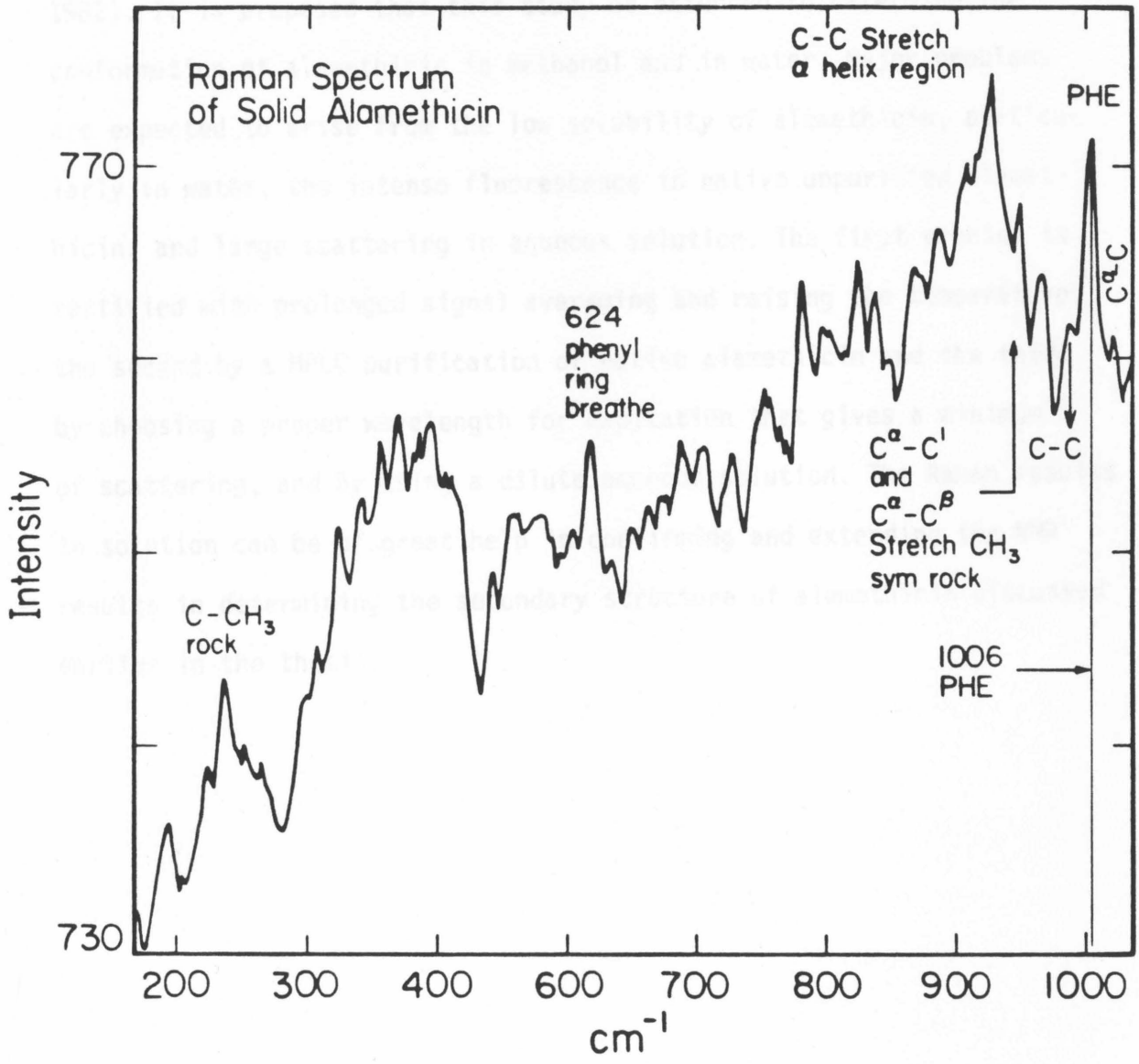
Raman Spectrum
of Solid Alamethicin
C-C Stretch
α helix region
PHE
624
phenyl
ring
breathe
C-CH3
rock
Cα-C'
and
Cα-Cβ
Stretch CH3
sym rock
C-C
1006
PHE
Cα-C
Intensity
770
730
200
300
400
600
700
800
900
1000
cm-1

$f_\alpha = .44$; $f_\beta = .4$; and $f_R = .16$

This compares very well with NMR results in solution described earlier and contrasts with the all helical crystal structure (Fox and Richards, 1982). It is proposed that this study be extended to determine the conformation of alamethicin in methanol and in water. Major problems are expected to arise from the low solubility of alamethicin, particularly in water, the intense fluorescence in native unpurified alamethicin, and large scattering in aqueous solution. The first problem is rectified with prolonged signal averaging and raising the temperature, the second by a HPLC purification of native alamethicin and the third by choosing a proper wavelength for excitation that gives a minimum of scattering, and by using a dilute aqueous solution. The Raman results in solution can be of great help in confirming and extending the NMR results in determining the secondary structure of alamethicin discussed earlier in the thesis.

References.

Fox, R.O. and Richards, F.M. (1982) Nature, 300, 325.

Iqbal, Z. and Weidekamm, E. (1980) Arch. Biochem. Biophys. 202, 639.

Lippert, J.L., Tyminski, D. and Desmeules, P.J. (1976) J. Am. Chem. Soc. 98, 7075.

Lippert, J.L., Gorczyca, L.E. and Meiklejohn, G. (1975) Biophys. Biochim. Acta, 382, 51.

Raman, C.V. and Krishnan, K.S. (1928) Nature, 121, 501.

Spiro, T.G. and Gaber, B.P. (1977) Ann. Rev. Biochem. 46, 553.

Yu, N.T. (1977) CRC Crit. Rev. Biochem. 4, 229.